ForestPaths

Co-designing holistic forest-based policy pathways for climate change mitigation

D3.1 Enhanced and evaluated forest ecosystem models

28.11.2024

Project authors: Thomas Pugh, Mart-Jan Schelhaas, Almut Arneth, Ioan Dutca, Annemarie Eckes-Shephard, Sara Filipek, Louis König, Silke Jacobs, Anna Maria Jönsson, Marco Patacca, Silke Jacobs, Bas Lerink, Mats Lindeskog, Rodrigo Munoz Avilez, Gert-Jan Nabuurs, Stefan Olin, Mikko Peltoniemi, Karl Piltz, Cornelius Senf, Ajdin Starcevic, Igor Staritsky, Alba Viana-Soto, Martin Wittenbrink.

External contributors: Julen Astigarraga, Emil Cienciala, Adriane Esquivel-Muelbert, Jonas Fridman, Leen Govaere, Fredrik Lagergren, Aleksi Lehtonen, Paul A. Miller, Lars Nieradzik, Anja Rammig, Paloma Ruiz Benito, Golo Stadelmann, Susanne Suvanto, Torbern Tagesson, Andrzej Talarczyk, Miguel A. Zavala, Haoming Zhong.

Funded by
the European Union

This project receives funding from the European Union's Horizon Europe Research and Innovation Programme (ID No 101056755), as well as from the United Kingdom Research and Innovation Council (UKRI). Views and opinions expressed are those of the author(s) only and do not necessarily reflect those of the European Union or the European Commission. Neither the EU nor the EC can be held responsible for them.

Prepared under contract from the European Commission and the United Kingdom Research and Innovation Council.
Grant agreement No. 101056755
EU Horizon Europe Research and Innovation Action

Project acronym:	**ForestPaths**
Project full title:	**Co-designing Holistic Forest-based Policy Pathways for Climate Change Mitigation**
Project duration:	01.09.2022 – 28.02.2027 (54 months)
Project coordinator:	Dr. Hans Verkerk, European Forest Institute (EFI)
Call:	HORIZON-CL5-2021-D1-01
Deliverable title:	Enhanced and evaluated forest ecosystem models
Deliverable n°:	D3.1
WP responsible:	WP3
Nature of the deliverable:	Report
Dissemination level:	Public
Lead partner:	ULUND
Recommended citation:	Pugh, T., Schelhaas, M.-J., Arneth, A., Dutca, I., Eckes-Shephard, A., Filipek, A., König, L., Jacobs, S., Jönsson, A. M., Patacca, M., Jacobs, S., Lerink, B., Lindeskog, M. Munoz Avilez, R., Nabuurs, G.-J., Olin, S., Peltoniemi, M., Piltz, K., Senf, C., Starcevic, A., Staritsky, I., Viana-Soto, A., Wittenbrink, M. (2024). Enhanced and evaluated forest ecosystem models. ForestPaths project deliverable D3.1.
Due date of deliverable:	Month 27
Actual submission date:	29.11.2024

Deliverable status:

Version	Status	Date	Author(s)
1.0	Draft	11.11.2024	See above
	Review	22.11.2024	Mikko Peltoniemi, Hans Verkerk
2.0	Final	28.11.2024	Thomas Pugh, Mart-Jan Schelhaas

Table of contents

Key takeaway messages

- Initialisation processes in both LPJ-GUESS and EFISCEN-Space have been updated and improved to provide starting points for the model simulations that correspond closely to the actual state of forests across Europe.
- EFISCEN-Space was expanded with mechanistic disturbance modules for fire and wind, whilst mechanistic wind and fire disturbance modules in LPJ-GUESS were tailored for simulations across Europe and a new spruce bark beetle module developed. These developments allow the evaluation of the effectiveness of different management interventions and policy pathway scenarios with both models.
- EFISCEN-Space was expanded with an empirical dynamic ingrowth module and an empirical dynamic mortality model, allowing longer realistic projections and coverage of a wider variety of forest structure conditions.
- Both LPJ-GUESS and EFISCEN-Space were expanded with empirical rule-based harvesting modules, allowing them to closely represent the dynamics of recent harvest behaviour in Europe and giving more flexibility regarding the implementation of alternative management scenarios.
- EFISCEN-Space can closely reproduce current forest structure due to its dependence on tree-by-tree forest inventory for initialisation. Due to its empirical foundations, the reliability of the projections decreases when climate, forest and management conditions depart from the calibration conditions. The model is capable of producing realistic business as usual scenarios for at least 3-4 decades, but uncertainty increases quickly over time. The model is especially sensitive to the harvest implementation. Different setups of harvest rules may lead to contrasting effects on longer-term increment levels, causing either a long-term increase or decrease in average growing stock.
- LPJ-GUESS can reproduce current forest structure using tree-by-tree inventory data where it is available and by using stand age data where it is not. Its process-based formulation currently results in some regional biases in the simulation of growth dynamics; it is stable, however, in making long-term simulations and provides a capable platform for exploring and attributing the responses of European forests under novel climate and/or management conditions.
- A flexible benchmarking tool has been developed that can be applied to evaluate forest models against eddy-covariance fluxes, national forest inventory statistics and satellite-based metrics.
- EFISCEN-Space was awarded the WENR quality A status for models and databases after an audit that focuses on modelling protocols, evaluations and quality assurance and quality control (QA/QC) procedures.

Summary

This deliverable describes the updates to two forest ecosystem models, LPJ-GUESS and EFISCEN-Space, which provide enhanced capacity for the models to capture current forest state and disturbance risks and to model management actions.

EFISCEN-Space was expanded with an empirical dynamic ingrowth module and an empirical dynamic mortality module, allowing longer realistic projections and coverage of a wider variety of forest structure conditions. Due to the long management history of European forests, observations in very dense stands and in stands with (very) large diameters are rare. The calibration data of the mortality module are therefore heavily dominated by observations in managed stands with small to medium-sized trees. Consequently, the mortality module reflects the self-thinning process under low to medium densities and is not capable of accurately predicting mortality under high densities and for large-sized trees (approximately 60 cm diameter and beyond). Secondly, EFISCEN-Space was expanded with an empirical rule-based harvesting module, allowing more flexibility regarding the implementation of alternative management scenarios. The projections proved to be very sensitive to alternative formulations of harvest mechanisms and parameters. Different setups of harvest rules may lead to contrasting effects on longer-term increment levels, causing either a long-term increase or decrease in average growing stock. Thirdly, EFISCEN-Space was expanded with mechanistic disturbance modules for fire and wind, allowing the evaluation of the effectiveness of adaptation scenarios. These modules are currently being tested and evaluated.

Overall, we found that EFISCEN-Space is able to closely reproduce current forest structure and harvest level due to its dependence on raw National Forest Inventory (NFI) data for initialization and harvest parameterisation. Due to its empirical foundations, the reliability of the projections decreases when climate, forest and management conditions depart from the calibration conditions. Uncertainty increases inside the EFISCEN-Space when moving away from the raw NFI observations (number of trees per diameter class), accumulating uncertainties of additional models for volume, biomass, biomass turnover and finally the soil module Yasso15. Performing an uncertainty analysis for such a complex simulation model proved to be a demanding task, partly due to its inherent complexity and partly because the uncertainty of incorporated models (for example for estimation of volume, biomass and increment) is not documented. We therefore limited our uncertainty analysis to the direct effects of uncertainty in the underlying NFI data. We conclude that EFISCEN-Space is capable of producing realistic business as usual scenarios for at least 3-4 decades, but uncertainty increases quickly over time.

LPJ-GUESS was updated with new routines for forest initialisation. Where systematic tree-by-tree forest inventory data is available, the model can now directly initialise vegetation composition and structure from this over large scales. Where such data is not available, the stand age initialisation process has been updated to allow a better representation of forests within Europe. Furthermore, we added a capability to directly force historical stand-replacing disturbances based on satellite observations, allowing to dynamically update large-scale forest structure from the base year of inventory observations to the present day. As such, LPJ-GUESS can now begin European-scale simulations from an unprecedented level of realism for a process-based vegetation model. The wind disturbance module for Sweden has been generalised for application

across Europe as a whole, whilst the fire disturbance modules have been reparameterised to enable improved simulations at the scale of European forests. A new spruce bark beetle module has been developed, allowing to simulate the complex dynamics of this important agent and its interactions with storm damage, drought and management. These disturbance modules complement the existing individual-tree mortality mechanisms substantially increasing the level of process-realism in the simulation of tree death. A new harvest module based on harvest frequency and intensity as derived from forest inventory data over 2000-2020 has been developed. The resulting harvest frequencies and intensities are responsive to the composition and structure of the simulated forest stands, providing a capability to simulate dynamic business-as-usual harvesting scenarios. The updated LPJ-GUESS module was extensively benchmarked against a range of observations of forest state and dynamics. The evaluation showed generally a high level of performance but also highlighted some regional biases in tree growth rate which should be addressed. Finally, new climate input datasets have been prepared, enabling simulations at 0.05° resolution across Europe.

1 Introduction

The overall objective of WP3 is to assemble a flexible framework of highly synergistic and complementary models for analysis of forests' role in Socio-Ecological Systems, in the Earth-System, and for Integrated Assessments. A key part of this is developing the capabilities of forest ecosystem models to represent disturbances and management, as well as to more closely inform the structure of the forest they are simulating with observations. In this deliverable, we describe the developments made two forest ecosystem models: LPJ-GUESS and EFISCEN-Space. LPJ-GUESS is a dynamic vegetation model with a detailed representation of forest demography which simulates growth, competition and mortality of age cohorts of trees of different species (or plant functional types). EFISCEN-Space is an empirical European forest resource model that simulates the development of NFI plots into the future. All submodules that represent important demographic processes (increment, mortality, ingrowth, harvest) are developed on a large database of repeated forest inventory measurements, spanning a large gradient within Europe.

In the following, we describe, for each of the models in turn, new developments in (a) the initialisation of vegetation composition and state, (b) the dynamic representation of important demographic processes, (c) the representation of major forest disturbance agents (wind, fire and bark beetle), (d) the representation of rule-based forest management regimes and (e) evaluation of model performance. We then provide a performance summary for some important metrics across the two models against independent data. We perform these demonstrations across a subset of the countries in Europe for which appropriate data has been available during this model development stage of ForestPaths and which give a good representation of the range of different forest types within Europe. We highlight collaborations with other projects to maximise the improvements of the model capabilities available to exploit in ForestPaths and beyond as well as explain where and why we have deviated from the original plan laid out in the grant agreement.

2 LPJ-GUESS

An overview of the model developments included in ForestPaths is given in Table 1. The development process was optimised by extensive collaborations with other projects with the aim to link and synergise work across projects to provide a more capable model than was originally envisaged in the grant agreement of any one project. These projects were the Horizon Europe projects CLIMB-Forest (101059888) and wildE (101081251), as well as the ForestValue EraNet project FORECO (www.foreco.org) and the Horizon 2020 project TreeMort (758873). We transparently show where these developments have been made in collaboration with other projects and also identify developments in other projects which have been brought into the model version available for use in ForestPaths. Details of the developments are provided in two publication-ready manuscripts which are attached to this deliverable as appendices. References to the explicit sections of these appendices can be found in the table.

Appendix A "Dynamic vegetation modelling for the past and future of Europe's forests" (Pugh et al. *in preparation*) describes the developments made to create a version of LPJ-GUESS optimised for simulating European forest present and futures. In ForestPaths, the developments primarily relate to Tasks 3.1 and 3.2.2. The appendix describes new capabilities to initialise LPJ-GUESS based on tree-by-tree NFI data or by using forest age data for Europe (Task 3.1.1), a generalisation of windthrow modelling capability for Sweden and a reparameterisation of the

global fire model, to allow them to be applied at European scale (Task 3.1.2), a new approach to specify harvest rates and intensity based on rules derived from national forest inventory data (Task 3.2.1) and a new benchmarking tool including evaluation against fluxes from the Integrated Carbon Observation System (ICOS), forest harvest and growth statistics from Forest Europe and forest regrowth rates from inventory plot observations (Task 3.1.3). The tool is designed to be applicable on any model with comparable outputs and in this deliverable is also applied to evaluate EFISCEN-Space in relevant aspects (see §4). The results in this work are typically demonstrated for a transect of ten European countries from Spain to Finland. Further to the work described in the appendix, we also made agreements with several national inventory networks to use their data to initialise and develop LPJ-GUESS within ForestPaths. Data processing pipelines have also been put in place to prepare input data for the remaining European countries that were not simulated as part of this study.

Appendix B "Combining empirical and mechanistic understanding of spruce bark beetle outbreak dynamics in vegetation modelling" (Lagergren et al. *in preparation*) describes the implementation and calibration of a spruce bark beetle damage module in LPJ-GUESS. We had originally anticipated developing a simple bark beetle model based on observations from WP2 (Task 2.3) in LPJ-GUESS. However, as it did not prove possible to cleanly separate storm and bark beetle damage in the remote sensing observations (Deliverable 2.3), we adopted an alternative approach, combining resources from ForestPaths with the CLIMB-Forest and FORECO projects to develop a new intermediate-complexity spruce bark beetle model for Europe. This model has a strong empirical foundation but also enough process detail to link the complex dynamics of bark beetle outbreaks, droughts and storm damage.

Table 1. LPJ-GUESS model features developed and added in ForestPaths and in collaborating projects. Details are provided in the referenced sections of Appendices A and B.

Aspect	Model feature	ForestPaths	Other projects
Initialisation	Age and composition initialisation	Collaborated with CLIMB- Forest and wildE projects to utilise the best components from each project. In ForestPaths we prepared the pipeline to process the forest genus map from WP2 for LPJ-GUESS initialisation	1. Prepared European forest age dataset for LPJ-GUESS initialisation. Technical updates to LPJ-GUESS to accommodate more detailed input (CLIMB-Forest) 2. Merged forest age and composition initialisation with land use dataset from HILDA+ (wildE)
Initialisation	NFI initialisation	Implemented capability to initialise LPJ-GUESS from forest inventory data on a systematic grid across European countries with suitable data. Appendix A, §4.6, §6.2	
Initialisation	High resolution input datasets	High resolution input datasets (0.05°) for climate and land-use change have been prepared.	

Disturbances	Fire disturbances (burnt area)	Reparameterisation of the SIMFIRE model for application to Europe, using maps from WP2. Appendix A, §4.1, §5.5	
Disturbances	Fire disturbances (BLAZE wildfire combustion)	-	The BLAZE fire combustion model has been recalibrated for Europe in the CLIMB-Forest project, further improving the fire disturbance representation available to ForestPaths Appendix A, §4.1, §5.5
Disturbances	Storm damage	An empirical wind damage probability risk map was developed together with WP2 and applied within LPJ-GUESS to provide appropriate pan-European risk assessment to link with an existing wind damage vulnerability model. Appendix A, §4.2, §5.4	Technical updates to the storm damage module to improve its capability to represent damage in different European countries from the (CLIMB-Forest). Code merge of storm damage code with latest European model version (FORECO).
Disturbances	Spruce bark beetle damage	Generalisation, calibration and evaluation of spruce bark beetle code across Europe in direct collaboration with the CLIMB-Forest project. Appendix B. Also summarised in Appendix A, §4.3, §5.4	Initial development of generic bark beetle concept and code (TreeMort) Specialisation for European spruce bark beetle (FORECO)
Disturbances	Satellite-forcing of historical stand-replacing disturbances	Additional to grant agreement plans, allowing improved historical assessment and model initialisation for future simulations. Appendix A, §4.4, §6.1	Joint effort with FORWARDS
Rule-based management	Probabilistic harvest	Conceptualisation, LPJ-GUESS code development and simulations, leveraging inventory data analysis made in the CLIMB-Forest project. Summarised in Appendix A, §4.5	
Evaluation	Model benchmarks	Collaborated across projects to utilise the best components from each project and implement them in an open access model evaluation framework, going beyond the initial plans detailed in the respective Grant Agreements. In ForestPaths this included	Y. Model evaluated against satellite GPP, gridded NFI statistics, FLUXNET (CLIMB-Forest) Appendix A, §5.1, §5.3

evaluation against ICOS fluxes, Forest Europe statistics and forest regrowth rates
Appendix A, §5.2

High-resolution climate. In addition to the above, high resolution climate data for use as input to LPJ-GUESS was provided by adopting the CHELSA algorithms, which are designed to perform spatial downscaling of near-surface climate data. The original implementation (Karger, 2022), scales ISIMIP3b temperature, precipitation, and downwelling shortwave radiation from an input resolution of 0.5° down to 0.01°. The code additionally requires three-dimensional data from the CMIP6 ensemble, as well as static data such as high-resolution surface elevation. The dataset has been processed for the MPI-ESM for historical period (1850-2014) and future projections (2015-2100) for SSP1-2.6, SSP3-7.0, SSP5-8.5, consistent with the cross-project climate scenario protocol developed as part of Task 5.1.1 and to be employed for the exploratory scenarios. Windspeed and air humidity (necessary for the fire-module in LPJ-GUESS) were interpolated. The data has been regridded to 0.05° to keep total file size (1.3 TB) and run-time for European continent-wide runs to a reasonable effort. Initial simulations that compare LPJ-GUESS output at standard 0.5° versus 0.05° resolution reveal significant differences in vegetation properties and fluxes, particularly in mountain regions with e.g. lower gross primary productivity in the high-resolution runs. The data is available for download through KIT/IMK-IFU's thredds storage server (Belda, 2024) and are made available under a CC BY-SA 4.0 license. As a next step it is foreseen to develop a simplified downscaling method for LPJ-GUESS that would allow the user to flexibly downscale other GCMs than MPI-ESM and for self-selected grid cells.

3 EFISCEN-Space

EFISCEN-Space is enhanced and applied in a range of (mostly EU-funded) projects. Developments relevant for ForestPaths are shared in particular with HoliSoils (101000289), Forwards (101084481) and Resonate (101000574), while a large part of the data collection underlying the parameterization of processes was done in TreeMort (758873), all funded by the European Commission. In Table 2 we present the recent model developments and indicate how the projects contributed to these developments. Here we provide a short summary of the developments, while Table 2 gives further references to either external sources or appendices to this deliverable.

In the first year of the ForestPaths project, a manual was produced (Schelhaas et al., 2022). The manual documents the state of the model at the start of the project, serves as a guide for developers and users of the model, and provides a thorough evaluation of the model. The manual was an important element based on which EFISCEN-Space was granted the WENR quality A status in October 2024 (Figure 1). This status is assigned after an internal independent audit, where the model has to fulfil minimum requirements concerning documentation, version control, protocols for coding and testing, and further quality assurance and quality control (QA/QC) measures.

Figure 1. EFISCEN-Space quality A status label

During the course of ForestPaths, we renewed the national forest inventory (NFI) data contracts with the countries, for some countries we received a more recent inventory cycle, and we managed to get data for some new countries. We improved the processing pipeline of these data,

using standardised scripts for harmonisation of species names, quality checks of the data and extraction of abiotic variables at the plot locations. We initialised all countries again with the improved procedures and checked the results against alternative data sources like State of Europe's Forests (Forest Europe, 2020) and country NFI reports. Initialisation for Romania was done by University of Brasov, who also performed a model uncertainty analysis (Appendix E). We developed a synthetic data approach for the countries where no NFI data are available, using a combination of remote-sensing based maps and NFI plots from neighbouring regions. However, this approach proved to be not feasible in practice due to a lack of base maps of sufficient quality.

Important improvements in the representation of model processes are the development of a dynamic ingrowth module, a dynamic mortality module and the development of a rule-based harvesting module. The new rule-based harvesting module was parameterised using the insights and results from WP1 (Feliciano et al. in prep.). We made a 100-year baseline projection for the same subset of countries as in LPJ-GUESS, using the rule-based harvesting system and the new dynamic ingrowth and mortality modules. Results were evaluated in both qualitative and quantitative terms. Next, this baseline will also be constructed for the remaining countries where we have initialisation data. The results will be shared with the country correspondents for feedback and these baselines will form the basis for the exploratory scenarios and cases in WP5.

We evaluated the dynamic ingrowth model (König et al., 2023) for a single country by monitoring the development of the stem number over time, as well as the distribution of trees over diameter classes. Without ingrowth, the stem number decreased continuously over time because trees are lost to mortality and harvesting (Figure 2a). Also, there was a generic "aging" of the tree population, visible as a shift of stem numbers to higher diameter classes as trees grow and no small trees are added to the simulation (Figure 2b). These problems are solved when introducing the dynamic ingrowth module. The tree number is more stable over time and new trees show up in the smaller diameter classes.

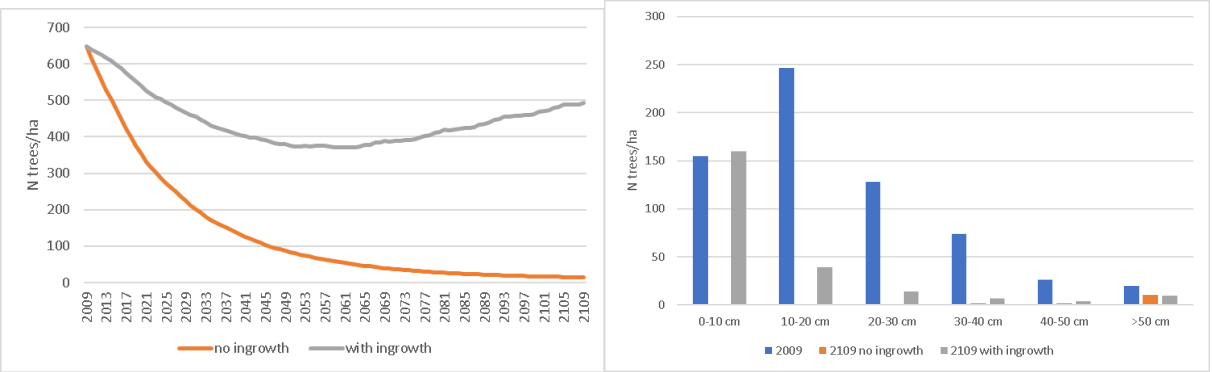

Figure 2. Development over time of average tree number per ha (a) and diameter class distribution (b) for Belgium-Flanders, using the static harvest and mortality module and without and with the new dynamic ingrowth module.

Also in the baseline applications, we found a relatively stable number of trees over the projection period for most countries, indicating that the trees that get harvested or die are replaced by new trees (Figure 3). However, Norway and Denmark show an initial fast increase in tree number. For Denmark this may be related to the fact that there are many recently afforested plots, in Norway there is no apparent reason. We also found that the distribution of ingrowth species resembles

the current patterns and species' ranges well, indicating the capability of the ingrowth model to produce realistic ingrowth of species. However, we found no regeneration of Sitka spruce at all, caused by a generic lack of observed ingrown trees of Sitka in our dataset. We have secured additional data from Norway, Denmark, Ireland and France and will refit the ingrowth parameters on this expanded dataset. We expect this will solve both the problem with number of ingrowth trees as well as the absence of Sitka spruce.

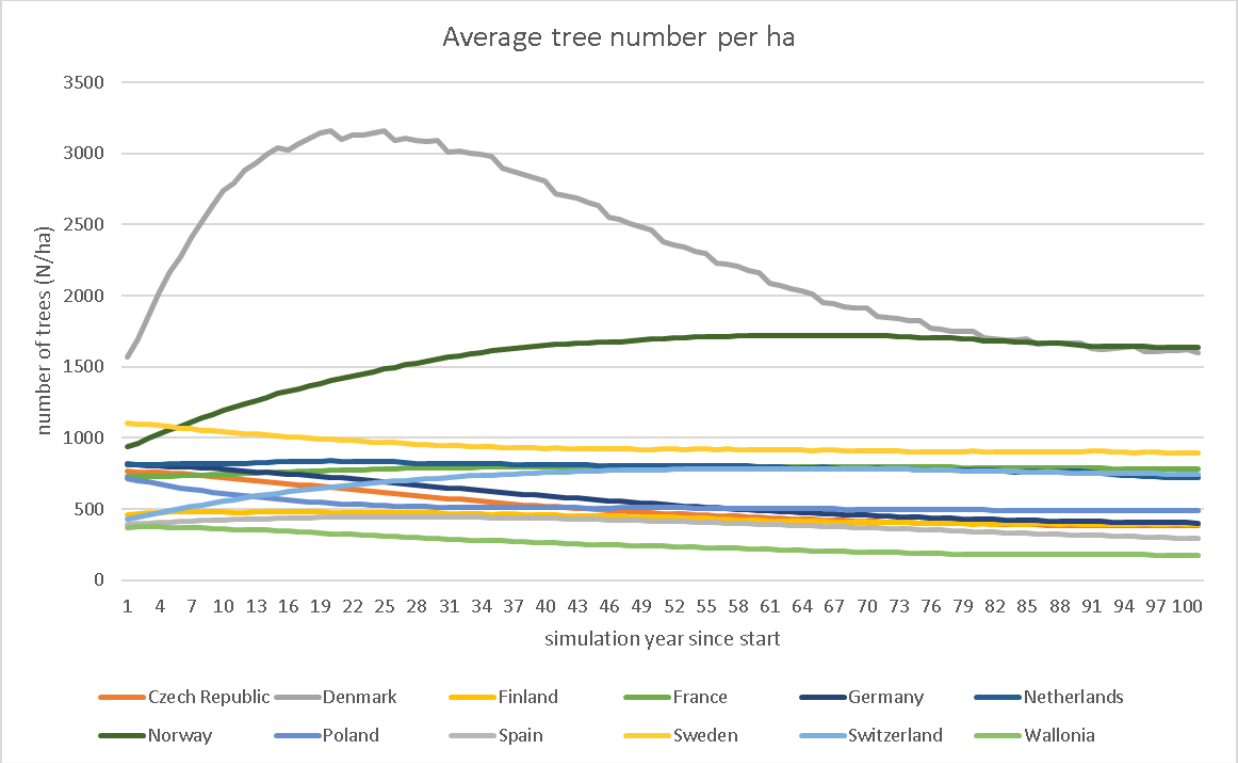

Figure 3. Development of stem number over time for the countries, using the static (i.e. pattern-based) harvest and mortality, with the new dynamic ingrowth module.

In the baselines, the simulated mortality rates using the dynamic mortality module (Appendix D) were close to observed values as reported by (Avitabile et al., 2024) (Figure D1). We then applied the dynamic mortality module to the test countries under unmanaged conditions. Under these conditions, EFISCEN-Space produced unrealistically high values of basal area (over 250 m^2 ha^{-1}) and volume (over 3000 m^3 ha^{-1}) for all countries (average at country level). Increment decreased only gradually and mortality increased more or less linearly with the increase in growing stock. We therefore concluded that the dynamic mortality module (but also the increment module) mostly represents the self-thinning process as observed under low to moderate stand densities. The vast majority of the European forests, and thus the NFI data used to feed the model calibration process, are currently in this stage. A lack of observations in very dense forests in various diameter ranges and a lack of observations in trees with very high diameters prevents the development of empirical models for such conditions, similar to the conclusions by Thrippleton et al. (2021). To prevent EFISCEN-Space to simulate unrealistically high values, we introduced a maximum basal area beyond which the trees will simply stop growing. We used the 99% percentile observed in our calibration dataset as maximum (Table D2), which gave reasonable results. However, we clearly lack understanding and empirical data how trees grow and die at

really high densities and at large dimensions, and the model should not be applied to such conditions. We estimate that the model can simulate 30-40 years of no management starting from managed conditions.

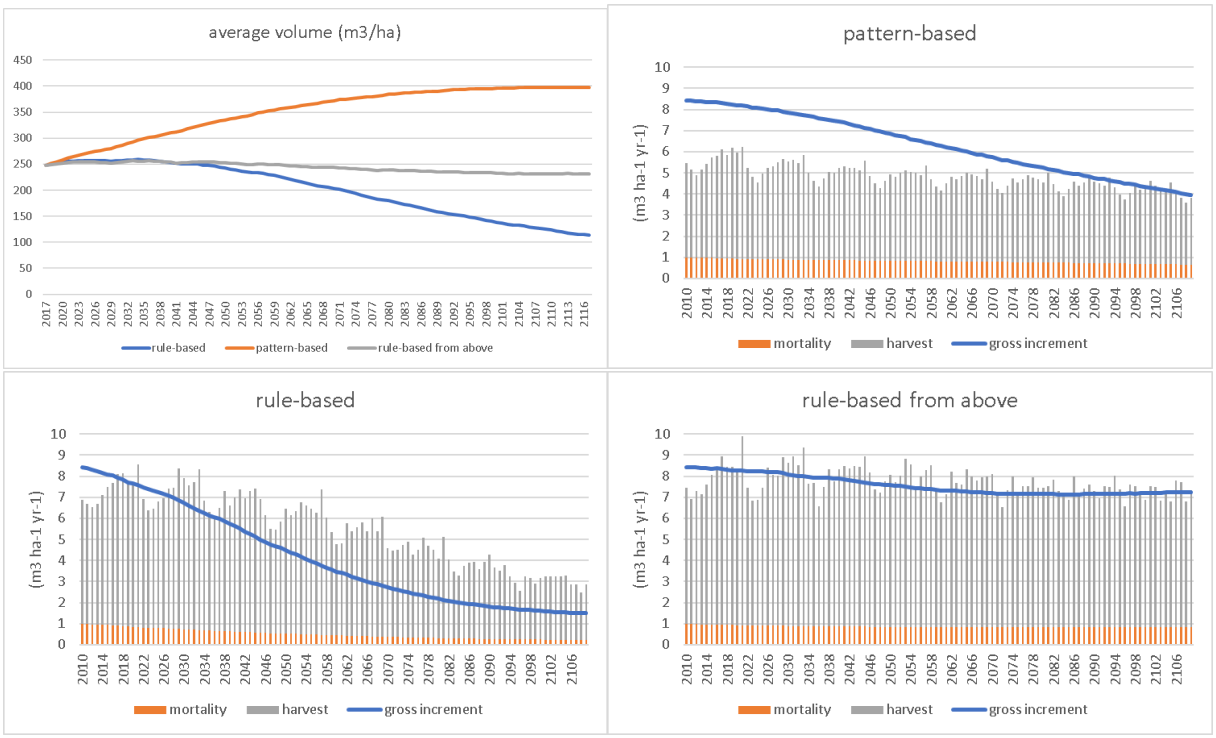

Figure 4. Development of growing stock and harvest/increment balance for Belgium-Flanders using three different harvest scenarios. The pattern-based scenario uses the old approach, where harvest probabilities are derived by species and diameter class from repeated NFI data (Schelhaas et al. 2018). The rule-based scenario uses the new approach, where harvesting rules are derived from the same data. The rule-based scenario with thinning from above has the same rules, but the shape parameter was changed such that the thinnings were targeting the larger trees rather than the smaller trees.

The rule-based harvesting module introduced more options and better precision in the simulation of harvesting activities, and greatly facilitates the implementation of the exploratory cases in WP5. After country-specific parameterisation and application in EFISCEN-Space we found that the simulated harvest level was generally close to the level as simulated with the previous pattern-based system, and also close to reported values (see Chapter 4). However, the model proved to be very sensitive to both the way harvest was implemented (rule-based or pattern-based) as well as to the parameters of the rule-based system. The pattern-based system is sensitive to missing observations, usually happening when the forest in a country is relatively young, and no large trees are present. During the simulation, trees will grow to larger diameter classes where no harvest was observed, and consequently these trees “escape” from harvesting. This effect became visible after 10-20 years and could make the difference between a long-term increase or decline in growing stock (Figure 4). Especially when the smaller, well-growing trees are targeted in harvest operations and only large slow-growing trees are left, the increment starts to decrease (rule-based scenario in Figure 2). At some point the harvest/increment ratio will surpass 100% and the growing stock starts to decline. However, this did not happen in all countries, which shows

there is a delicate balance between several processes in the model, in interaction with the current state of the forest.

Furthermore, EFISCEN-Space was expanded by two modules, representing disturbances by wind and fire. Bark beetles are not included due to a generic lack of data for empirical modelling and a lack of process understanding (Deliverable 2.3), resulting in a lack of suitable model approaches for inclusion in EFISCEN-Space. For both wind and fire, we apply an external scenario, indicating which plots will be affected by what disturbance in what year. These scenarios can be derived from those as developed in WP2 in the ForestPaths project, or WP4 from the RESONATE project. For the impact of wind on the forest stand we coupled the mechanistic model ForestGALES (Gardiner et al., 2008; Hale et al., 2015). For the impact of fire on the forest stand we calculate fire severity based on the fuel load by the available litter, calculated a tree susceptibility to fire based on tree size and the annual Canadian Fire Weather Index of the European fire season (JJA), and apply a mortality factor based on tree's susceptibility and species specific bark thickness (Schumacher and Bugmann, 2006; Seidl et al., 2014). Both disturbance modules are currently being tested.

Table 2. Summary of EFISCEN-Space improvements and evaluation during the ForestPaths project and contribution from other projects

Aspect	Model feature	ForestPaths WP/Contributing projects	Reference
Initialisation	Renewed NFI-based initialisation	All projects	HoliSoils deliverable D6.2 (Flores et al. 2024)
Disturbance	Burned area scenario (fire)	WP2, Resonate	Appendix C
Disturbance	Fire disturbances (impact)	Resonate, Forwards	Appendix C
Disturbance	Wind disturbances scenario (disturbed area)	WP2, Resonate	Appendix C
Disturbance	Wind disturbances (impact)	Resonate, Forwards	Appendix C
Rule-based management	Rule-based management (concept and implementation)	HoliSoils	HoliSoils deliverable D6.1 (Luyssaert et al. 2022)
Rule-based management	Rule-based management (parameterisation)	WP1	ForestPaths deliverable D1.3 (Feliciano et al. In prep)
Processes	Dynamic ingrowth module	TreeMort, WUR PhD project PE&RC	König et al. (in prep)
Processes	Dynamic mortality module	TreeMort	Appendix D
Evaluation	Initial model evaluation	All projects	Schelhaas et al. (2022) Chapter 4
Evaluation	Quality status A	All projects	Figure 1
Evaluation	Uncertainty analysis		Appendix E
Evaluation	Additional model evaluation		This deliverable Chapter 4

4 Joint evaluation

Whilst each of LPJ-GUESS and EFISCEN-Space have their own, model-specific, evaluation processes, as described in the previous sections and the associated appendices, we also carried out a joint evaluation against country-level statistics to provide a summary of model performance. The evaluation was carried out using the TellMe Europe tool, described in Appendix A. We made comparisons against observations for the period 2013-2017 for net annual increment (NAI) and harvest (Forest Europe, 2020). LPJ-GUESS simulations were set up to represent the observational period as closely as possible (Appendix A, §3) and modelled results were compared for the corresponding years. EFISCEN-Space simulations were based on a 100-year business-as-usual projection, with means over the first five simulation years being compared. The projection started from the state of the forest in the most recently available NFI census (generally dated in the period 2005-2015) and continued under repeated present-day climate, being the average of the period 2000-2015. LPJ-GUESS simulations were made at 0.5° x 0.5° resolution and plots simulated by EFISCEN-Space were aggregated up to the same resolution. Country totals for forest area for both models were then obtained by multiplying the forest values for each grid cell by the forested area based on Fuchs et al. (2015).

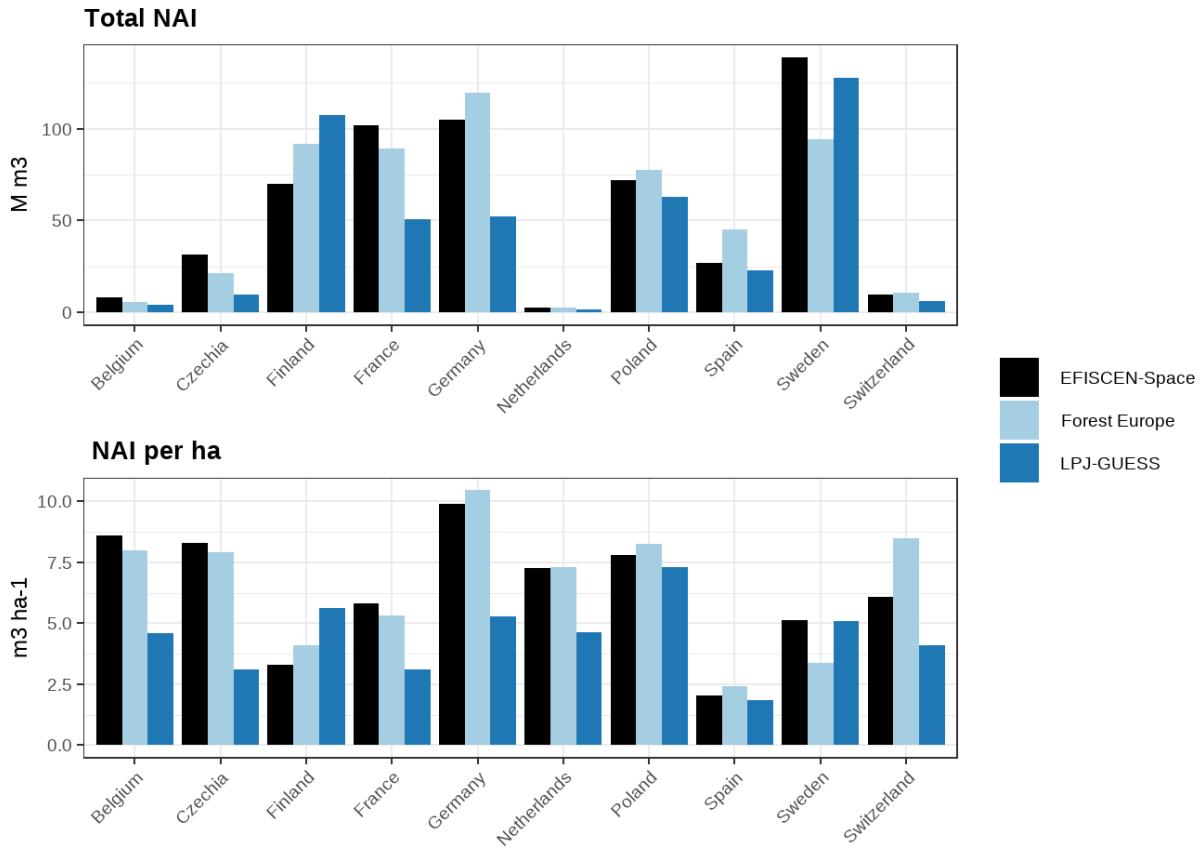

Figure 5. Evaluation of net annual increment (NAI) for country totals (top) and per unit area (bottom). The comparison is made for all forested land in each country.

Both models displayed good overall performance in simulating NAI (Figure 5). Uncertainties are not available for the Forest Europe statistics nor the model simulations, much can still be inferred from the results however. LPJ-GUESS showed very close correspondence with Forest Europe in

NAI per hectare for Spain and Poland, along with moderate overestimations for Sweden and Finland. These estimations result from overly high simulated productivity in the north of the Nordic countries. In contrast, productivity, and thus NAI, is underestimated in Czechia, Belgium, France, Germany and Switzerland. Productivity in the intermediate zone in southern Sweden and northern Germany was well represented (Appendix A, Figure 6). These biases were somewhat moderated by the parameter update and calibration process described in Appendix A (Section 4.7) but remained persistent in the final version. The reasons for this are still under investigation but are believed to be at least partially linked to the use of a single parameter set for species that have broad climatic ranges. For instance, Scots Pine and Norway Spruce are two of the most dominant tree species in Europe, with ranges that run from central Europe to the Arctic circle. It appears that the existing variation in productivity resulting from climate operating on the photosynthesis, respiration and nitrogen cycling in LPJ-GUESS is insufficient on its own to capture the observed productivity gradient in these species. Intraspecific variation in traits as a function of climate across the species ranges is being investigated as a possible solution for this in the medium-term.

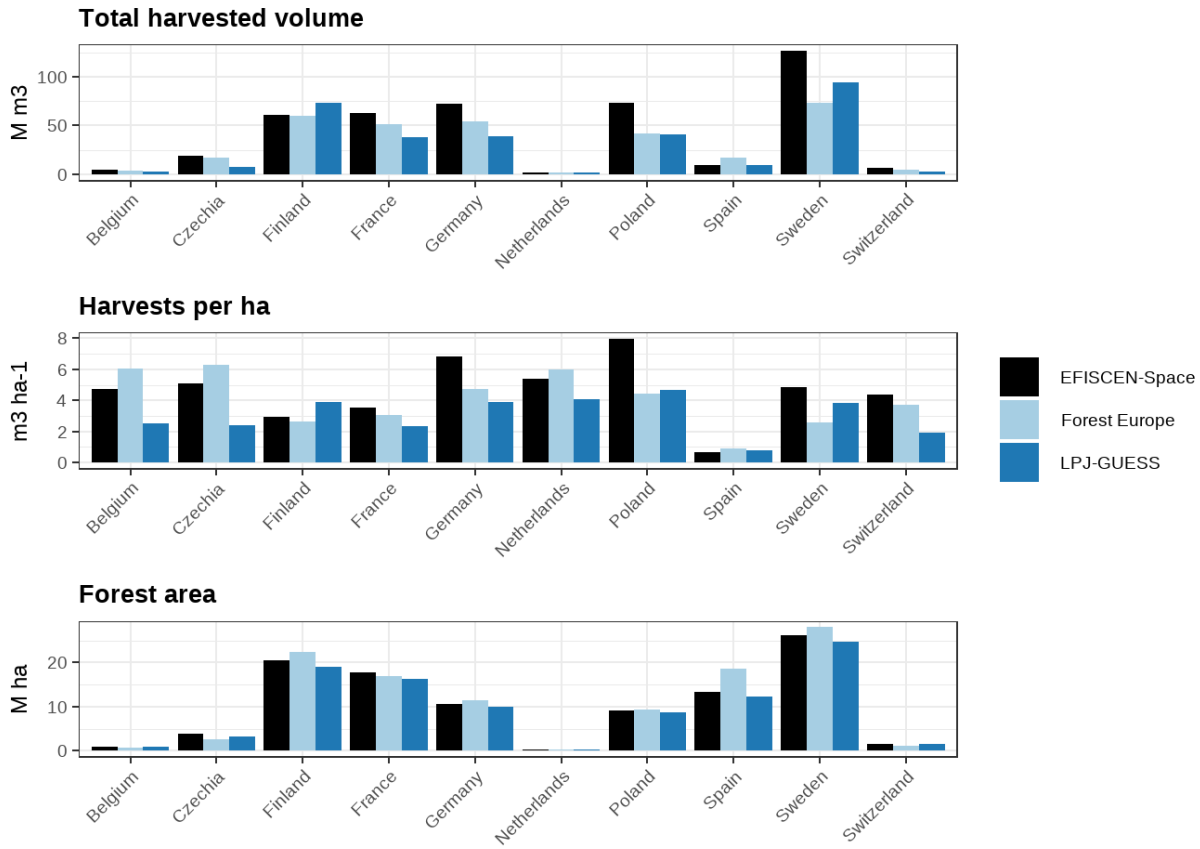

Figure 6. Total harvested volume (top), harvest per unit area (middle) and forest area (bottom) as compared to Forest Europe for the period 2013-2017). Forest area is not simulated by the models, but it is included to illustrate the extent to which different assumptions regarding forest area affect the comparisons.

EFISCEN-Space tended to simulate NAI quite well for most countries. The underestimation in Switzerland may be caused by the resolution of the underlying map, not delineating the country

borders very well. The simulated NAI using the model output directly was 9.3 m^3 ha^{-1} yr^{-1}, close to the reported value. The overestimation in Sweden is partly related to the definition of the area. The NFI data received relate to productive forest only, while the reported values likely include additional (unproductive) forest, causing the average productivity to be lower. Furthermore, Forest Europe uses a diameter threshold of 10 cm in their definition of volume, while EFISCEN-Space includes all above a 5 cm threshold. Despite these definition-related differences, EFISCEN-Space still overestimates the increment. Sweden reports a decline in increment since 2013, probably related to more adverse weather conditions (Roberge et al., 2024). The increment and mortality modules of EFISCEN-Space are fitted with data mostly prior 2013, and the projections assume constant weather conditions. The simulated gross annual increment of 126 million m^3 yr^{-1} is similar to the value reported for 2013. EFISCEN-Space thus seems not to capture the recent decline in increment in Sweden. This may partly be due to the assumption of constant climate in the projections and partly a lack of empirical observations. A similar trend of declining increment is reported in other European countries (Korosuo et al., 2023), which may not be captured fully in the EFISCEN-Space model.

Harvested wood volume based on the new harvest schemes developed in ForestPaths is a key variable for future simulations, in which representation of the current forest management intensity is important to provide a realistic counterfactual for different management interventions, as well as to link smoothly with the CRAFTY land-use modelling. LPJ-GUESS harvest per hectare agreed closely with Forest Europe statistics for France, Germany, Poland, Spain and only deviated substantially for Switzerland, Belgium and Czechia (Figure 6). These deviations are almost entirely a function of differences between the modelled forest structure and the actual structure. Tests applying the probabilistic forest harvest module directly on NFI data produced a very close representation of observed harvest (Suvanto et al., in prep, not shown). We expect that the simulated harvest rates will converge with the observations as we increasingly apply forest state initialisation based on tree-by-tree data instead of stand age (Appendix A, Section 4.6). However, we note that in order to maintain consistency between the simulated biomass and the dynamics, tree-by-tree initialisation should only be applied in regions where growth rate biases have been minimised, otherwise relative change projections and particularly net ecosystem carbon balances will be biased.

Generally, the comparison of models and observations at the country level reflects the NAI per hectare results. Where deviations occur, these can be attributed to differences between the forest area mask used in Forest Europe and the one applied to scale the models here (Figure 6 bottom). This is particularly notable at the edges of forest distribution, notably for Spain and Sweden and emphasises the importance of agreeing on appropriate and unified datasets for forest area. The harvest comparisons also show reasonably good comparisons, but more work is needed for a few countries where results deviate.

5 Conclusions

The developments presented herein have provided substantial improvements to the capabilities of the EFISCEN-Space and LPJ-GUESS models to simulate the dynamics of European forests. These are consistent with the intentions expressed in the grant agreement. The only notable deviation from the grant agreement stems from the finding in WP2 that bark beetles could not be separated from storm disturbances in the remote sensing datasets. We have dealt with this by developing a spruce bark beetle module using an alternative approach within the LPJ-GUESS model, creating the capability to explore the impact of this important disturbance agent within WP5 of ForestPaths. These methods are demonstrated for a selection of countries. At this moment in time, EFISCEN-Space is prepared to make simulations for all countries for which tree-by-tree NFI data is available (18 countries). The stand-age initialisation in LPJ-GUESS is also able simulate the remaining countries in the EU27+3. ForestPaths is therefore well prepared to simulate forests across the whole EU27+3, with the approach used following data availability.

Naturally, the updated models are not perfect representations of reality and do diverge in some respects from the evaluation data. In addition to the described improvements, the work carried out in WP3 of ForestPaths has allowed us to clearly identify remaining biases and develop plans for addressing them. This work will continue beyond the timespan of this deliverable and it is anticipated that further updates may be available for application later in ForestPaths. Nonetheless, even in regions where biases in variables such as growth rate do exist, with appropriate simulation setup choices the models remain self-consistent worlds in which impacts of forest management actions and disturbances on forest structure and function can be explored in the context of the exploratory scenarios and policy pathways planned in ForestPaths.

A key theme throughout the work covered here has been cooperation across multiple projects to synergise and leverage developments for both EFISCEN-Space and LPJ-GUESS between them. This has allowed to create forest ecosystem models that are more capable and flexible than anticipated in any of those projects alone. We expect that the simulation work in WP5 of ForestPaths will continue to benefit from ongoing developments in other projects throughout the project duration.

6 References

Avitabile, V., Pilli, R., Migliavacca, M., Duveiller, G., Camia, A., Blujdea, V., Adolt, R., Alberdi, I., Barreiro, S., Bender, S., Borota, D., Bosela, M., Bouriaud, O., Breidenbach, J., Cañellas, I., Čavlović, J., Colin, A., Di Cosmo, L., Donis, J., Fischer, C., Freudenschuss, A., Fridman, J., Gasparini, P., Gschwantner, T., Hernández, L., Korhonen, K., Kulbokas, G., Kvist, V., Latte, N., Lazdins, A., Lejeune, P., Makovskis, K., Marin, G., Maslo, J., Michorczyk, A., Mionskowski, M., Morneau, F., Myszkowski, M., Nagy, K., Nilsson, M., Nord-Larsen, T., Pantic, D., Perin, J., Redmond, J., Rizzo, M., Šebeň, V., Skudnik, M., Snorrason, A., Sroga, R., Stoyanov, T., Svensson, A., Talarczyk, A., Teeuwen, S., Thürig, E., Uva, J., and Mubareka, S.: Harmonised statistics and maps of forest biomass and increment in Europe, Sci Data, 11, 274, https://doi.org/10.1038/s41597-023-02868-8, 2024.

CHELSA climate input data for LPJ-GUESS:

Forest Europe: State of Europe's Forests 2020, Ministerial Conference on the Protection of Forests in Europe, Bratislava, 394 pp., 2020.

Fuchs, R., Herold, M., Verburg, P. H., Clevers, J. G. P. W., and Eberle, J.: Gross changes in reconstructions of historic land cover/use for Europe between 1900 and 2010, Glob Chang Biol, 21, 299–313, https://doi.org/10.1111/gcb.12714, 2015.

Gardiner, B., Byrne, K., Hale, S., Kamimura, K., Mitchell, S. J., Peltola, H., and Ruel, J. C.: A review of mechanistic modelling of wind damage risk to forests, Forestry, 81, 447–463, https://doi.org/10.1093/forestry/cpn022, 2008.

Hale, S. E., Gardiner, B., Peace, A., Nicoll, B., Taylor, P., and Pizzirani, S.: Comparison and validation of three versions of a forest wind risk model, Environmental Modelling & Software, 68, 27–41, https://doi.org/10.1016/j.envsoft.2015.01.016, 2015.

CHELSA_ISIMIP3b_BA_1km:

König, L. A., Mohren, F., Schelhaas, M.-J., Astigarraga, J., Cienciala, E., Fridman, J., Govaere, L., Lehtonen, A., Esquivel-Muelbert, A., Pugh, T. A. M., Rohner, B., Ruiz-Benito, P., Suvanto, S., Talarczyk, A., Zavala, M. A., Medina Vega, J., Staritsky, I., Hengeveld, G., and Nabuurs, G.-J.: Combining national forest inventories reveals distinct role of climate on tree recruitment in European forests, submitted, 2023.

Korosuo, A., Pilli, R., Abad Viñas, R., Blujdea, V. N. B., Colditz, R. R., Fiorese, G., Rossi, S., Vizzarri, M., and Grassi, G.: The role of forests in the EU climate policy: are we on the right track?, Carbon Balance Manag, 18, 15, https://doi.org/10.1186/s13021-023-00234-0, 2023.

Roberge, C., Dahlgren, J., Nilsson, P., Wikberg, P.-E., and Fridman, J.: Forest Statistics 2024. Official statistics of Sweden, Umeå, 2024.

Schelhaas, M.-J., Hengeveld, G., Filipek, S., König, L., Lerink, B., Staritsky, I., de Jong, A., and Nabuurs, G.-J.: EFISCEN-Space 1.0 model documentation and manual, 2022.

Schumacher, S. and Bugmann, H.: The relative importance of climatic effects, wildfires and management for future forest landscape dynamics in the Swiss Alps, Glob Chang Biol, 12, 1435–1450, https://doi.org/10.1111/j.1365-2486.2006.01188.x, 2006.

Seidl, R., Rammer, W., and Spies, T. A.: Disturbance legacies increase the resilience of forest ecosystem structure, composition, and functioning, Ecological Applications, 24, 2063–2077, https://doi.org/10.1890/14-0255.1, 2014.

Thrippleton, T., Hülsmann, L., Cailleret, M., and Bugmann, H.: An evaluation of multi-species empirical tree mortality algorithms for dynamic vegetation modelling, Sci Rep, 11, 19845, https://doi.org/10.1038/s41598-021-98880-2, 2021.

Appendix A: Dynamic vegetation modelling for the past and future of Europe's forests

Dynamic vegetation modelling for the past and future of Europe's forests

Thomas A. M. Pugh[1,2,3], Almut Arneth[4], Annemarie H. Eckes-Shephard[1], Anna Maria Jönsson[1], Fredrik Lagergren[1], Mats Lindeskog[1], Paul A. Miller[1], Lars Nieradzik[1], Stefan Olin[1], Karl Piltz[1], Anja Rammig[5], Susanne Suvanto[6], Martin Wittenbrink[4], Haoming Zhong[1], Julen Astigarraga[7], Emil Cienciala[8,9], Adriane Esquivel-Muelbert[2,3], Jonas Fridman[10], Aleksi Lehtonen[5], Paloma Ruiz Benito[7], Mikko Peltoniemi[5], Mart-Jan Schelhaas[11], Cornelius Senf[4], Alba Viana-Soto[4], Golo Stadelmann[12], Torbern Tagesson[1], Andrzej Talarczyk[13,14], Miguel A. Zavala[7].

[1] Department of Physical Geography and Ecosystem Science, Lund University, Lund, Sweden.
[2] School of Geography, Earth and Environmental Sciences, University of Birmingham, Birmingham, UK.
[3] Birmingham Institute of Forest Research, University of Birmingham, Birmingham, UK.
[4] Karlsruhe Institute of Technology, IMK-IFU, Garmisch-Partenkirchen, Germany.
[5] Technical University of Munich, School of Life Sciences, Hans-Carl-von-Carlowitz-Platz 2, 85354 Freising, Germany
[6] Natural Resources Institute Finland (Luke), Latokartanonkaari 9, 00790 Helsinki, Finland
[7] Universidad de Alcalá, Forest Ecology & Restoration Group (FORECO), Departamento de Ciencias de la Vida, 28805 Alcalá de Henares, Madrid, Spain
[8] IFER - Institute of Forest Ecosystem Research, Cs. armady 655, 254 01 Jilove u Prahy, Czech Republic
[6] Global Change Research Institute CAS, Belidla 986/4a, 603 00 Brno, Czech Republic
[10] Department of Forest Resource Management, Swedish University of Agricultural Sciences, Umeå, Sweden
[11] Wageningen Environmental Research (WENR), Wageningen University and Research, Wageningen, The Netherlands
[12] Forest Resources and Management, Swiss Federal Institute for Forest, Snow and Landscape Research WSL, Switzerland
[13] Forest and Natural Resources Research Centre, ul. Płomyka 56A, 02-491 Warszawa, Poland
[14] Bureau for Forest Management and Geodesy, ul. Leśników 3, 05-090 Sękocin Stary, Poland

Abstract

In an age of high-resolution satellite observations and artificial intelligence, the capability of humanity to observe and analyse the world's forests has never been larger. Yet these technologies start to meet their limits where the question demands information on variables that cannot be observed by monitoring electromagnetic signals, when attributing observed changes to underlying causes, or where it starts to explore the future. Dynamic models have a crucial role to play, applying process knowledge to fill these gaps. Here, we present a new version of the dynamic global vegetation model LPJ-GUESS tailored to represent European forests, and especially disturbance dynamics, with unprecedented realism. This new version builds on previous work to represent individual tree species and forest management to offer a range of new capabilities to explore questions around the state, dynamics and future of forests across Europe. Novel capabilities equip it to draw on big data from satellites and forest inventories and combine these with new process representations. These include (a) direct initialisation of vegetation state from forest inventory observations, (b) forcing of historical natural and human disturbances by satellite observations, (c) prognostic storm, spruce bark beetle and fire disturbance models tailored to the European context, and (d) dynamic representation of forest harvest frequency and intensity based on empirical observations of harvest probabilities. We have further updated the functional trait parameters of the 20 major species represented based on a synthesis of observations and carried out a calibration process to constrain woody growth rates. Taken together, this unique set of developments mean that european-wide simulations are now constrained to match actual forest structure,
can directly leverage large-scale observations to capture trends in forest dynamics over the last recent decades and directly propagate these into scenario simulations of future productivity, vulnerability and carbon cycling. The model is evaluated against a series of benchmarks of state, dynamics and fluxes within a coherent benchmarking framework. These new capabilities offer powerful possibilities to apply LPJ-GUESS to important policy-relevant questions such as the permanence of forest-based carbon mitigation efforts, as well as to add value to forest monitoring observations by calculating well-constrained and spatially-consistent fields of quantities unobserved at large scale such as carbon cycling.

1. Introduction

Europe's forests are complex socio-ecological systems, their current state strongly affected by legacies of past management decisions and their future increasingly influenced by climate change and demand for a broad range of services. Forests are expected to provide wood products to feed a large forest-based sector (Mishra et al., 2022; Talvitie et al., 2023), as well as to provide major carbon sinks (Daigneault et al., 2022), reservoirs of biodiversity (Ulyshen et al., 2023) and various cultural ecosystem services (Winkel et al., 2022). Trying to fulfil these, often competing, objectives to the best extent possible is generating increasing demand to understand European forests, both in terms of monitoring ongoing changes (European Commission, 2023) and projecting the impacts of different policies. Facilitating joined-up policy making at the continental level requires methodologies to make consistent assessments at this scale.

Forests within Europe have been the focus of extensive monitoring efforts going back as much as a hundred years or more (Breidenbach et al., 2020). Almost all countries have national forest inventories (NFI) making systematic samples of biomass stocks, growth, losses and other variables, typically at five or ten year intervals (Tomppo et al., 2010). These observations are increasingly being supplemented by remote-sensing based approaches, which can give wall-to-wall and more frequently updated estimates of quantities directly observable with electromagnetic sensors or quantities directly derivable from these, such as forest disturbances (Hansen et al., 2013; Senf and Seidl, 2021), forest biomass (Santoro et al., 2021) and vegetation condition (Buras et al., 2021) Yet whilst both NFI and remote sensing are incredibly powerful tools, they each have their own limitations; NFI is infrequent and discrete in time and space and remote sensing only observes a portion of the dynamics of interest. Furthermore, because they observe the forests in different ways, with different definitions, using different metrics, they can also be difficult to compare consistently (Palahí et al., 2021; International Tree Mortality Network et al., under review). Methodologies linking together and extending the monitoring operations are needed as a complement to provide holistic assessments of forest changes over recent decades.

To explore future forest development, empirical forest simulators are widely used at national (Lämås et al., 2023), and increasingly continental (Kurz et al., 2009; Schelhaas et al., 2022), extents. Typically based directly on empirical observations of forest growth and initialised directly from observations of forest state, these simulators are powerful for historical and relatively short-term projections, corresponding very closely to observations. However, they are limited in their ability to explore novel systems under changing environmental or management conditions that are not well represented in the training data. Process-based modelling approaches, which aim to represent forest dynamics from fundamental biological and physical principles, have long been regularly applied at large-scales, for instance as part of the annual Global Carbon Budget assessments (Friedlingstein et al., 2023). However, the more detailed process representations often result in relatively large biases in individual models (Seiler et al., 2022), especially with respect to disturbances and wider tree mortality (Pugh et al., 2020). Furthermore, realistic representations of present-day forest state have been strongly reliant on historical reconstructions of land-use change and forest management (e.g. Hurtt et al., 2020), which are highly uncertain and often result in large biases in present-day model state at the regional level (e.g. Yu et al., 2022). Neither empirical nor process-

based models have generally included realistic representations of disturbance and harvest processes that are suitable to be applied at continental scales.

There is thus a need for continental-scale process-based forest simulators that can draw on the range of ground-based and remote-sensing observations to generate accurate representations of the actual state and dynamics of Europe's forests. Explicit representations of forest demography and different agents of demographic change (e.g. harvest, disturbances by wind, fire or insects) can allow for consistent comparisons between different measurement types, for instance converting satellite-observed canopy losses to stem mortality rates that can be compared with NFIs (Scheel et al., 2022). It is also crucial to be able to make smooth past-to-future simulations that faithfully represent the state of the real forest and which draw on mechanistic links between forest state, environmental state and change, and disturbance vulnerability. A new class of models is starting to emerge that can satisfy all or part of these needs at the continental scale, originating from either global-scale or landscape-scale modelling backgrounds (Lasch-Born et al., 2020; Naudts et al., 2016; Rammer and Seidl, 2019).

The LPJ-GUESS dynamic vegetation model has been widely used to study land ecosystems, and especially forests, globally (Smith et al., 2014). For instance, LPJ-GUESS has been a contributor to the annual Global Carbon Project assessments since they started in 2013 (Le Quéré et al., 2013). In recent years, efforts have been made to utilise inventory and satellite observations to increase accuracy of these global simulations (Pugh et al., 2019a, b), to represent detailed forest management processes (Lindeskog et al., 2021), as well as to develop new fire modelling capabilities (Rabin et al., 2022). Previous efforts have also been directed to develop a version of the model specially adapted for European studies, with Hickler et al. (2012) creating the capability to represent Europe's forest with explicit simulation of 16 major tree species. At the national scale, process-based wind and spruce bark beetle disturbance models have previously been developed within LPJ-GUESS for Sweden (Jönsson et al., 2012; Lagergren et al., 2012). These capabilities provide a strong base on which to develop high-quality continental-scale modelling of Europe's forests.

In this paper, we describe a suite of updates that make use of large-scale datasets and new process-modelling developments to provide a new version of LPJ-GUESS tailored for Europe. These updates include:

- A new scheme to force disturbance and clearcut harvest rates directly from remote sensing observations.
- Updates to the wind and fire disturbance mechanisms that enable European-scale applications.
- A new capability to initialise forest structure and composition directly from forest inventory observations.
- Update of key functional parameters for a set of European tree species, including a recalibration of poorly constrained parameters linked to woody growth.

Additionally, we provide short overviews of new schemes presented elsewhere which are core to the capabilities of the updated model:

- A harvest scheme based directly on empirical probabilities of tree removal.
- A scheme for simulating spruce bark beetle outbreaks and their impact on the forest.

We also present a new benchmarking scheme tailored towards assessing forest dynamics with independent data and make some demonstrations of the capabilities of the new model

version. We begin with a short general description of LPJ-GUESS (§2), then describe the simulation setup used for evaluation and demonstration (§3), followed by a description of the new updates (§4), a presentation of the evaluation framework and results of the evaluation (§5), demonstration applications for a selection of the components (§6) and finally an outlook and conclusions section (§7).

2. General description of LPJ-GUESS

LPJ-GUESS is a dynamic global vegetation model which has been widely applied over the last 25 years for studies of the terrestrial biosphere and carbon cycling (Smith et al., 2001, 2014). The model includes detailed representations of forest, grassland, croplands, pasture, peatlands and arctic vegetation, as well as the land-use changes between them (Bayer et al., 2017; Rabin et al., 2020). In this description we focus on those components of the model most relevant to the simulation of European forests.

LPJ-GUESS simulates vegetation and soils as a series of pools of carbon and nitrogen, whose sizes are governed by the fluxes between them and between the pools and the atmosphere. The processes of photosynthesis and respiration, along with updates of hydrology, are carried out on a daily timestep, whilst vegetation growth and mortality are assessed annually. The basic processes of photosynthesis, respiration, carbon allocation and vegetation dynamics are described in Smith et al. (2014). These processes are forced by externally-provided boundary conditions of climate, atmospheric CO_2 mixing ratio, nitrogen deposition and soil type. This information is provided in grid cells, whose size is primarily determined by the spatial scale of the boundary conditions provided. Whilst global simulations are typically run at 0.5° x 0.5°, higher resolution simulations can also be run regionally (e.g. 3km, Lagergren et al., 2024), or even at the local catchment scale (e.g. 50m, Gustafson et al., 2021).

Within a grid cell, the basic unit of an LPJ-GUESS simulation is the 0.1 ha patch. Within patches, age cohorts of different plant functional types (PFTs) compete for light, water and nitrogen. In the European version of LPJ-GUESS, vegetation is represented by 24 plant functional types, 20 of which are directly parameterised based on major tree species (Hickler et al., 2012; Lindeskog et al., 2021). Vegetation structure is vertically resolved, such that taller vegetation shades the vegetation underneath. Because the processes of vegetation establishment and mortality have a strong stochastic component, multiple replicate patches are typically simulated to provide a realistic representation of the range of trajectories that patches might take. Replicate patches are forced by the same external boundary conditions of climate, soil type, atmospheric CO_2 mixing ratio and nitrogen deposition. Patches themselves are contained within “stands”, with the group of patches forming a representative sample of the vegetation within the stand. Stands loosely conform to an area of trees established at the same time, similar to the terminology in forestry. However, in LPJ-GUESS, all vegetation areas of the same type and management rules, established at the same time, are spatially aggregated within a grid cell and are contained within the same stand. Whilst patch size is fixed (as patches are samples, analogous to forest inventory plots), stands are initiated covering a fraction of a grid cell, which can be reduced over time as a result of land-use change or management interventions. The established stands are defined by a “stand type” which determines the type of PFTs that can grow there and the “management type” that is applied there. Management types are a similar concept that define sets of management rules. A wide range of management interventions are possible including thinning, clearcuts

and planting according to user-specified rules. The combination of stand types and management types is very flexible, such that a stand type can have different management types active at different points in time. Finally, stands are grouped within a “land-cover type”, which describes the major groups of vegetation representations contained within LPJ-GUESS. Land-cover types include “Managed Forest”, “Natural” (which represents natural forest and grassland vegetation without management interventions), “cropland”, “pasture” and “peatland”. A diagrammatic overview of the patch to stand to land-cover to grid-cell structure of LPJ-GUESS is shown in Figure 1. A more complete description of this structure and the existing forest management capabilities is provided in Lindeskog et al. (2021).

Land-use history can be a powerful driver of vegetation dynamics and carbon cycling (Krause et al., 2020) and LPJ-GUESS explicitly represents this by transferring grid cell area between land-cover types and stands on an annual basis, according to supplied input datasets. Transfers can either be specified at the land-cover level, with internal rules used to decide which stand types and thus stands to convert, or at the stand type level with an additional stand-type input file. A new stand is then created with the new land-cover type and/or stand type. On initiation of the new stand, the previous vegetation is usually killed, but the soil and litter carbon and nitrogen pools are transferred from the parent stand, thus allowing land-use history to influence the subsequent vegetation growth and carbon cycling, while ensuring that nitrogen, carbon and water are conserved. A full description of the land-use change functionality is given by Bayer et al. (2017), Lindeskog et al. (2013), Olin et al. (2015).

In principle, detailed historical land-use and management information should be enough to simulate a present-day forest that well represents the age structure and species composition found in the real world. In reality, however, such accurate and detailed information is only available for a limited part of the world and for a relatively short time period compared to the century or longer timescales over which past events can influence forest structure and composition. With LPJ-GUESS we have previously developed a process to use observations of forest stand age for a recent base year to initialise forest structure in LPJ-GUESS (Lindeskog et al., 2021; Pugh et al., 2019b). Treating stand age as the time since last stand-replacing disturbance we spin-up an LPJ-GUESS simulation with a natural vegetation stand type and gradually convert this into the appropriate managed forest stand type at the appropriate year of the simulation according to the stand age observations. For instance, assuming that the stand age dataset is representative of the year 2010, a 40-year-old stand would be created by converting from the natural vegetation stand type in the year 1971 and initialising a new managed forest stand in that year. Where land-use history information also exists, a stand type corresponding to a different initial land cover than natural vegetation can be used (e.g. cropland).

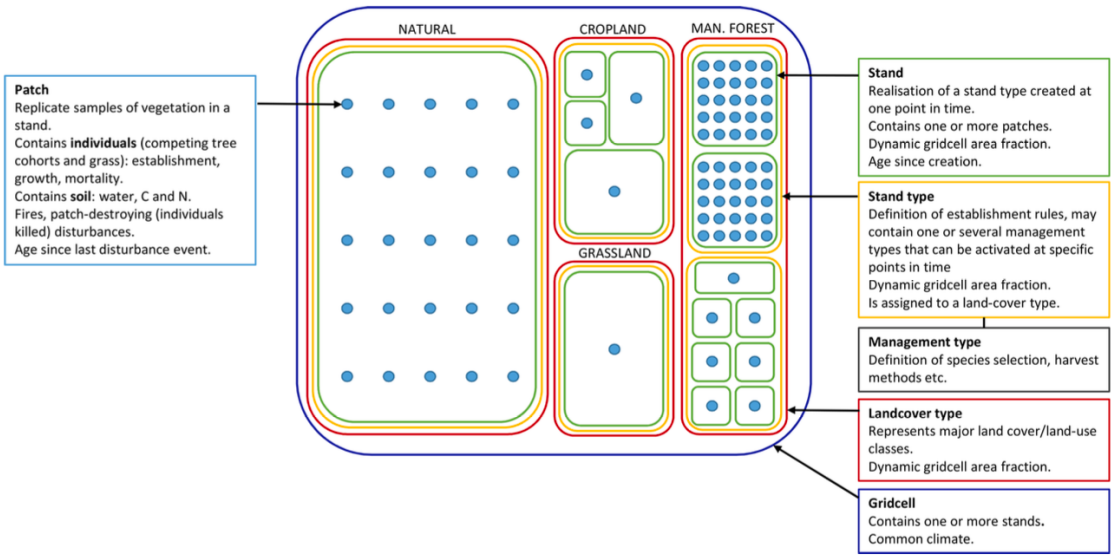

Figure 1. Data structures in LPJ-GUESS relevant for this study reproduced from Lindeskog et al. (2021). During land-cover change events, stands belonging to forest stand types can only be reduced in size. Expansion of such stand types results in new stands.

3. General simulation setup

Unless otherwise indicated, we apply a general simulation setup to benchmark and demonstrate the LPJ-GUESS developments described in this paper. We run the model at 0.5° x 0.5° resolution for the countries of Spain, France, Switzerland, Belgium, Netherlands, Germany, Czech Republic, Poland, Sweden and Finland. Only forest was simulated with the forest area per grid cell set according to the HILDA v2.0 dataset (Fuchs et al., 2015). Simulations began with a 500-year spin-up phase starting in the year 1401 and using repeated climate and atmospheric forcing (see below) starting from bare ground to provide a first initialisation of vegetation and soil pools. Following the spin-up, a simulation phase following transient climate was initiated from the year 1901. Stand age was initialised based on the European forest age 1870-2010 dataset of Pucher et al. (2022). The age dataset was aggregated to 0.5° resolution and then converted into a timeseries of land-cover and stand type input files which allowed to reconstruct the stand age distribution observed in circa 2010 using the same functionality used to represent land-use change (§2). This timeseries began in the year 1801. From 1801-1870 an area equivalent to the 1870 forest area was gradually converted from the potential natural vegetation land cover to managed forest land cover to allow a representation of forests older than 140 years in 2010. Clearcut harvest and disturbances prior to 2010 are accounted for based on this stand-age initialisation process, therefore as soon as a forest stand was established following the age distribution input, further clearcutting or stand-replacing disturbance before 2010 was disallowed. Non-stand-replacing harvests were specified following a probabilistic empirically-based harvest scheme (described in Section 4.5 and in Suvanto et al., in prep.).

Forest species composition was initialised based on observations from the NFI in each grid cell. 27 stand types were specified including both monospecific and mixed species stands, to represent the variety of tree species combinations found in the simulation domain. The stand type definitions used the European PFTs corresponding to the observations when possible.

Species observed in the data but not included in the European PFTs were categorised based on the species type (conifer/broadleaved) and shade tolerance (tolerant/intermediate/intolerant) and European PFTs with corresponding characteristics were used in the stand type definition. Full details of the process used to select the 27 stand types is given in Suvanto et al. (in prep.).

In calibration simulations (§4.7), we run LPJ-GUESS using monthly CRU-NCEP climate data (Wei et al., 2014) which covers the period 1901-2015 and is downscaled to daily values using a weather generator, atmospheric CO_2 mixing ratios (Le Quéré et al., 2018) and atmospheric nitrogen deposition (Lamarque et al., 2013). Prior to 1901, repeated 1901-1930 was used for climate and 1901 values were used for CO_2 mixing ratio and nitrogen deposition. We use output values from 2001-2010 in the calibration and benchmarking. In making demonstration simulations for the new model capabilities we use the same set-up as above, but extend the simulated period by using CRU-JRA v2.4 climate data which covers the period 1901-2022 at a daily resolution (Friedlingstein et al., 2022). After year 2015, the CO_2 value for that year was used and after 2009, the N deposition values for that year were used. We then apply the new capabilities (disturbance forcing, initialisation from forest inventory, new disturbance mechanisms) over the period 2011-2022.

Simulations were made with the european_applications branch in the LPJ-GUESS community code repository with subversion revision r13031 and the standard trunk version of the model r11481, which is an update of the v4.1.1 release of the model (Nord et al., 2021; Smith et al., in prep.).

4. Descriptions of new model components and updates

The main new components described in this paper are designed to fit together in a coherent system to explore the recent past and future of European forests, making use of tight constraints on forest structure, disturbance rates and harvest regimes to maximise the consistency between the simulated and the real forests (Figure 2). All of the components can, however, be applied individually or over different time periods than those shown here, depending on the scientific question.

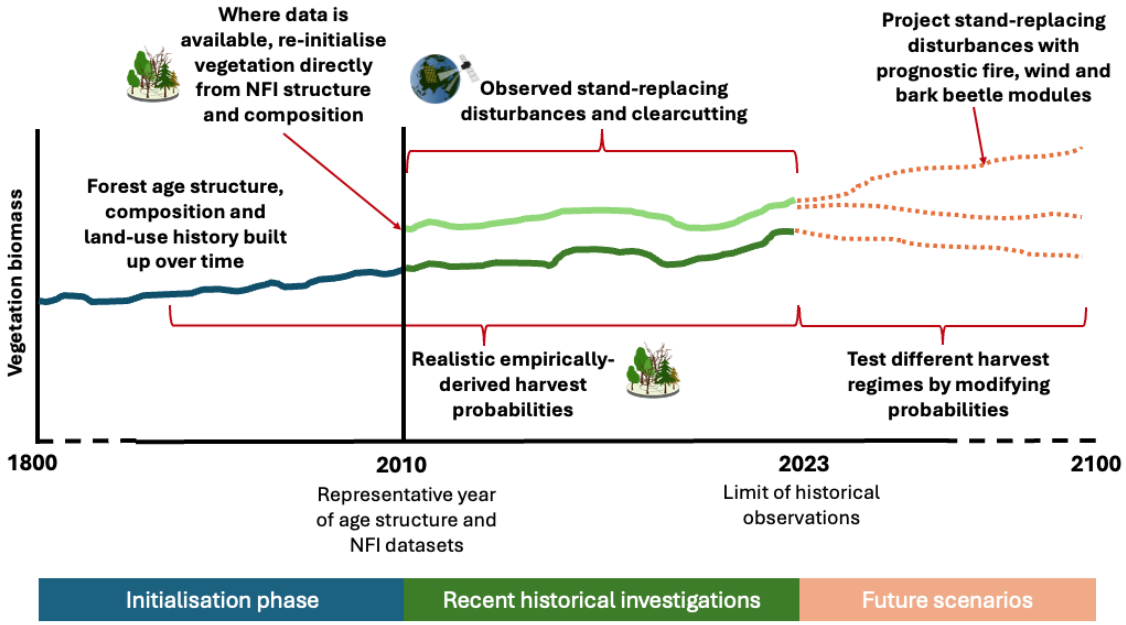

Figure 2. Conceptual figure showing how the different developments described in this paper link together to enable well-constrained simulations of recent historical and future forest dynamics. Years on the x-axis are examples and can be selected based on data availability and the questions being investigated.

4.1. Fire disturbances

Fire disturbances in LPJ-GUESS operate using two sub-models, a statistical burnt area model SIMFIRE (Knorr et al., 2014) and a combustion model BLAZE (BLAZe induced biosphere-atmosphere flux Estimator; (Rabin et al., 2017; Nieradzik et al., in prep) which is used to compute the fluxes from combusted biomass. Both SIMFIRE and BLAZE were first developed for global applications and here we describe their implementation and parameterisation for European-specific applications.

SIMFIRE is a statistical model that predicts burnt area per grid cell and year based on land cover, biomass available for burning, climate data, and population density. Burnt area predictions by SIMFIRE are calculated as follows:

$$f_{i,t} = a(l_i) F_i^b N_{i,t}^c logit(d + eP_i) \qquad \text{Eq. 1}$$

where *i* denotes location, *t* time (year), *l* land cover, *F* fAPAR (fraction of absorbed photosynthetic active radiation), *N* the Nesterov-Index (Thonicke et al., 2010;a fire danger index based on air temperature, dew point temperature and precipitation), *P* the population density, and *a, b, c, d* and *e* the optimization parameters. $f_{i,t}$ stands for the SIMFIRE prediction of the fraction of a grid cell *i* in year *t* that is burned. Whenever parameter *d* is small, the function changes to:

$$f_{i,t} = a(l_i) F_i^b N_{i,t}^c exp(eP_i) \qquad \text{Eq. 2}$$

We updated the SIMFIRE parameters using the following datasets: Information on land cover is represented in SIMFIRE by eight different so-called “fire biomes”. In the global SIMFIRE parameterisation these are based on a remote sensing product of dominant land cover type. We replaced the eight global fire biomes with seven fire biomes tailored for the European context by using the land-use dataset HILDA+ (Winkler et al., 2021) to identify the most common land-use clusters (common combinations of land-cover fractions per grid cell) in Europe. As a proxy for biomass available for burning, we use fAPAR data from the Global Land Surface Satellite project (Liang et al., 2021) based on MODIS remote sensing data at a spatial resolution of 0.5°. For the updated SIMFIRE parameterization, we computed yearly maximum values of fAPAR per 0.5° pixel. For the Nesterov Index, we used the maximum temperature, minimum temperature, and precipitation from the W5E5 dataset (Lange et al., 2021). We calculated yearly maxima of the Nesterov Index per 0.5° grid cell following the method of Thonicke et al. (2010). Population density data was taken from the Landscan Global dataset (Sims et al., 2022), whose original spatial resolution of 30 arc-seconds was aggregated to a resolution of 0.5° by averaging the population density of all grid cells within the 0.5° grid cell.

The original SIMFIRE parameterization (Knorr et al., 2014) was based on burned area data from GFED3 (Giglio et al., 2010). Agricultural fires were excluded from the parameterization process by filtering out grid cells where agricultural land exceeded 50% of the area. For the updated SIMFIRE model (“SIMFIRE-EU”), we use a combination of two remote sensing-based burned area datasets: forest fire disturbance data from the European Forest Disturbance Atlas (EFDA; (Viana-Soto and Senf, 2024, ForestPaths Deliverable 2.1) and 'natural' non-forest burned area data from GFED5 (Chen et al., 2023). The EFDA offers annual high-resolution forest disturbance information from Landsat remote sensing, categorised by disturbance causes such as wind, bark beetle, harvest, and fire. We used the forest fire disturbance rate at a 0.5° resolution (calculated as the number of pixels disturbed by fire divided by the total number of forest pixels per 0.5° grid cell). GFED5 provides monthly burned area data at 0.25° resolution for various land cover types. We classified the burned areas in 'Temperate mosaic,' 'Temperate shrublands,' 'Temperate grasslands,' 'Wetlands,' 'Sparse boreal forest,' and 'Tundra' categories as 'natural' non-forest burned areas. To update the SIMFIRE-EU parameters, we aggregated the GFED5 data to annual sums at a 0.5° resolution and normalised it by the area of GFED5 'natural' land cover types per grid cell. As a target variable for SIMFIRE-EU, we use a weighted average of the two burned area rates (forest fire from EFDA and „natural” fire from GFED5). This average is weighted according to the area of forest and unmanaged land per 0.5° grid cell as provided by HILDA+. The SIMFIRE-EU parameters (*a, b, c and d*) were optimised for a list of 2686 grid locations covering the EU, Norway, Switzerland and the UK. We used data from 2001 to 2019 for the SIMFIRE parameter update as all utilised datasets are available during that period. As we used annual data for all predictors, the updated SIMFIRE-EU formula takes the following form:

$$f_{i,t} = a(l_{i,t})F_{i,t}^{b}N_{i,t}^{c}exp(eP_{i,t}) \qquad \text{Eq. 3}$$

The parameter optimization was carried out using Python's SciPy library (Virtanen et al., 2020), with the parameters being optimised with a Trust Region Reflective algorithm. The loss function was defined as the weighted sum of squared errors (SSE), where the weights were derived from the combined areas of forest and natural land cover per 0.5° grid cell, as provided

by HILDA+. To ensure a robust search for optimal parameters, we performed multiple optimizations with randomly initialised parameter values. From these runs, we selected the parameter set that yielded the lowest weighted SSE, indicating the best fit to the target data. The updated parameter set is provided in Table A1.3.

Running within LPJ-GUESS, SIMFIRE-EU derives the fire biome per pixel directly from the land use data, with population density data provided externally. The annual maximum Nesterov index is calculated using the climate data forcing data, whilst fAPAR is simulated by LPJ-GUESS. Except for the fire biome calculation, the implementation follows the methods described by (Knorr et al., 2016).

SIMFIRE-EU annual burned area fraction (B) is computed for the past 365 days on every day in LPJ-GUESS and daily burned area is derived by applying a monthly fire-climatology generated from MODIS burned area (product MCD64A1.061 over 2000-2016; Giglio et al., 2021) and subsequent division by the number of days of a month for each cell *i* as:

$$B_{i,doy} = B_{i,t}(doy) \cdot P[i,m]/lom \qquad \text{Eq. 4}$$

where *doy* is "day of year", *t* year, *m* month, *lom* "length of month" in days and *P* the probability of a fire occurring in cell *i* in month *m*. To ensure a climatology for every grid cell, even if there has not been a fire during the period covered by the dataset, a nearest neighbour averaging approach was applied.

The BLAZE model calculates the fluxes from litter to atmosphere and from live biomass to both atmosphere and litter resulting from a fire. This is done in a three-stage approach:

1) BLAZE utilizes the daily output of SIMFIRE-EU as "fraction of grid-cell burned" to check whether a fire occurs. This is done by using random numbers for each patch with a minimum biomass of 120 g C m^{-2} in this cell. A burning patch is considered to be burned completely.
2) In case of a fire each tree tests against a survival probability depending on its physiognomy, climate-region, allometry like height or diameter at breast height, and fire-line intensity which itself depends on available fuel and fire weather conditions.
3) Carbon fluxes are computed from litter biomass to the atmosphere as well as from live biomass to litter and atmosphere based on look-up tables depending on fire-line intensity and the carbon pools are updated accordingly.

In the tuning and evaluation phase we fed GFED4 burned area to BLAZE and analysed the C-emissions and compared them to the European totals. We used the flammability of so-called readily available fuels that have a high surface-to-volume ratio and normally burn instantly including leaves, twigs, the metabolic top soil-layer, and coarse woody debris (CWD). CWD in LPJ-GUESS includes dead tree stems (standing and lying) which do not readily burn and, therefore, a tuning factor has been implemented reflecting the fraction of CWD that is readily flammable. This factor is 0.02 for boreal CWD and 0.0025 for temperate. The seemingly low values reflect the fact that, in LPJ-GUESS, dead trees are included in CWD.

4.2. Storm disturbances

The Lagergren et al. (2012) module of wind damage originally developed for Sweden has been re-implemented in LPJ-GUESS for application at the European scale. In the module a wind damage sensitivity index is calculated at cohort level. The index is primarily based on the height of the cohort related to surrounding trees in the patch to and surrounding patches in the grid cell, its height to diameter relationship and the time since the last thinning. The sensitivity index is multiplied with a wind load resulting in a fraction of a cohort that would be killed during a severe storm event. As the module was originally developed for Sweden, some changes have been carried out compared to the previously published implementation to allow application across Europe in this new version of LPJ-GUESS. This includes the impact of forest fragmentation on cohort exposure, which was previously assessed by relating the typical size of a forest stand (i.e. a contiguous patch of forest) to the total forest area in the grid cell (Eq. 7 of Lagergren et al., 2012). The unit size was derived from clearcut size statistics at the county level. To generalise across Europe, the average forest stand size has been set to a fixed value of 3 ha based on average unit size of even-aged silvicultural systems in Europe (Aszalós et al., 2022). The original model was constructed to give a range of storm sensitivities for similar forest patches, to get a better distribution of damage levels as a consequence of different wind exposure. This was based on specifying wind load separately for six different sectors of wind direction and giving each patch a random sensitivity for each sector (Eq. 8 of Lagergren et al., 2012). This approach, however, requires running a large number of patches for a good representation of the mean, which is often not feasible for continental-scale simulations with complex land-use history. In the new implementation, wind load is set to the same value for all sectors (0.05) and the random factor is set to a constant value of 0.5. Wind load can be read from a pre-prepared external ascii-file or directly calculated from the wind fields in the climate data used to drive LPJ-GUESS simulations. Alternatively, a constant wind-load of a severe storm can be used, which results in annual estimates of storm sensitivity expressed as the tree biomass lost in the event of a severe storm. For runs with dynamic wind load, the application of wind mortality can be turned off, for generating output of wind sensitivity when the disturbances are driven by other functionality (e.g. §4.4).

In the original implementation the PFT-specific sensitivity parameter “storm_sensiv” (Eq. 13 of Lagergren et al., 2012) had only three levels; 1 for Norway spruce, 0.5 for other evergreen conifers and 0.1 for remaining PFTs. Based on Gardiner (2021) the “storm_sensiv” parameters have been updated as 1/”stability rating”, giving a smoother distribution which remains consistent with the original implementation. The update of the PFT allometric parameters (see §4.7) also affects the “allometric-relationship index at cohort level” as it is sensitive to the height to diameter ratio (Eq. 13 of Lagergren et al., 2012). With the new parameters, *Picea abies* sensitivity increased, *Pinus sylvestris* sensitivity decreased. *Fagus sylvatica* gained an increased sensitivity that peaked already at a diameter of 21 cm (Figure 3).

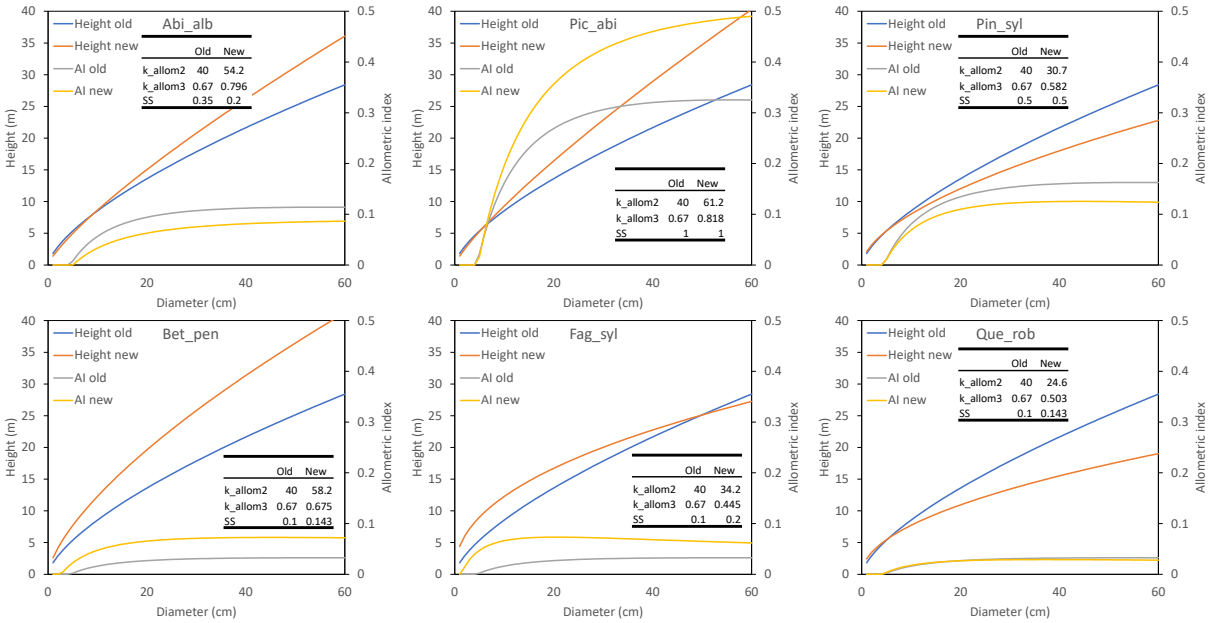

Figure 3. Diameter-height and diameter-Allometric index (AI) relationships with the old and new parameters for six selected PFTs. AI relationships determine the storm sensitivity of the species. Abi_alb = *Abies alba*; Pic_abi = *Picea abies*; Pin_syl = *Pinus sylvestris*; Bet_pen = *Betula pendula*; Fag_Syl = *Fagus_sylvatica*; Que_rob = *Quercus robur*.

The challenge in moving from average storm damage in a severe storm to actual damage predictions is the threshold for the severity of a storm to result in damage. This challenge is particularly acute because storm damage is dependent on the above-canopy wind speed, which can be very poorly associated with the mean wind speed recorded at the synoptic scale (i.e. the scale of the weather data used to drive LPJ-GUESS) (Chen et al., 2018). Here we circumvent this challenge by creating a wind disturbance probability map which combines historical observations of wind disturbance damage with information on wind speed return intervals and maximum wind gust speed. The approach makes the implicit assumption that all regions affected by severe storms contain stands of similar vulnerability. Despite the obvious limitations of this assumption, we consider it much superior to a direct parameterisation against mean grid cell wind speed from the model driving climate data which would not consider the complex relationship between synoptic wind speed and above-canopy wind speed, mediated as it is by the local topography. Given the uncertainty regarding future wind speeds (Severino et al., 2024) we do not include a climate change component on the wind disturbance probability; instead the wind module in LPJ-GUESS will calculate how the combination of location and stand structure influences wind disturbance damage.

The wind disturbance probability map was based on a satellite-derived product of storm-related forest disturbances over 1985-2016 at 30 m resolution across Europe (Senf and Seidl, 2021). We aggregated all wind disturbances from this disturbance map to a grid of 10 x 10 km and assigned each grid cell as zero if no wind disturbance was included and as one if at least one disturbance was included. Using this data, we modelled the occurrence probability of a wind disturbance. To do so, we calibrated a binomial generalised additive model with 5-year wind speed return intervals and maximum storm gusts as predictor variables. That is, we predict the occurrence of a wind disturbance event based on historical storm data, expecting a higher probability in areas of higher historic storm intensity. The 5-year storm wind speed return intervals and maximum storm gusts were obtained from the Copernicus storm database

(https://doi.org/10.24381/cds.9b4ea013), which is a pan-European database of storm reanalysis.From the calibrated model, we predicted the average occurrence probability for each grid cell (i.e. what is the probability that a wind disturbance occurs in this grid cell) and divided the probability by the number of years to obtain an annual wind disturbance probability. We did not use additional topographic predictors, because topographic data was already used for the reanalysis of the storm database. The map is shown in Figure 10b.

In a second step, we aggregated all wind disturbance events to a 10 x 10 km grid and modelled the spatial wind disturbance occurrence probability. To do so, we calibrated a binomial generalized additive model with 5-year storm wind speed return intervals and maximum storm gusts as predictor variables. That is, we predict the occurrence of a wind disturbance event based on historical storm data, expecting a higher occurrence probability in areas of higher historic storm intensity. The 5-year storm wind speed return intervals and maximum storm gusts were obtained from the Copernicus storm database (https://doi.org/10.24381/cds.9b4ea013), which is a pan-European database of storm reanalysis. The database provides the most accurate representation of storm conditions for Europe to date. From the model, we predicted average occurrence probability for each grid cell (i.e. what is the probability that a wind disturbance occurs in this grid cell) and divided the probability by the number of years to obtain an annual wind disturbance probability. We did not use additional topographic predictors, because topographic data was already used for the reanalysis of the storm database. The map is shown in Figure 10b.

The wind disturbance probability map is then multiplied by the average damage in a severe storm and a calibration factor to calculate an estimate of actual damage. To set the calibration factor (previously set to 9.35 in Lagergren et al., 2012) the average storm damage in a severe storm over the period 1986-2020 calculated by LPJ-GUESS was multiplied with the wind disturbance probability map. This step was done offline, using calculations of average damage in a severe storm output from the simulation described in §3. This resulted in a map of expected annual wood damaged in the simulated grid cells. The results were aggregated by country, multiplied with 35 years and compared to the total wind damage 1986-2020 in the Database of Forest Disturbances in Europe (DFDE). For the period 1986-2019 we used the expert gap filled data compiled by Patacca et al. (2023) and for 2020 we used data directly from the database (https://dfde.efi.int/db/dfde_app.php, accessed 7 Aug 2024, search terms: Period start 2020; Period end 2020; cause wind). The values compared quite well (R^2 = 0.66) but as expected the m_stormfactor from Lagergren et al. (2012) was no longer appropriate, giving predicted damage levels about 33% lower on average than DFDE. The slope between modelled results and the DFDE data (1.49) was used to calibrate the “m_stormfactor” (new value 9.35 × 1.49 = 13.93). As the calibration factor is based on damage volume, which is the only independent large-scale statistic available, it will be sensitive to any efforts which reduce biases in the simulated stock volume (§5.1). For this reason, we have automated the calibration process of m_stormfactor as part of the model benchmarking scheme (§5), such that the value remains appropriate following other model updates.

4.3. Spruce bark beetle disturbances

The new spruce bark beetle disturbance module is described in detail in Lagergren et al. (Appendix B), but summarised here as it forms an integral part of the new model version. The aim was to develop a simple mechanistic module that is suitable for large-scale application, drawing strongly on empirical understanding. The module simulates an index of spruce bark

beetle population at patch level (P_{patch}), which is directly related to the availability of brood substrate of the right species and size (spruce with diameter > 15 cm). The rate of change (R) of P_{patch} ($P_{patch} = e^{R} P_{patch\ t-1}$) depends on factors related to drought, temperature driven phenology, P_{patch} averaged to grid-cell level ($P_{gridcell}$), P_{patch} and spruce trees newly killed by other mortality reasons than bark beetles (L) (Figure 5), a concept found in both empirical (Marini et al., 2017) and mechanistic (Jönsson et al., 2012) models. The module was applied together with the storm damage module (Section 4.3), and as storms cause large amounts of L, they can trigger bark beetle outbreaks in the simulations. The storm damage can either be provided by the storm module described in Section 4.2 or read in as an input file.

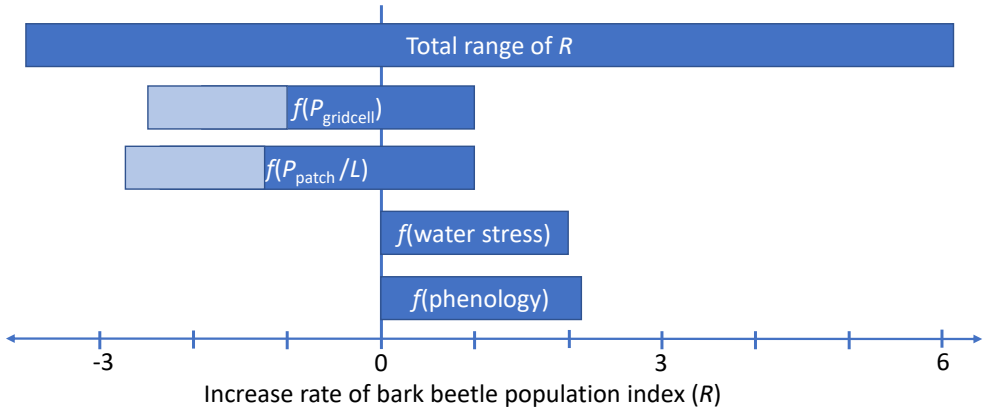

Figure 5. The different components of the rate of change of the spruce bark beetle population index ($R = f(P_{gridcell}) + f(P_{patch} / L) + f(\text{water stress}) + f(\text{phenology})$). For $f(P_{gridcell})$ and $f(P_{patch} / L)$, the light shaded areas show the range with different parameters for the minimum of $f(P_{gridcell})$ and $f(P_{patch} / L)$. To have the possible total negative feedback from the population index constant, the minimums of the ranges were depending on each other so that the sum always equalled -3.8 in the calibration.

The module also has functionality to account for salvage logging by reducing L and sanitary cutting by reducing P_{patch}. Like for the wind module, there is an option to run the module to calculate grid-cell-level bark beetle population sizes ($P_{gridcell}$) and phenology parameters to assess vulnerability without applying the resulting damage to the modelled vegetation. Calibration of the model was based on European storm and bark beetle damage statistics from Marini et al. (2017), for South Sweden, North-East France, Switzerland and Austria and is described in detail in Lagergren et al. (Appendix B).

4.4. Satellite-forcing of historical stand-replacing disturbances

Disturbances are episodic events and the prognostic modules to describe their dynamics in Sections 4.1-4.3 all utilise a strong probabilistic component to capture the characteristics of the disturbance regime. For application of LPJ-GUESS to the historical period, however, a probabilistic formulation means that the timing and location of major disturbance events will differ from the historical record if this record includes observed disturbance events. This limits the extent to which the model can be applied to explore recent forest dynamics and their implications, for instance, for interannual variation in the forest carbon sink. To improve the capability of LPJ-GUESS to explore such dynamics, we added a capability to directly force stand-replacing disturbances with observations of disturbance occurrence from satellite information. We processed 30 x 30 m resolution annual observations of disturbance

occurrence (Viana-Soto and Senf, 2024) to create input files containing the fraction of forest disturbed per model grid cell (here 0.5° x 0.5°) for each year in the time series and separated by agent type (forestry clear-cut; fire, wind and bark-beetle disturbances). As the observations do not provide a split between wind and bark-beetle disturbances, we made a preliminary assumption of an equal split between the two disturbance types. Each simulation year, all the forest stands within a grid cell are ranked for vulnerability to the different disturbance types. The prescribed forest disturbances were then applied to the stands in the order of vulnerability to the different disturbance types. The different disturbance types were applied in the order: clearcut, fire, wind and bark-beetle mortality.

Disturbance vulnerability of stands was determined as follows. For forestry clearcuts, we ranked standards according to their quadratic mean diameter at breast height (DBH), preferentially harvesting stands with higher values. Fire vulnerability was ranked using the BLAZE model (§4.1) and wind vulnerability was ranked using the storm module (§4.2). For bark beetles, we assumed that disturbance was primarily spruce bark beetles. We thus ranked stands by quadratic mean DBH and further weighted disturbance likelihood according to stand composition, with *Picea abies* individuals given a weight of 100, other needle-leaved trees a weight of 10 and broadleaved trees a weight of 1. It was assumed that all the trees within a disturbed area were killed, with the exception of fire disturbances where we used the BLAZE model to calculate tree mortality on disturbed areas. Different assumptions can be made about the fate of the disturbed vegetation, depending on the disturbance type. For clearcut harvest we followed the standard model assumption that 90% of the stem biomass and 40% of branches, 30% of leaves and 10% of coarse roots are removed from the ecosystem. For fire, we allowed combustion of vegetation to follow the BLAZE model calculations. For wind and bark beetle disturbances the base assumption is that the disturbed material is transferred directly to the litter, but it is also possible to specify a harvest setting that accounts for salvage logging.

4.5. Probabilistic harvest regimes

An empirically-based harvest scheme has been developed based on harvest rates observed in forest inventory data. This functionality is presented in full in Suvanto et al. (in prep.), but it is summarised here as it forms an integral part of the new model version. The scheme is based on the analysis of harvest regimes in national forest inventory data of Suvanto et al. (2024) which covered 10 European countries: Spain, France, Germany, Poland, Switzerland, the Netherlands, Belgium, Sweden, Norway and Finland, as well as the national landscape inventory of the Czech Republic. The aim was to create a harvest scheme that reflects the frequency, intensity and form of harvest that is really carried out in European forests, rather than relying on idealised harvest rules which do not reflect reality (Schelhaas et al., 2018). A decision tree was created which is assessed at the level of each forest patch within LPJ-GUESS. Each stage of the decision tree is evaluated probabilistically based on a random draw from a uniform distribution assessed against empirically-defined harvest probabilities. First it is determined whether or not harvest occurs in the patch in that year. If harvest is determined to occur, then it is subsequently determined whether that harvest is partial or clearcut. Clearcut harvests are implemented with harvest of all trees on the patch. For partial harvests a further decision stage determines the intensity of the harvest (i.e. what fraction of trees are removed), followed by a determination of whether smaller trees (i.e. thinning from below) or larger trees (thinning from above) are preferentially removed. The empirical probabilities are composed of

matrices where the probability varies as a function of the patch basal area, the quadratic mean DBH and whether the PFT composition is primarily needleleaved or broadleaved. The probability matrices are defined regionally, where the regions reflect a combination of the prevailing harvest regime (Suvanto et al., 2023) and the country. Linking the harvest probability to stand characteristics in this way means that we do not simply apply observed harvest rates, but rather the harvest rates are responsive to the state of the forest following the prevailing harvest regime. This means that the scheme is suitable to be applied as a baseline management case in simulations of the future of European forests. To explore different management scenarios, it is possible to manipulate the probability tables, for instance to increase the likelihood of clearcut harvest or change the stand basal area and/or quadratic mean DBH at which it is most probable to occur. These harvest probability matrices can be defined for any country for which suitable NFI data is available, following the process described in Suvanto et al. (in prep.). Finally, an option is included in LPJ-GUESS to allow clearcut harvest from this scheme to be replaced by clearcut information from satellite (Section 4.4).

4.6. Forest state initialisation

The stand-age initialisation procedure previously developed within LPJ-GUESS has provided a big step forward in capability to represent current forest structure accurately, and thus make improved assessments of important behaviours such as forest carbon uptake and harvest rates (Lindeskog et al., 2021; Pugh et al., 2019b; Scheel et al., 2022). Stand age initialisation, however, does have some limitations. Whilst it sets a maximum age for trees on the stand, it provides no information on the progression of stand development over the intervening years. This information, however, is important, since a potential occurrence of thinning or non-stand-replacing disturbance can have major impacts on the size, number and composition of trees (Suvanto et al., in prep.), impacting the forest's response to e.g. disturbances. Large-scale datasets of stand age also lack a breakdown of how age cross-references with forest species composition (Besnard et al., 2021; Poulter et al., 2019), requiring to make assumptions about how stand age and composition relate to each other. Finally, using stand age means that any biases in modelled growth are compounded into the current forest structure. To avoid these limitations, we have developed an approach to directly initialise the vegetation in LPJ-GUESS using tree-by-tree data from forest inventory datasets.

The state initialisation process equates one field sample plot to one LPJ-GUESS patch. Field sample plots vary in size (Tomppo et al., 2010), but are typically of the order 0.05 ha and thus of a similar magnitude to the 0.1 ha patches of LPJ-GUESS. Inventory data is pre-processed to first assign each species to one of the LPJ-GUESS PFTs according to its functional traits and then to group individual trees on each plot with the same PFT classification to DBH size cohorts in bins of 10 cm (10-150 cm plus one bin >150 cm). This preprocessed dataset is then provided to LPJ-GUESS as an input file. Because LPJ-GUESS uses stochastic process descriptions to simulate re-establishment and mortality, a good representation of the future development of an initialised plot requires multiple replicates. Therefore, standard practice is to simulate each inventory plot as one stand, composed of 10 replicate patches, each initialised from the same plot data, which are identical at the time of forest initialisation. There is no fixed limit on the number of plots that can be initialised in any model grid cell, with each additional plot being initialised as an additional stand with associated replicate patches. In practice, however, the density of NFI plots varies substantially across Europe. We tested the

initialisation process with the NFIs of Germany and Sweden, which contain forests with very different harvest regimes (and therefore structures) (Suvanto et al., 2023) and sampling protocols (Tomppo et al., 2010). The density of NFI plots varies between the two countries. To standardise the model inputs, we used a fixed number of 30 plots per grid cell. Since the sampling method can influence model results, we implemented a straightforward approach by categorising grid cells based on plot frequency. Grid cells with fewer than 5 plots were excluded, while those with 5 to 30 plots retained their original plots, with random duplications added to reach 30. For grid cells with more than 30 plots, a random selection limited the number to 30. In Germany, 90% of grid cells have more than 30 plots, compared to 57% in Sweden. This method ensures consistent input data, though further research into the effects of different sampling techniques is necessary.

The forest state initialisation process does not affect the soil and litter carbon and nitrogen pools. To initialise these to an appropriate level, it is therefore necessary to carry out a historical simulation following the standard LPJ-GUESS spin-up procedure and some representation of the kind of vegetation that has been growing at that location over the previous ca. 100 years. Here, we apply the simulation set-up described in Section 3 for this purpose, but in principle, any level of complexity of historical land-use change and management is possible. At the time of vegetation initialisation, vegetation in all forest stands is killed and all biomass is removed from the system, all soil carbon and nitrogen pools and water content are pooled so the new stands all begin from the same soil state, but soil state at the level of the forest land cover conserves the information from before vegetation initialisation. The trees are then introduced in the stands, using the input PFT, DBH and tree density information described above. Leaf-to-sapwood area ratio, leaf and sap carbon/nitrogen quotient and sapwood fraction of wood biomass (per 10-cm diameter-class) were sampled from the previous 20-year period in corresponding trees growing in the model. Because LPJ-GUESS currently uses an age-based approach to assess mortality risk for older trees, but tree age is not generally available in the inventory data, a simplistic DBH-age relationship (age in years equals ten times DBH in mm) was applied to the initialised trees.

4.7. Updates of PFT parameters and code base

PFT parameters for which direct and good quality trait observations are available were updated directly with those values, taking the approach that LPJ-GUESS should be as closely tied to real-world observations as possible. These parameters were specific leaf area (SLA) (based on TRY data request 6033), wood density (Global wood density database;Chave et al., 2009) and allometric parameters calculated based on the TALLO database (Jucker et al., 2022). Specifically, the allometric parameters were k_{allom1}, k_{allom2}, k_{allom3} and k_{rp}, as used in the equations (Sitch et al., 2003; Smith et al., 2014) relating DBH (D) to height (H),

$$H = k_{allom2}\, D^{kallom3}, \qquad \text{Eq. 5.}$$

and DBH to crown projective area (CA),

$$CA = k_{allom1}\, D^{krp}. \qquad \text{Eq. 6.}$$

In all cases we took the trait values for the species corresponding to the name of the LPJ-GUESS PFT and used the median of the individual entries per species to update the

parameters. Only tree PFTs were updated. An additional parameter, *reprage*, was defined as a minimum age below which trees do not allocate any carbon to reproduction. Above *reprage* the standard 10% of net primary productivity is allocated to reproductive processes (Smith et al., 2014). Values for *reprage* were set based on Miller et al. (2008), supplemented by centroid values from (Leuschner and Meier, 2018) for species which were not included. We further modified the bole height ratio (fraction of tree height at which the crown begins), which is set at 0.0 in standard LPJ-GUESS to 0.5 for all PFTs. A full list of the updated parameter values for the PFTs can be found in Table A4.2 and the consequences of the updated allometric coefficients for height and crown area are shown in Figures A4.2 and A4.3.

In addition to the PFT parameter updates we also made some changes to the underlying code base relating to allocation where we reformulated the carbon allocation so that it is more numerically stable (by avoiding non-integer exponents in power functions), avoiding side effects such as negative height increments that could occur with the previous implementation. We further implemented a modification to avoid unintended behaviour in monocultures where, if only one woody PFT was specified, establishment was increased by a factor of 3.

Based upon an initial assessment of LPJ-GUESS performance against the benchmarking datasets described in Section 5.1, it was identified that there was a general low bias in biomass and in woody growth rate. Given that the simulations were initialised based on observed stand age, woody growth rate was identified as the core variable in need of improvement. It was also identified that the carbon use efficiency (NPP/GPP) was generally very low compared to independent estimates (Zhang et al., 2014). Using expert judgement, we identified parameters which are known to have a substantial impact on woody growth rate, but for which strong observational constraints are not available. Based on this, the autotrophic respiration coefficient (respcoeff, i.e. the base respiration rate at 10°C with units g C g N^{-1} day^{-1}) and sapwood turnover rate (turnover_sap, units: yr^{-1}) were identified for calibration. Sapwood turnover rate is generally set at the shade-tolerance class level, so this split was maintained, giving a total of 3 parameters to calibrate. Respcoeff is included in the model to account for the differences in baseline respiration rates as a result of climate adaptation, but is set to 1.0 across the whole of Europe. Given that climate is the primary driver (Atkin et al., 2015), we split the species/PFTs into two groups based on whether they were predominantly boreal or north-central temperate zone (cold) or southern temperate zone (warm), we also split it into needleleaved and broadleaved following Atkin et al. (2015). This gave a total of 7 parameters for the calibration process.

A calibration transect of 59 grid cells was selected from the simulation setup described in Section 3 above, randomly selecting one for each degree of latitude. In order to avoid inadvertently calibrating LPJ-GUESS against extreme values, only grid cells with observed growth rate values between the 25th and 75th quartiles were available for selection. We performed 6760 simulations across the gradient with the permutations (steps of 4 between the values given in Table A4.1) for the 7 selected parameters that met the following constraints: (a) turnover_sap for the more shade tolerant should always be lower or equal to that of a less shade tolerant class; (b) respcoeff should be higher for the warm class within its leaf physiognomic class. This latter response was based on assessments showing carbon use efficiency to tend towards higher values at cooler locations (Zhang et al., 2014). We selected the top performing simulations by maximising the ratio of the correlation coefficient and RMSE calculated in comparison with the observations of growth rate. Woody growth rate is the only

variable included in the objective function because it is the only part of the inventory observations whose values are not heavily determined by assumptions regarding the thinning regime. The optimal parameter set, *euro_opt*, is based on the mean of the top 10 simulations based on this metric (Table 1).

Table 1. European simulations conducted and results of the calibration.

Simulation name	respcoeff ($g\ C\ g\ N^{-1}\ day^{-1}$)				turnover_sap (yr^{-1})		
	Broad Cold	Broad Warm	Needle Cold	Needle Warm	shade tolerant	intermediate shade tolerant	shade intolerant
trunk	1	1	1	1	0.05	0.075	0.1
euro_opt	0.67	0.97	0.58	0.62	0.072	0.1	0.117
euro_opt1	0.67	0.83	0.58	0.58	0.075	0.1	0.108
euro_opt2	0.67	0.83	0.58	0.75	0.075	0.1	0.108
euro_opt3	0.67	1	0.58	0.42	0.075	0.1	0.108
euro_opt4	0.67	1	0.58	0.42	0.075	0.1	0.125
euro_opt5	0.67	1	0.58	0.58	0.058	0.1	0.125
euro_opt6	0.67	1	0.58	0.58	0.075	0.1	0.108
euro_opt7	0.67	1	0.58	0.58	0.075	0.1	0.125
euro_opt8	0.67	1	0.58	0.75	0.058	0.1	0.125
euro_opt9	0.67	1	0.58	0.75	0.075	0.1	0.108
euro_opt10	0.67	1	0.58	0.75	0.075	0.1	0.125

euro_opt: fully calibrated *optimal* setup, based on the mean of the ten best parameter sets
euro_opt1,..., euro_opt10: calibration results for each of the ten best parameter sets. trunk: standard version of LPJ-GUESS.

5. Benchmarking

A range of benchmark tests have been developed and integrated within a flexible suite written in R, which can be applied directly on LPJ-GUESS results or on any other model with comparable outputs. In this section we describe the different benchmark tests that have been

implemented and present the performance of the updated European version of LPJ-GUESS against them.

5.1. European forest state and dynamics

To test model performance against the actual state and dynamics of European forests, we created gridded benchmarks of current forest structure and productivity across eleven European countries based on information from NFI plots (or other forest inventory data in the case of the Czech Republic and Finland; Table A5.1). Plot-level information was averaged on a 0.5° grid in order to have enough sample plots per grid cell. The grid information provides a representative assessment of the actual forest structure and dynamics which could be used to benchmark module simulations set up to provide best-estimate simulations of the regions covered. Only trees with minimum diameter at breast height of 10 cm (except a minimum of 12 cm for Switzerland) were considered from any of the data sets. Trees were weighted by their inverse sampling probability on a hectare to account for different plot sizes and designs between the countries. The evaluation data contained the following variables:

- Average plot quadratic mean diameter (mm)
- Woody biomass (Mg ha^{-1})
- Average plot stem density (stems ha^{-1})
- Gross biomass growth (Mg ha^{-1} y^{-1}), calculated as the biomass in census 2 minus the biomass in census 1, plus the biomass lost to mortality and harvest during the census period. Henceforth referred to as woody growth rate.

The census periods for which the NFI data were calculated are provided in Table A5.1.

In addition to the NFI data we benchmarked against a satellite-derived dataset of annual gross primary productivity (GPP) covering the period 1982-2015 (kgC m^{-2} y^{-1}) from Tagesson et al. (2021). To focus on forest areas, we first extracted the 0.05° pixels covered with forest according to the Corine Land Cover dataset (CLC) (100m) (European Environment Agency, 2023). These 0.05° pixels were then aggregated to 0.5° by taking the mean. All 0.5° grid cells with at least 80% forest cover were used for the benchmark.

We compared LPJ-GUESS simulations initialised based on observational stand-age structure (§3) against these NFI- and satellite-based values, as this provides a rigorous test of the structure which emerges from the model processes and the forcing datasets because the stands are grown from their year of establishment. When the forest structure is directly initialised from the same underlying dataset (i.e. forest state initialisation, §4.6), then these benchmarks would only test the initialisation process against the NFI data and not the underlying model dynamics. The updates described in this paper which influence performance in these benchmarks are thus parameter updates (§4.7) and the thinning component of probabilistic harvest (Section 4.5) which was applied over the historical period.

We find relatively low absolute biases in GPP and woody growth rate overall following the calibration (§4.7), but a tendency remains to underestimate these fluxes in central Europe and overestimate them in northern Europe. These biases accumulate sufficiently over stand development to lead to substantial underestimations of biomass and mean tree size (quadratic mean DBH) in central Europe (Figure 6 and Figure 7). Whilst non-negligible, these biases represent a substantial improvement over the previous LPJ-GUESS v4.1 implementation which showed a substantial overestimation of GPP and stem density, whilst tending to

underestimate woody growth rate (not shown). The improvement in GPP - a result of the reparameterisation and calibration described in §4.7 - is particularly notable as no direct measures were taken to improve this.

It is important to consider that these benchmarks are not a pure test of model process representations and parameterisation, but rather of the full combination of those representations and parameterisation with available input datasets. For example, there are substantial differences between stand age distributions in the Pucher et al. (2022) dataset used here and the Poulter et al. (2019) dataset, despite both of them being based on the same underlying NFI data and referenced to the same base year of *ca.* 2010.

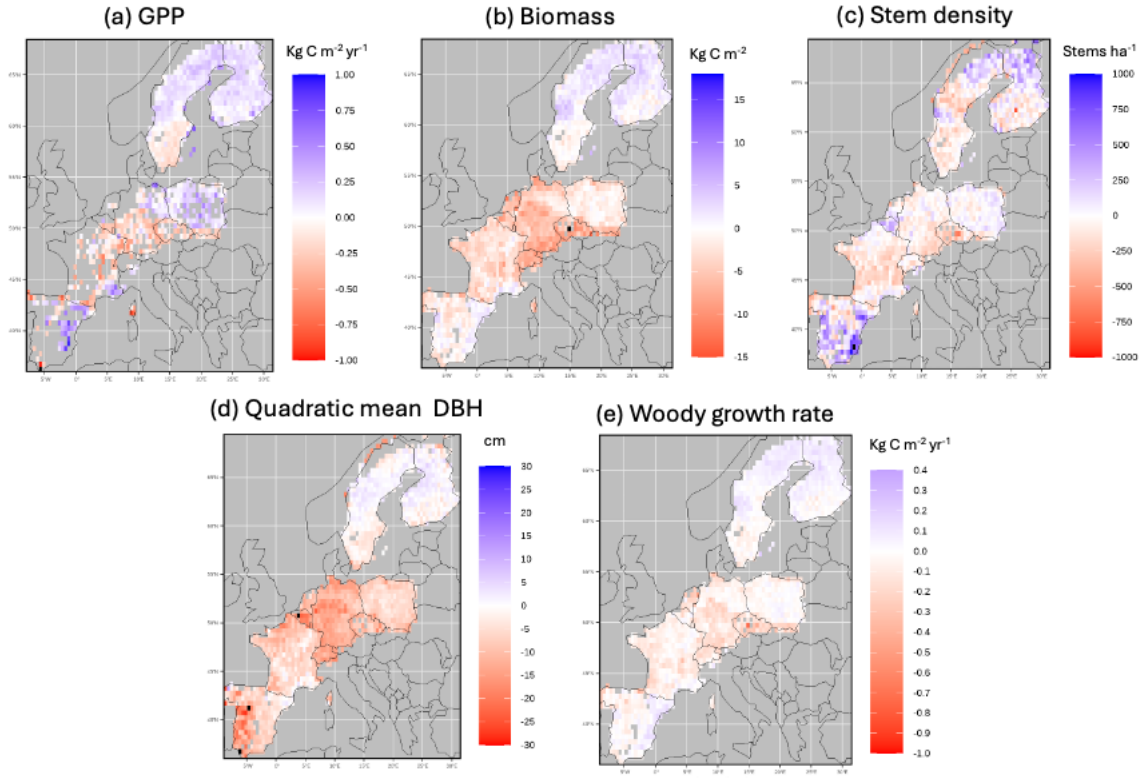

Figure 6. Difference maps showing benchmarking of the stand-age initialised LPJ-GUESS simulations against forest inventory data and satellite-based productivity (GPP). Negative values mean that the modelled values are lower than the observations.

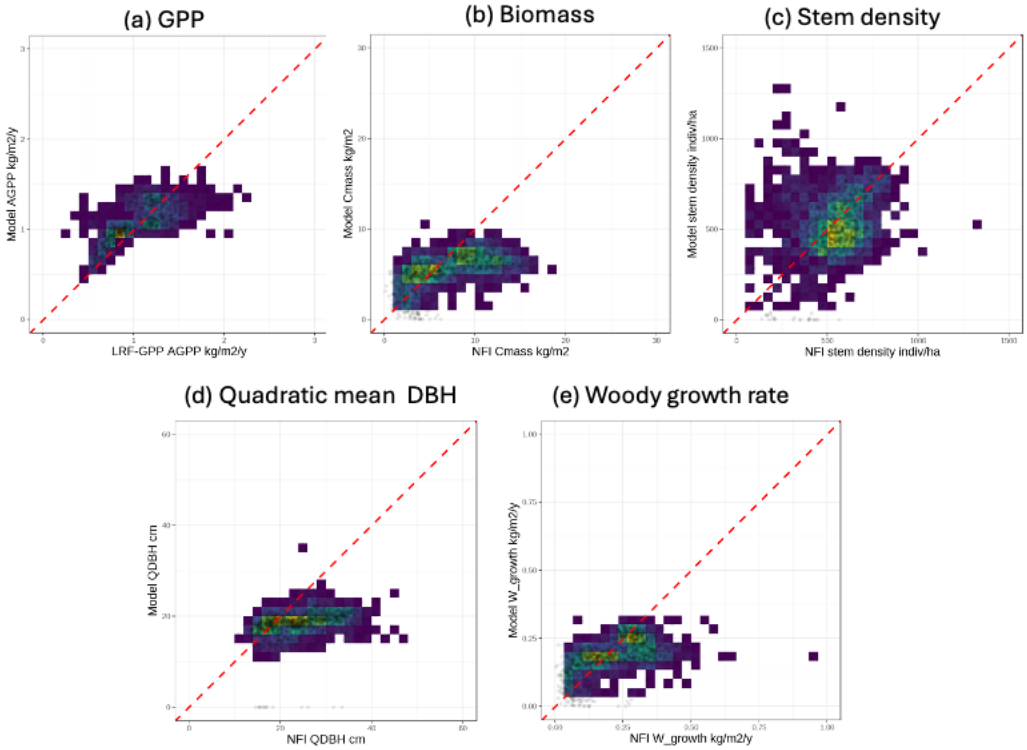

Figure 7. Scatter plots showing benchmarking of the stand age initialised LPJ-GUESS simulations against forest inventory data and satellite GPP. Brighter colours indicate a higher density of grid cells.

5.2 Forest regrowth rates

To assess the realism of simulated aboveground woody carbon dynamics during forest recovery, we benchmark a subset of locations against chronosequences of regrowing forest from sites from temperate and boreal Europe. The observational dataset of temperate regrowth curves of aboveground woody carbon are derived from chronosequence data in Teobaldelli et al. (2009), omitting foliage and root biomass pools. For boreal biome-level data, we used biomass chronosequence data calculated for Repo et al. (2021) based on Finnish national forest inventory plots from NFI9 to NFI12 (Tomppo et al., 2010). We also selected a subset of NFI plots, which were either conserved or had low-intensity management (last management > 30 years ago) across southern and central Finland. To arrive at above-ground woody carbon, we removed the foliage biomass fraction from existing total above-ground biomass estimates based on stand-age-based biomass expansion factors (BEFs) using age-dependent foliage-total biomass relationships calculated from Lehtonen et al. (2004). Regrowth data is organised in 20-year age bins and we report the median, 10th percentile and 90th percentile boundary. At least 20 observations are in each bin, following Pugh et al. (2019b).

LPJ-GUESS simulates regrowth in the way that the regrowing vegetation composition emerges from the combination of PFT bioclimatic limits and inter-PFT competition. To simulate regrowth at the locations for which observations were available in LPJ-GUESS, we killed all vegetation and initiated stand regrowth for each location according to the stand age. We set this year of stand initiation based on the publication year, subtracting 5 years from this to

account for data processing delays. We carried out this process to arrive at approximately corresponding climatic and CO_2 conditions for each of the regrowing simulated forest stands. For sites from temperate data (Teobaldelli et al., 2009), we used the mean publication date of the main sources reported in (Cannell, 1982)and (Usoltsev, 2001) and subtract the stand age and 5 additional years. We additionally removed temperate forest coordinates for regrowing stands in Sweden, due to a strong productivity gradient found between Sweden and continental Europe. For the boreal data, disturbance years were created based on the publication date of Repo et al 2019, the midpoint of stand age binned data provided and – again subtracted by 5 years. As we do not have the exact locations of the regrowing stands in Finland, the grid cells to be disturbed were selected randomly from 0.5° grid cells located the same broad region of Finland as the observations. To account for the 20-year range of age bins, we added stochastic noise to the disturbance year. In total, we simulated 43 regrowing forest stands across temperate Europe, with the oldest being disturbed in 1704 and the youngest in 1988 and 156 sites in boreal Europe (Finland), with the oldest being disturbed in 1795, and the youngest in 2014.

In boreal forests, the simulations show a steady increase in aboveground woody carbon, continuing even beyond 100 years, where observations indicate a plateau (Figure 8), with median woody carbon content stabilising around 15 kg C m^{-2}. The model remains within observational bounds until the forest age goes beyond 180 years. The lack of disturbance mortality events, with only age-related mortality active, likely causes to the unrealistic continued increase in woody carbon beyond 100 years. In temperate forests, the simulated carbon trajectory peaks and declines about 40 years earlier than observed, leading to a slight overestimation of woody carbon content between stand ages of 41-80 years. Despite this, the simulated regrowth dynamics of natural forests across both biomes generally align with observed patterns, particularly over the next 40 years, a critical timeframe for policy relevance.

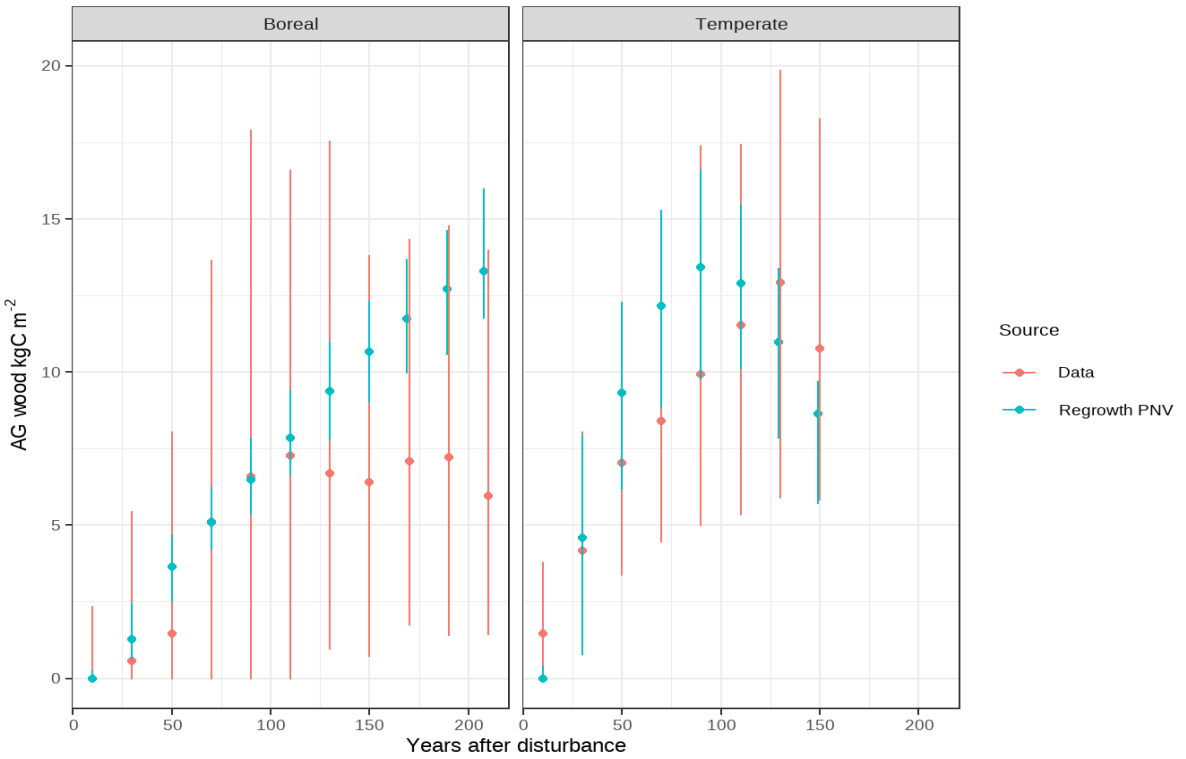

Figure 8. Forest regrowth benchmark of aboveground woody carbon recovery of multiple plots grouped into 20-year age bins, along years after disturbance for boreal (South and central Finland) and temperate forests in Europe.

5.3 Land-atmosphere fluxes

We implemented a benchmark to read GPP and evapotranspiration (ET) observations directly from the standard formats used by the ICOS Carbon Portal (https://www.icos-cp.eu/observations/carbon-portal). We extracted these data for 17 flux tower sites in forests across Europe and aggregated by season. We ran LPJ-GUESS at each flux tower site. Because forest age and management history were not available for all the sites, we ran LPJ-GUESS in potential natural vegetation mode, allowing the composition and state of the forest to emerge as a function of the grid cell boundary conditions. Whilst this approach does not allow like-for-like assessment of ecosystem respiration or net ecosystem exchange, it should have a relatively modest impact on GPP and ET which are primarily vegetation fluxes. This showed close correspondence between the model and observations for GPP across the four seasons, with deviations from the 1:1 line only notable for three sites during the spring season (Figure 9). For evapotranspiration, agreement was similarly good, although with divergence between model and observations notable for five sites in either the spring or summer season. In the future it is anticipated to improve this benchmark by including specific forest management histories for each site.

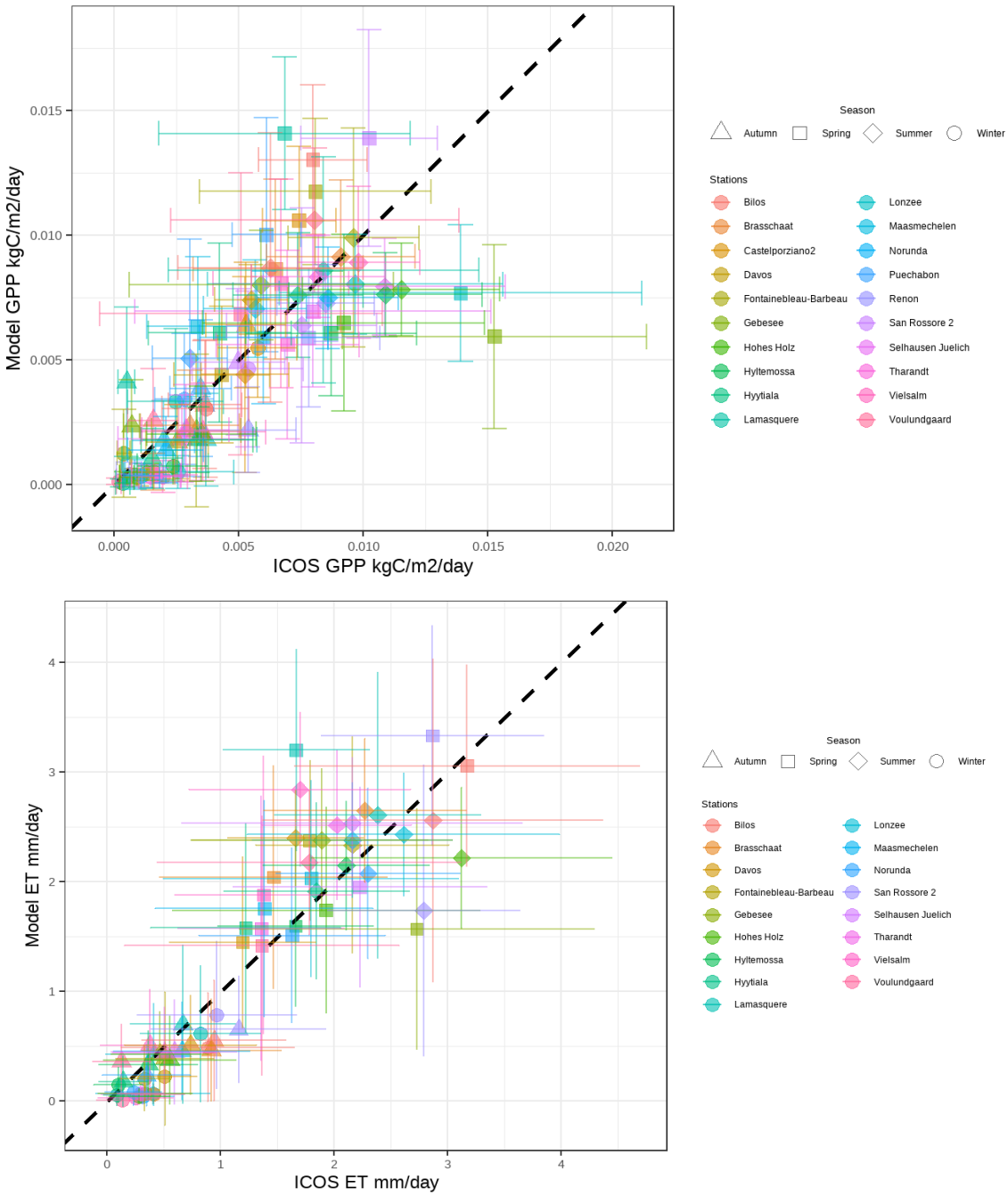

Figure 9. Scatter plots of ICOS GPP (top) and ET (bottom) vs LPJ-GUESS simulations. Each dot shows one simulation year, with separate icons for spring and autumn. Error bars show the standard deviation of daily values. The black dashed line is the 1:1 line.

5.4 Storm disturbances

Figure 10 shows the simulated wind damage in a severe storm averaged over the period 1986-2020 and how this combines with annual storm probability to produce an estimate of annual wind damage. The results across the simulation domain are benchmarked to observation-based damage statistics from the DFDE database (Table 2). The relationship between the modelled and reported damage was used to get the calibrated numbers. Reported damage comes from the DFDE database (Patacca et al., 2023) and modelled damage was calculated

from simulated damage in a severe storm and wind damage probability. For France and the Czech Republic, which have very high observed damage, the calibrated storm damage model underestimates damage, whilst for Spain with low damage (and to some extent Finland) it overestimates. A reason for underestimation in Czechia could be the difficulty in separating storm and spruce bark beetle damage in the most recent years (years 2017-2019 have about 18% of the damage of the whole period). For the other large countries Germany, Sweden and Poland the damage is similar to DFDE statistics.

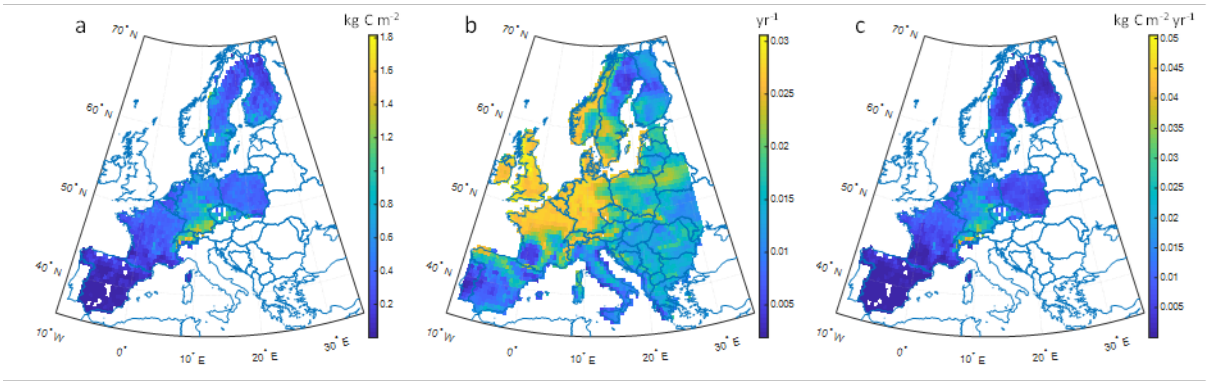

Figure 10. a) Simulated mean wind damage in a severe storm over the European Application Domain. **b)** annual wind disturbance probability map. **c)** expected annual wind damage; a result of multiplying the data in maps 3a and 3b. These are the results post-calibration.

Table 2. Total reported and modelled wind damage 1986-2020 by country (million m^3).

Country	Spain	France	Belgium	Nether-lands	Switzer-land	Sweden	Czech Republic	Germany	Poland	Finland
Code	ES	FR	BE	NL	CH	SE	CZ	DE	PL	FI
Report	4.1	246.8	5.6	0.7	26.2	157.4	99.8	192.9	59.4	32.0
Mod uncal.	12.1	75.2	4.8	2.6	22.7	127.0	27.7	147.0	50.3	56.6
Mod cal.	18.0	111.6	7.1	3.8	33.8	188.6	41.1	218.4	74.7	84.1

5.5 Fire disturbances

The spatial distribution of burned area predicted by SIMFIRE-EU aligns relatively well with the observed patterns, especially in southern Europe, and the total annual burned area in Europe falls within the range of observed data (Figure 11). Discrepancies between spatial patterns of observed and modelled burned can largely be attributed to the fact that observations of burned area per year are spatially very heterogeneous and statistically do not follow a normal distribution, which makes it difficult for a simple model like SIMFIRE-EU to accurately replicate spatial patterns across regions. Moreover, local wildfire dynamics driven by the distinct fire behaviours of the different tree species are not considered by SIMFIRE-EU. Because the agent attribution algorithm in the forest disturbance observation dataset is latitude-dependent,

the observed burned area noticeably increases below a certain latitude, therefore comparison between SIMFIRE-EU and the observations is most valid in Southern Europe.

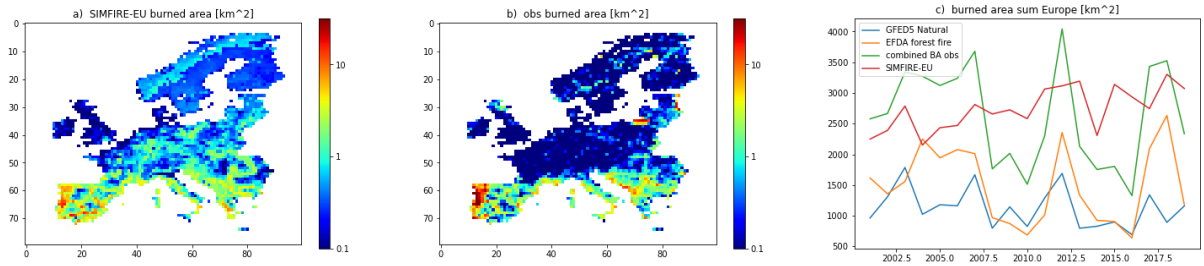

Figure 11. Mean 2001-2019 burned area as predicted by SIMFIRE-EU (left), observed by a combination of remote sensing products (center) and annual European burned area (right) predicted and observed. Burned area in km² per grid cell resulting from multiplying burned area rates with respective land-cover type areas. Note the log colour scale.

6. Demonstration applications

6.1 Outputs from satellite disturbances.

To demonstrate the satellite-driven disturbance capability we applied satellite-derived forcing of historically observed disturbances annually over the period 2011-2022 (Section 3). Coupling LPJ-GUESS to the observations in this way allows to derive downstream quantities that are not directly observed. Some examples of these are shown in Figure 11. LPJ-GUESS can directly convert the canopy area losses from satellite into estimates of vegetation carbon killed (Figure 11a,b), showing how these vary spatially and as a function of time. It can also relate these losses to other ecosystem aspects, such as total C flux associated with tree death (Figure 11c), which cannot be assessed from satellite and are challenging to derive by directly combining satellite and inventory measurements because of the very different forms of the observations. In a similar vein, it can relate estimates of the C flux from clearcut harvests to harvests of all types, allowing to smoothly combine information from satellite and ground-based sources to make combined assessments of harvest dynamics (Figure 11d). Because the satellite disturbance observations are regularly updated to the previous year (Viana-Soto and Senf, 2024) the satellite-driven disturbance capability also allows to update stand structure based on forest inventory to the present day, maintaining maximum consistency with reality and therefore an optimal starting point for future simulations.

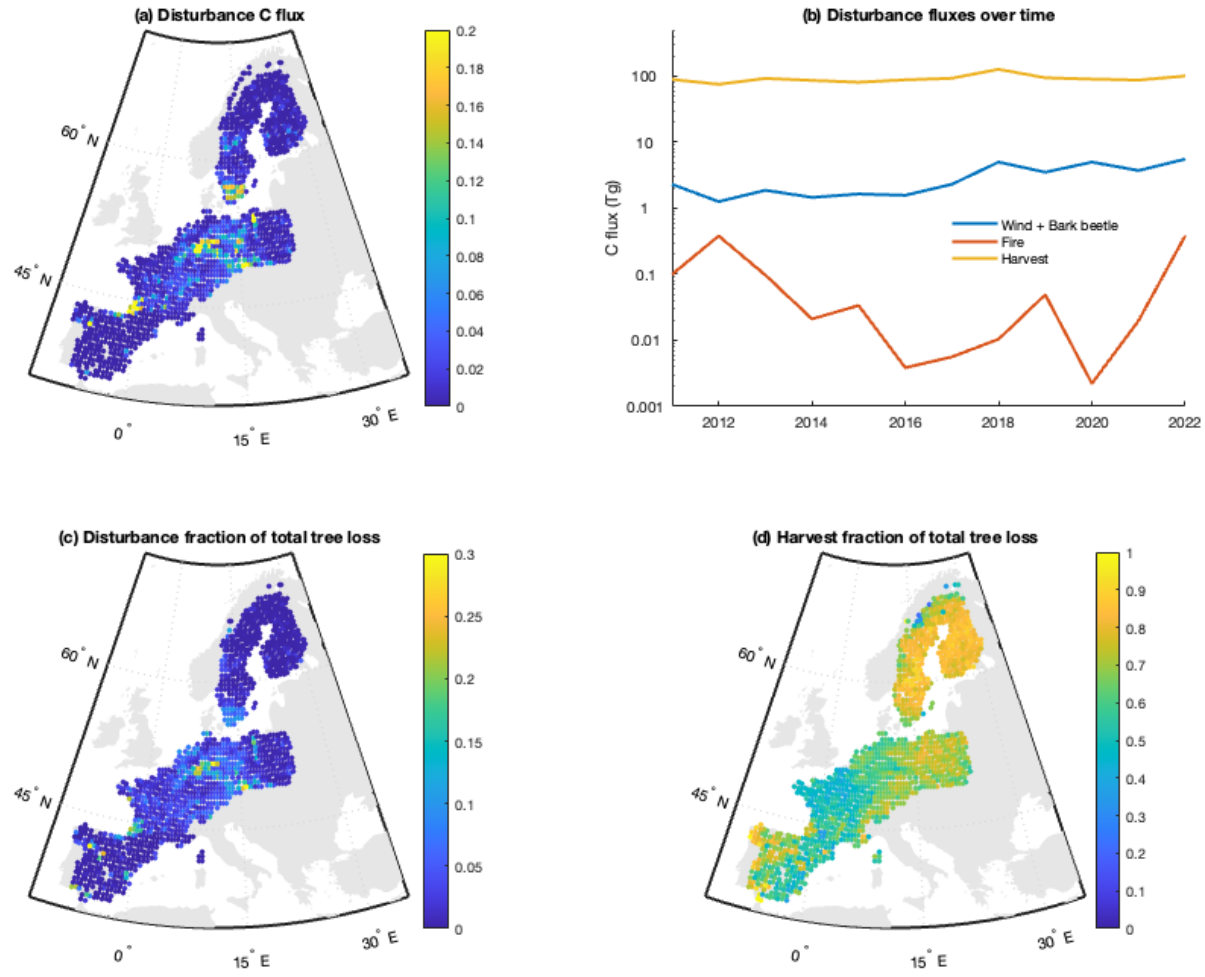

Figure 12. Example quantities derived based on observed stand-replacing disturbance rates using LPJ-GUESS. Maps present averages over the period 2011-2022, whilst panel b shows the summed C flux of vegetation death over the whole simulation domain.

6.2 Initialisation of forest structure and composition from forest inventories

In this section, we apply the approach outlined in §4.6 to national forest inventory data from Sweden and Germany, initialising the simulations in the year 2005, using the NFI census that best corresponded to that year. The sample set of 30 plots per grid cell yielded very similar results for carbon mass per forest area in 2005 compared to the full dataset. In Germany, the carbon mass was 11.99 and 11.90 kg/m², while in Sweden it was 4.12 and 4.14 kg/m² across the two samples, with good consistency between the samples spatially (Figure 12a).

We initialised LPJ-GUESS with the NFI census data closest to the year 2005. The model goes through an initial period during which trees which exist in the real world, but which cannot exist in the simplified physics and biology of the model world, die. This “relaxation period” takes about 5 years to resolve. As a result, we consider the effective year of initialisation to be 2010. We then compared the biomass estimates for 2010 with the NFI census data for the same year, aggregated to the grid cell level (Figure 12b). The fit between the model and observations remains good but is somewhat degraded compared to the original sample shown in Figure

12a. The model calculated higher biomass in Sweden and lower biomass in Germany compared to the NFI data. Specifically, the estimated carbon mass in Germany was 10.25 kg/m², while the NFI reported 12.19 kg/m². In Sweden, the model estimated carbon mass at 4.95 kg/m², compared to the NFI estimate of 4.45 kg/m². The lower modelled biomass in Germany in 2010 follows as some of the heavily populated stands found in reality cannot be reproduced in the model world and the biomass therefore “relaxes” to consistency with the model world through the death of some trees (Figure 13). We note, however, that the census interval of the German NFI (Table A5.1) is not short enough to clearly differentiate biomass in 2005 and 2010, meaning that the comparisons, whilst informative, are imprecise.

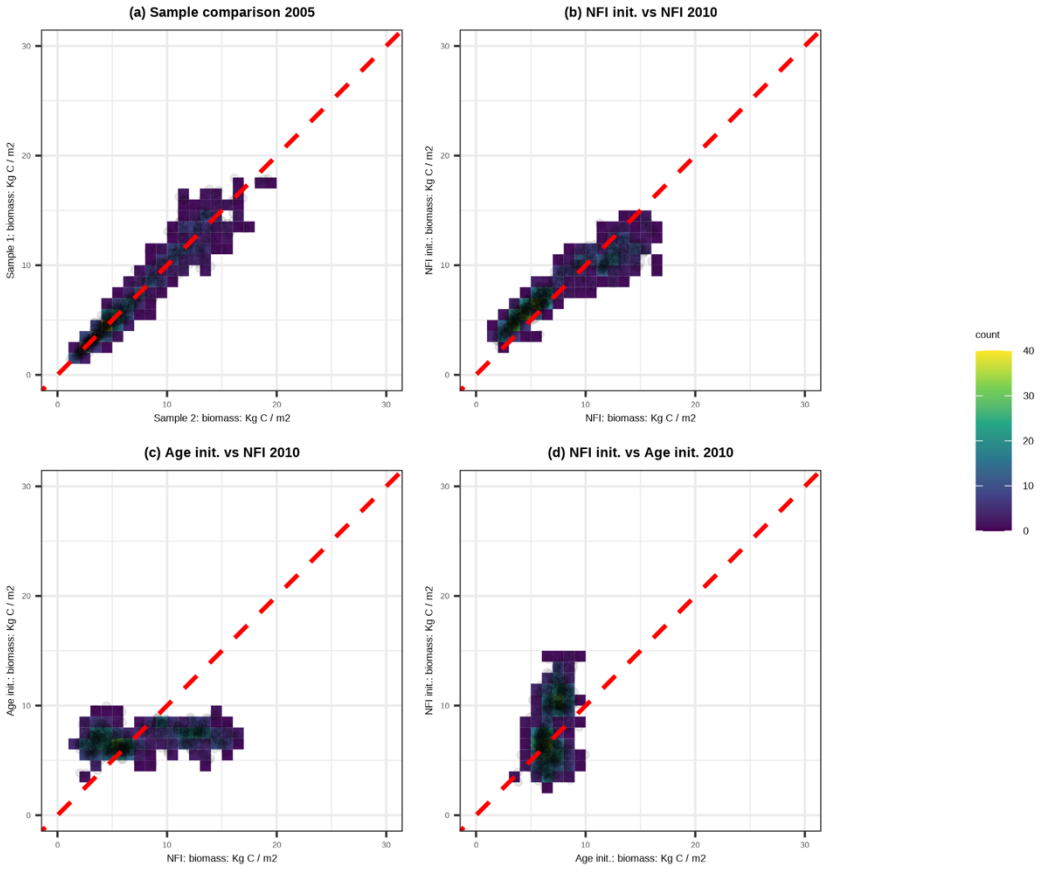

Figure 13. NFI initialisation compared to age initialisation. (a) Biomass mass comparison between the sample used to initialise LPJ-GUESS and all plots in each grid cell. (b) Biomass comparison between LPJ-GUESS initialised from NFI and grid-cell-level NFI observations in 2010. (c) Equivalent comparison for age initialisation against grid-cell-level NFI observations. (d) Comparison of NFI and age initialisation methods. Brighter colours indicate a higher density of grid cells.

When comparing the NFI initialisation method with the stand age initialisation described in §3, we observed significant differences in vegetation carbon after initialising the model in 2005 (Figures 12c,d, 13). In Germany, the NFI initialised biomass in 2010 was much higher than achieved with the age initialisation. This difference primarily results from the low growth bias for, especially southern, Germany compared to observations that was identified in §5.1. However, it can also result from the impact of unknown levels of thinning and mortality that have occurred within the stand since its establishment, which the age initialisation approach

does not have information for. Following initialisation, the trajectory of biomass change is similar in both initialisation methods. In contrast, Sweden exhibited a relatively low initial carbon mass from the NFI, compared to that from age initialisation, which adjusted over the first year and then increased rapidly, primarily due to new plant establishments.

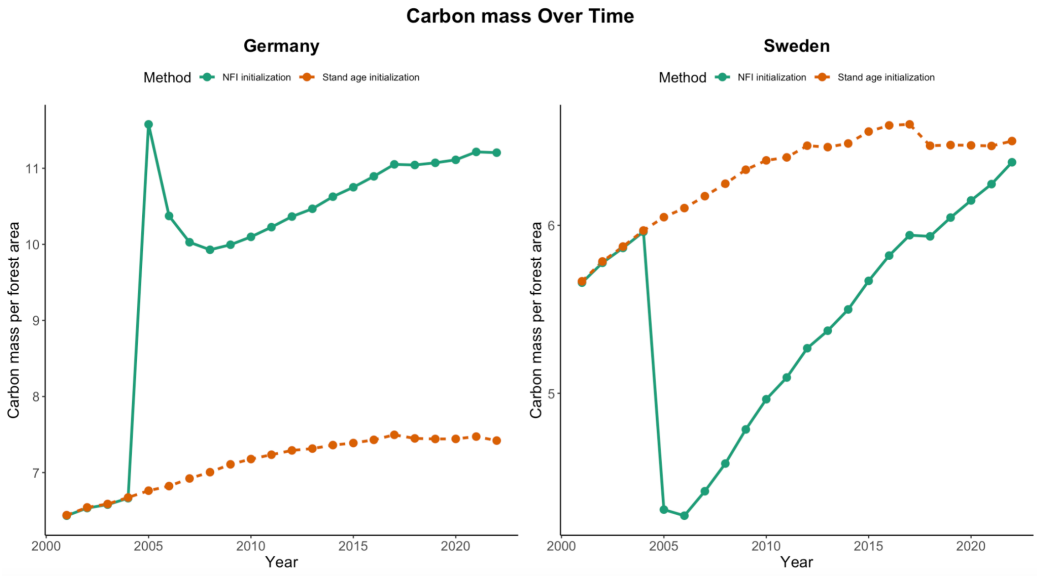

Figure 14. Temporal changes in carbon mass under two initialization methods in Germany and Sweden. Note different y-axis scales.

The NFI initialisation thus largely addresses both the cumulative effect of historical growth biases and the unknown management and mortality that occurred during the period of stand development. We conclude that NFI initialisation substantially improved carbon mass predictions compared to stand-age initialisation (Figure 12). The level of biomass “relaxation” seen in the Germany case study, however, indicates that further work to reduces structural biases in the model representation of forests will allow to improve the skill of this approach. We expect that these biases relate to allometric representations of trees how trees are structured in the model patches. We also note, however, that the allometries used to convert the measured DBH to biomass in forest inventories are not direct measurements and thus also contain a measure of uncertainty.

7. Conclusions

We have presented here extensive updates to the LPJ-GUESS dynamic vegetation model to improve its capability to simulate the state and dynamics of European forest. The updated model offers improved performance on forest-specific metrics at the European scale compared to the previous release of LPJ-GUESS. The detailed representation of forest demography in LPJ-GUESS enabled the leveraging of the power of forest inventory data to carry out an extensive benchmarking of the model performance which, for forests, offers a powerful constraint beyond the flux-tower-based and satellite-dataset approach commonly used to evaluate models of this type (Anav et al., 2013; Kelley et al., 2013; Seiler et al., 2022). The benchmarking revealed biases in woody growth rate, GPP and stem density that we were able to reduce through a calibration process. Work is required to further reduce the growth

bias identified, however, the model already offers a useful process-based complement to empirical growth simulators, enabling the exploration of the impact of novel environmental and management conditions on forest growth, structure and carbon cycling.

The updated version of LPJ-GUESS includes new capabilities to represent and explore the effects of disturbances, including the three major disturbance agents active in Europe: storm, fire and bark beetles (Patacca et al., 2023; Seidl et al., 2014). As well as the new/updated disturbance sub-models, the new initialisation capability provides a major step forward, given that forest disturbance risk is strongly dependent on the state of the forest. Predicting accurate damage levels for fire, wind and bark beetles under novel environments remains highly uncertain, however the disturbance sub-models presented offer the capability to explore this uncertainty, and we anticipate that they will prove powerful in assessing the direction of changes, as well as to rank forest stands according to their vulnerability. The prognostic disturbance models for the three disturbance agents are linked, either directly in the case of windthrown spruce trees acting as brood material bark beetles or because of the effect that they have on state variables. For instance fires can reduce the height of other stands in the grid cell, increasing the vulnerability of remaining stands to windthrow. These links will allow to explore some of the potential for interactions between disturbances.

The extensive integration of observations through initialisation from NFI tree size and composition, forcing historical disturbance rates using satellite-based maps and assessing harvest probability based on extensive repeated NFI observations also opens new opportunities in the field of forest monitoring. The model provides a complete, internally consistent and wall-to-wall set of states and fluxes that is not available from any individual observation platform. Constraining some of the most uncertain components of forest dynamics can allow to utilise the model to gain insights that would not otherwise be readily available at continental scales, for instance the net annual exchange of carbon between forests and the atmosphere, the direct impact and legacy of disturbances on ecosystem carbon fluxes, and the attribution of observed trends between different environmental drivers. The model allows to consistently compare satellite observations made on a canopy-area basis with NFI observations made on a stem basis. LPJ-GUESS directly simulates both of these components linked observation-based tree allometries and by tree packing constraints. As such the model can potentially be a useful tool in unpicking apparent differences between, for instance, trends in tree mortality or harvest from satellite products and from NFI (Palahí et al., 2021; Scheel et al., 2022).

Whilst the developments herein have focused on the European context, all of them have potential applications beyond the bounds of that continent. Key in most instances is the availability of the types of observations on which they rely. Several of the developments described in this paper were indeed only possible because of cooperation between model developers and the scientists and organisations behind the ground-based monitoring of Europe’s forests. Ground-based inventory observations provide unparalleled information about forest structure, dynamics and composition across large scales, much of which cannot be directly or accurately derived from remote sensing. Maintaining and further building such cooperations is key to making the most of the opportunities for improved digital representations of our forests.

Acknowledgements

The model developments described in this paper have been funded under the European Union's Horizon Europe research and innovation programme (grant agreement numbers 101059888, CLIMB-Forest; 101056755, ForestPaths; 101084481, FORWARDS; 101081251 wildE; 101000574, RESONATE) and the Horizon 2020 programme (grant agreement no. 758873, TreeMort), as well as from the ForestValue programme, the European Commission, Vinnova, the Swedish Energy Agency and Formas for the project FORECO. This study is a contribution to the Swedish government's strategic research areas BECC and MERGE and the Nature-based Future Solutions profile area at Lund University. We thank the TRY database (request number: 6033) for providing the SLA trait information and Andreas Krause for reviewing the draft manuscript. We extend our gratitude to the institutions and teams behind the Flemish Forest Inventory, CzechTerra Landscape Inventory, Finnish Forest Health Monitoring Network, Dutch Forest Inventory, Polish National Forest Inventory, Spanish National Forest Inventory, Swedish National Forest Inventory, and the United States Forest Service Forest Inventory and Analysis research program. The Spanish National Forest Inventory is available thanks to the Ministry for the Ecological Transition and the Demographic Challenge and the Polish National Forest Inventory was funded by the General State Directorate of Forests.

References

Anav, A., Friedlingstein, P., Kidston, M., Bopp, L., Ciais, P., Cox, P., Jones, C., Jung, M., Myneni, R., and Zhu, Z.: Evaluating the land and ocean components of the global carbon cycle in the CMIP5 earth system models, J Clim, 26, 6801–6843, https://doi.org/10.1175/JCLI-D-12-00417.1, 2013.

Aszalós, R., Thom, D., Aakala, T., Angelstam, P., Brūmelis, G., Gálhidy, L., Gratzer, G., Hlásny, T., Katzensteiner, K., Kovács, B., Knoke, T., Larrieu, L., Motta, R., Müller, J., Ódor, P., Roženbergar, D., Paillet, Y., Pitar, D., Standovár, T., Svoboda, M., Szwagrzyk, J., Toscani, P., and Keeton, W. S.: Natural disturbance regimes as a guide for sustainable forest management in Europe, Ecological Applications, 32, https://doi.org/10.1002/eap.2596, 2022.

Atkin, O. K., Bloomfield, K. J., Reich, P. B., Tjoelker, M. G., Asner, G. P., Bonal, D., Bönisch, G., Bradford, M. G., Cernusak, L. A., Cosio, E. G., Creek, D., Crous, K. Y., Domingues, T. F., Dukes, J. S., Egerton, J. J. G., Evans, J. R., Farquhar, G. D., Fyllas, N. M., Gauthier, P. P. G., Gloor, E., Gimeno, T. E., Griffin, K. L., Guerrieri, R., Heskel, M. A., Huntingford, C., Ishida, F. Y., Kattge, J., Lambers, H., Liddell, M. J., Lloyd, J., Lusk, C. H., Martin, R. E., Maksimov, A. P., Maximov, T. C., Malhi, Y., Medlyn, B. E., Meir, P., Mercado, L. M., Mirotchnick, N., Ng, D., Niinemets, Ü., O'Sullivan, O. S., Phillips, O. L., Poorter, L., Poot, P., Prentice, I. C., Salinas, N., Rowland, L. M., Ryan, M. G., Sitch, S., Slot, M., Smith, N. G., Turnbull, M. H., VanderWel, M. C., Valladares, F., Veneklaas, E. J., Weerasinghe, L. K., Wirth, C., Wright, I. J., Wythers, K. R., Xiang, J., Xiang, S., and Zaragoza-Castells, J.: Global variability in leaf respiration in relation to climate, plant functional types and leaf traits, New Phytologist, 206, 614–636, https://doi.org/10.1111/nph.13253, 2015.

Bayer, A. D., Lindeskog, M., Pugh, T. A. M., Anthoni, P. M., Fuchs, R., and Arneth, A.: Uncertainties in the land-use flux resulting from land-use change reconstructions and gross land transitions, Earth System Dynamics, 8, 91–111, https://doi.org/10.5194/esd-8-91-2017, 2017.

Besnard, S., Koirala, S., Santoro, M., Weber, U., Nelson, J., Gütter, J., Herault, B., Kassi, J., N'Guessan, A., Neigh, C., Poulter, B., Zhang, T., and Carvalhais, N.: Mapping global forest age from forest inventories, biomass and climate data, Earth Syst Sci Data, 13, 4881–4896, https://doi.org/10.5194/essd-13-4881-2021, 2021.

Breidenbach, J., Granhus, A., Hylen, G., Eriksen, R., and Astrup, R.: A century of National Forest Inventory in Norway – informing past, present, and future decisions, For Ecosyst, 7, https://doi.org/10.1186/s40663-020-00261-0, 2020.

Buras, A., Rammig, A., and Zang, C. S.: The European Forest Condition Monitor: Using Remotely Sensed Forest Greenness to Identify Hot Spots of Forest Decline, Front Plant Sci, 12, https://doi.org/10.3389/fpls.2021.689220, 2021.

Cannell, M. G. R.: World forest biomass and primary production data, Academic Press, 1982.

Chave, J., Coomes, D., Jansen, S., Lewis, S. L., Swenson, N. G., and Zanne, A. E.: Towards a worldwide wood economics spectrum, Ecol Lett, 12, 351–366, https://doi.org/10.1111/j.1461-0248.2009.01285.x, 2009.

Chen, Y., Hall, J., van Wees, D., Andela, N., Hantson, S., Giglio, L., van der Werf, G. R., Morton, D. C., and Randerson, J. T.: Multi-decadal trends and variability in burned area from the fifth version of the Global Fire Emissions Database (GFED5), Earth Syst Sci Data, 15, 5227–5259, https://doi.org/10.5194/essd-15-5227-2023, 2023.

Chen, Y. Y., Gardiner, B., Pasztor, F., Blennow, K., Ryder, J., Valade, A., Naudts, K., Otto, J., McGrath, M. J., Planque, C., and Luyssaert, S.: Simulating damage for wind storms in the land surface model ORCHIDEE-CAN (revision 4262), Geosci Model Dev, 11, 771–791, https://doi.org/10.5194/gmd-11-771-2018, 2018.

Daigneault, A., Baker, J. S., Guo, J., Lauri, P., Favero, A., Forsell, N., Johnston, C., Ohrel, S. B., and Sohngen, B.: How the future of the global forest sink depends on timber demand, forest management, and carbon policies, Global Environmental Change, 76, https://doi.org/10.1016/j.gloenvcha.2022.102582, 2022.

European Commission: Proposal for a REGULATION OF THE EUROPEAN PARLIAMENT AND OF THE COUNCIL on a monitoring framework for resilient European forests, Brussels, 2023.

European Environment Agency: CORINE Land Cover 2018 (raster 100 m), Europe, 6-yearly - version 2020_20u1, May 2020 , 2023.

Friedlingstein, P., O'Sullivan, M., Jones, M. W., Andrew, R. M., Gregor, L., Hauck, J., Le Quéré, C., Luijkx, I. T., Olsen, A., Peters, G. P., Peters, W., Pongratz, J., Schwingshackl, C., Sitch, S., Canadell, J. G., Ciais, P., Jackson, R. B., Alin, S. R., Alkama, R., Arneth, A., Arora, V. K., Bates, N. R., Becker, M., Bellouin, N., Bittig, H. C., Bopp, L., Chevallier, F., Chini, L. P., Cronin, M., Evans, W., Falk, S., Feely, R. A., Gasser, T., Gehlen, M., Gkritzalis, T., Gloege, L., Grassi, G., Gruber, N., Gürses, Ö., Harris, I., Hefner, M., Houghton, R. A., Hurtt, G. C., Iida, Y., Ilyina, T., Jain, A. K., Jersild, A., Kadono, K., Kato, E., Kennedy, D., Klein Goldewijk, K., Knauer, J., Korsbakken, J. I., Landschützer, P., Lefèvre, N., Lindsay, K., Liu, J., Liu, Z., Marland, G., Mayot, N., McGrath, M. J., Metzl, N., Monacci, N. M., Munro, D. R., Nakaoka, S.-I., Niwa, Y., O'Brien, K., Ono, T., Palmer, P. I., Pan, N., Pierrot, D., Pocock, K., Poulter, B., Resplandy, L., Robertson, E., Rödenbeck, C., Rodriguez, C., Rosan, T. M., Schwinger, J., Séférian, R., Shutler, J. D., Skjelvan, I., Steinhoff, T., Sun, Q., Sutton, A. J., Sweeney, C., Takao, S., Tanhua, T., Tans, P. P., Tian, X., Tian, H., Tilbrook, B., Tsujino, H., Tubiello, F., van der Werf, G. R., Walker, A. P., Wanninkhof, R., Whitehead, C., Willstrand Wranne, A., et al.: Global Carbon Budget 2022, Earth Syst Sci Data, 14, 4811–4900, https://doi.org/10.5194/essd-14-4811-2022, 2022.

Friedlingstein, P., O'Sullivan, M., Jones, M. W., Andrew, R. M., Bakker, D. C. E., Hauck, J., Landschützer, P., Le Quéré, C., Luijkx, I. T., Peters, G. P., Peters, W., Pongratz, J., Schwingshackl, C., Sitch, S., Canadell, J. G., Ciais, P., Jackson, R. B., Alin, S. R., Anthoni, P., Barbero, L., Bates, N. R., Becker, M., Bellouin, N., Decharme, B., Bopp, L., Brasika, I. B. M., Cadule, P., Chamberlain, M. A., Chandra, N., Chau, T. T. T., Chevallier, F., Chini, L. P., Cronin, M., Dou, X., Enyo, K., Evans, W., Falk, S., Feely, R. A., Feng, L., Ford, D. J., Gasser, T., Ghattas, J., Gkritzalis, T., Grassi, G., Gregor, L., Gruber, N., Gürses, Ö., Harris, I., Hefner, M., Heinke, J., Houghton, R. A., Hurtt, G. C., Iida, Y., Ilyina, T., Jacobson, A. R., Jain, A., Jarníková, T., Jersild, A., Jiang, F., Jin, Z., Joos, F., Kato, E., Keeling, R. F., Kennedy, D., Goldewijk, K. K., Knauer, J., Korsbakken, J. I., Körtzinger, A., Lan, X., Lefèvre, N., Li, H., Liu, J., Liu, Z., Ma, L., Marland, G., Mayot, N., McGuire, P. C., McKinley, G. A., Meyer, G., Morgan, E. J., Munro, D. R., Nakaoka, S. I., Niwa, Y., O'Brien, K. M., Olsen, A., Omar, A. M., Ono, T., Paulsen, M., Pierrot, D., Pocock, K., Poulter, B., Powis, C. M., Rehder, G., Resplandy, L., Robertson, E., Rödenbeck, C., Rosan, T. M., Schwinger, J., Séférian, R., et al.: Global Carbon Budget 2023, Earth Syst Sci Data, 15, 5301–5369, https://doi.org/10.5194/essd-15-5301-2023, 2023.

Fuchs, R., Herold, M., Verburg, P. H., Clevers, J. G. P. W., and Eberle, J.: Gross changes in reconstructions of historic land cover/use for Europe between 1900 and 2010, Glob Chang Biol, 21, 299–313, https://doi.org/10.1111/gcb.12714, 2015.

Gardiner, B.: Wind damage to forests and trees: a review with an emphasis on planted and managed forests, Journal of Forest Research, 26, 248–266, https://doi.org/10.1080/13416979.2021.1940665, 2021.

Giglio, L., Randerson, J. T., van der Werf, G. R., Kasibhatla, P. S., Collatz, G. J., Morton, D. C., and DeFries, R. S.: Assessing variability and long-term trends in burned area by merging multiple satellite fire products, Biogeosciences, 7, 1171–1186, https://doi.org/10.5194/bg-7-1171-2010, 2010.

Giglio, L., Justice, C., Boschetti, L., and Roy, D.: MODIS/Terra+Aqua Burned Area Monthly L3 Global 500m SIN Grid V061., 2021.

Gustafson, A., Miller, P. A., Björk, R. G., Olin, S., and Smith, B.: Nitrogen restricts future sub-arctic treeline advance in an individual-based dynamic vegetation model, Biogeosciences, 18, 6329–6347, https://doi.org/10.5194/bg-18-6329-2021, 2021.

Hansen, M. C., Potapov, P. V., Moore, R., Hancher, M., Turubanova, S. A., Tyukavina, A., Thau, D., Stehman, S. V., Goetz, S. J., Loveland, T. R., Kommareddy, A., Egorov, A., Chini, L., Justice, C. O., and Townshend, J. R. G.: High-resolution global maps of 21st-century

forest cover change, Science (1979), 342, 850–853, https://doi.org/10.1126/science.1244693, 2013.
Hickler, T., Vohland, K., Feehan, J., Miller, P. A., Smith, B., Costa, L., Giesecke, T., Fronzek, S., Carter, T. R., Cramer, W., Kühn, I., and Sykes, M. T.: Projecting the future distribution of European potential natural vegetation zones with a generalized, tree species-based dynamic vegetation model, Global Ecology and Biogeography, 21, 50–63, https://doi.org/10.1111/j.1466-8238.2010.00613.x, 2012.
Hurtt, G. C., Chini, L., Sahajpal, R., Frolking, S., Bodirsky, B. L., Calvin, K., Doelman, J. C., Fisk, J., Fujimori, S., Goldewijk, K. K., Hasegawa, T., Havlik, P., Heinimann, A., Humpenöder, F., Jungclaus, J., Kaplan, J. O., Kennedy, J., Krisztin, T., Lawrence, D., Lawrence, P., Ma, L., Mertz, O., Pongratz, J., Popp, A., Poulter, B., Riahi, K., Shevliakova, E., Stehfest, E., Thornton, P., Tubiello, F. N., van Vuuren, D. P., and Zhang, X.: Harmonization of global land use change and management for the period 850-2100 (LUH2) for CMIP6, Geosci Model Dev, 13, 5425–5464, https://doi.org/10.5194/gmd-13-5425-2020, 2020.
Jönsson, A. M., Schroeder, L. M., Lagergren, F., Anderbrant, O., and Smith, B.: Guess the impact of Ips typographus-An ecosystem modelling approach for simulating spruce bark beetle outbreaks, Agric For Meteorol, 166–167, 188–200, https://doi.org/10.1016/j.agrformet.2012.07.012, 2012.
Jucker, T., Fischer, F. J., Chave, J., Coomes, D. A., Caspersen, J., Ali, A., Loubota Panzou, G. J., Feldpausch, T. R., Falster, D., Usoltsev, V. A., Adu-Bredu, S., Alves, L. F., Aminpour, M., Angoboy, I. B., Anten, N. P. R., Antin, C., Askari, Y., Muñoz, R., Ayyappan, N., Balvanera, P., Banin, L., Barbier, N., Battles, J. J., Beeckman, H., Bocko, Y. E., Bond-Lamberty, B., Bongers, F., Bowers, S., Brade, T., van Breugel, M., Chantrain, A., Chaudhary, R., Dai, J., Dalponte, M., Dimobe, K., Domec, J., Doucet, J., Duursma, R. A., Enríquez, M., van Ewijk, K. Y., Farfán-Rios, W., Fayolle, A., Forni, E., Forrester, D. I., Gilani, H., Godlee, J. L., Gourlet-Fleury, S., Haeni, M., Hall, J. S., He, J., Hemp, A., Hernández-Stefanoni, J. L., Higgins, S. I., Holdaway, R. J., Hussain, K., Hutley, L. B., Ichie, T., Iida, Y., Jiang, H., Joshi, P. R., Kaboli, H., Larsary, M. K., Kenzo, T., Kloeppel, B. D., Kohyama, T., Kunwar, S., Kuyah, S., Kvasnica, J., Lin, S., Lines, E. R., Liu, H., Lorimer, C., Loumeto, J., Malhi, Y., Marshall, P. L., Mattsson, E., Matula, R., Meave, J. A., Mensah, S., Mi, X., Momo, S., Moncrieff, G. R., Mora, F., Nissanka, S. P., O'Hara, K. L., Pearce, S., Pelissier, R., Peri, P. L., Ploton, P., Poorter, L., Pour, M. J., Pourbabaei, H., Dupuy-Rada, J. M., Ribeiro, S. C., Ryan, C., Sanaei, A., Sanger, J., Schlund, M., Sellan, G., et al.: Tallo: A global tree allometry and crown architecture database, Glob Chang Biol, 28, 5254–5268, https://doi.org/10.1111/gcb.16302, 2022.
Kelley, D. I., Prentice, I. C., Harrison, S. P., Wang, H., Simard, M., Fisher, J. B., and Willis, K. O.: A comprehensive benchmarking system for evaluating global vegetation models, Biogeosciences, 10, 3313–3340, https://doi.org/10.5194/bg-10-3313-2013, 2013.
Knorr, W., Kaminski, T., Arneth, A., and Weber, U.: Impact of human population density on fire frequency at the global scale, Biogeosciences, 11, 1085–1102, https://doi.org/10.5194/bg-11-1085-2014, 2014.
Knorr, W., Jiang, L., and Arneth, A.: Climate, CO2 and human population impacts on global wildfire emissions, Biogeosciences, 13, 267–282, https://doi.org/10.5194/bg-13-267-2016, 2016.
Krause, A., Arneth, A., Anthoni, P., and Rammig, A.: Legacy Effects from Historical Environmental Changes Dominate Future Terrestrial Carbon Uptake, Earths Future, 8, https://doi.org/10.1029/2020EF001674, 2020.
Kurz, W. A., Dymond, C. C., White, T. M., Stinson, G., Shaw, C. H., Rampley, G. J., Smyth, C., Simpson, B. N., Neilson, E. T., Trofymow, J. A., Metsaranta, J., and Apps, M. J.: CBM-CFS3: A model of carbon-dynamics in forestry and land-use change implementing IPCC standards, Ecol Modell, 220, 480–504, https://doi.org/10.1016/j.ecolmodel.2008.10.018, 2009.

Lagergren, F., Jönsson, A. M., Blennow, K., and Smith, B.: Implementing storm damage in a dynamic vegetation model for regional applications in Sweden, Ecol Modell, 247, 71–82, https://doi.org/10.1016/j.ecolmodel.2012.08.011, 2012.
Lagergren, F., Björk, R. G., Andersson, C., Belušić, D., Björkman, M. P., Kjellström, E., Lind, P., Lindstedt, D., Olenius, T., Pleijel, H., Rosqvist, G., and Miller, P. A.: Kilometre-scale simulations over Fennoscandia reveal a large loss of tundra due to climate warming, Biogeosciences, 21, 1093–1116, https://doi.org/10.5194/bg-21-1093-2024, 2024.
Lamarque, J. F., Dentener, F., McConnell, J., Ro, C. U., Shaw, M., Vet, R., Bergmann, D., Cameron-Smith, P., Dalsoren, S., Doherty, R., Faluvegi, G., Ghan, S. J., Josse, B., Lee, Y. H., Mackenzie, I. A., Plummer, D., Shindell, D. T., Skeie, R. B., Stevenson, D. S., Strode, S., Zeng, G., Curran, M., Dahl-Jensen, D., Das, S., Fritzsche, D., and Nolan, M.: Multi-model mean nitrogen and sulfur deposition from the atmospheric chemistry and climate model intercomparison project (ACCMIP): Evaluation of historical and projected future changes, Atmos Chem Phys, 13, 7997–8018, https://doi.org/10.5194/acp-13-7997-2013, 2013.
Lämås, T., Sängstuvall, L., Öhman, K., Lundström, J., Årevall, J., Holmström, H., Nilsson, L., Nordström, E. M., Wikberg, P. E., Wikström, P., and Eggers, J.: The multi-faceted Swedish Heureka forest decision support system: context, functionality, design, and 10 years experiences of its use, Frontiers in Forests and Global Change, 6, https://doi.org/10.3389/ffgc.2023.1163105, 2023.
Lange, S., Menz, C., Gleixner, S., Cucchi, M., Weedon, G. P., Amici, A., Bellouin, N., Müller Schmeid, H., Hersbach, H., Buontempo, C., and Cagnazzo, C.: WFDE5 over land merged with ERA5 over the ocean (W5E5 v2.0), 2021.
Lasch-Born, P., Suckow, F., Reyer, C. P. O., Gutsch, M., Kollas, C., Badeck, F.-W., Bugmann, H. K. M., Grote, R., Fürstenau, C., Lindner, M., and Schaber, J.: Description and evaluation of the process-based forest model 4C v2.2 at four European forest sites, Geosci Model Dev, 13, 5311–5343, https://doi.org/10.5194/gmd-13-5311-2020, 2020.
Lehtonen, A., Mäkipää, R., Heikkinen, J., Sievänen, R., and Liski, J.: Biomass expansion factors (BEFs) for Scots pine, Norway spruce and birch according to stand age for boreal forests, For Ecol Manage, 188, 211–224, https://doi.org/10.1016/j.foreco.2003.07.008, 2004.
Leuschner, C. and Meier, I. C.: The ecology of Central European tree species: Trait spectra, functional trade-offs, and ecological classification of adult trees, Perspect Plant Ecol Evol Syst, 33, 89–103, https://doi.org/10.1016/j.ppees.2018.05.003, 2018.
Liang, S., Cheng, J., Jia, K., Jiang, B., Liu, Q., Xiao, Z., Yao, Y., Yuan, W., Zhang, X., Zhao, X., and Zhou, J.: The Global Land Surface Satellite (GLASS) Product Suite, Bull Am Meteorol Soc, 102, E323–E337, https://doi.org/10.1175/BAMS-D-18-0341.1, 2021.
Lindeskog, M., Arneth, A., Bondeau, A., Waha, K., Seaquist, J., Olin, S., and Smith, B.: Implications of accounting for land use in simulations of ecosystem carbon cycling in Africa, Earth System Dynamics, 4, 385–407, https://doi.org/10.5194/esd-4-385-2013, 2013.
Lindeskog, M., Lagergren, F., Smith, B., and Rammig, A.: Accounting for forest management in the estimation of forest carbon balance using the dynamic vegetation model LPJ-GUESS (v4.0, r9710): Implementation and evaluation of simulations for Europe, Geosci Model Dev, 14, 6071–6112, https://doi.org/10.5194/gmd-2020-440, 2021.
Marini, L., Økland, B., Jönsson, A. M., Bentz, B., Carroll, A., Forster, B., Grégoire, J. C., Hurling, R., Nageleisen, L. M., Netherer, S., Ravn, H. P., Weed, A., and Schroeder, M.: Climate drivers of bark beetle outbreak dynamics in Norway spruce forests, Ecography, 40, 1426–1435, https://doi.org/10.1111/ecog.02769, 2017.
Miller, P. A., Giesecke, T., Hickler, T., Bradshaw, R. H. W., Smith, B., Seppä, H., Valdes, P. J., and Sykes, M. T.: Exploring climatic and biotic controls on Holocene vegetation change in Fennoscandia, Journal of Ecology, 96, 247–259, https://doi.org/10.1111/j.1365-2745.2007.01342.x, 2008.
Mishra, A., Humpenöder, F., Churkina, G., Reyer, C. P. O., Beier, F., Bodirsky, B. L., Schellnhuber, H. J., Lotze-Campen, H., and Popp, A.: Land use change and carbon emissions of a transformation to timber cities, Nat Commun, 13, https://doi.org/10.1038/s41467-022-32244-w, 2022.

Naudts, K., Chen, Y., McGrath, M. J., Ryder, J., Valade, A., Otto, J., and Luyssaert, S.: Europe's forest management did not mitigate climate warming, Science (1979), 351, 597–600, https://doi.org/10.1126/science.aad7270, 2016.
Nord, J., Anthoni, P., Gregor, K., Gustafson, A., Hantson, S., Lindeskog, M., Meyer, B., Miller, P., Nieradzik, L., Olin, S., Papastefanou, P., Smith, B., Tang, J., and Wårlind, D.: LPJ-GUESS Release v4.1.1 model code, 2021.
Olin, S., Lindeskog, M., Pugh, T. A. M., Schurgers, G., and Wårlind, D.: Soil carbon management in large-scale Earth system modelling: implications for crop yields and nitrogen leaching, Earth System Dynamics Discussions, 6, 1047–1100, https://doi.org/10.5194/esdd-6-1047-2015, 2015.
Palahí, M., Valbuena, R., Senf, C., Acil, N., Pugh, T. A. M., Sadler, J., Seidl, R., Potapov, P., Gardiner, B., Hetemäki, L., Chirici, G., Francini, S., Hlásny, T., Lerink, B. J. W., Olsson, H., González Olabarria, J. R., Ascoli, D., Asikainen, A., Bauhus, J., Berndes, G., Donis, J., Fridman, J., Hanewinkel, M., Jactel, H., Lindner, M., Marchetti, M., Marušák, R., Sheil, D., Tomé, M., Trasobares, A., Verkerk, P. J., Korhonen, M., and Nabuurs, G.-J.: Concerns about reported harvests in European forests, Nature, 592, E15–E17, https://doi.org/10.1038/s41586-021-03292-x, 2021.
Patacca, M., Lindner, M., Lucas-Borja, M. E., Cordonnier, T., Fidej, G., Gardiner, B., Hauf, Y., Jasinevičius, G., Labonne, S., Linkevičius, E., Mahnken, M., Milanovic, S., Nabuurs, G., Nagel, T. A., Nikinmaa, L., Panyatov, M., Bercak, R., Seidl, R., Ostrogović Sever, M. Z., Socha, J., Thom, D., Vuletic, D., Zudin, S., and Schelhaas, M.: Significant increase in natural disturbance impacts on European forests since 1950, Glob Chang Biol, 29, 1359–1376, https://doi.org/10.1111/gcb.16531, 2023.
Poulter, B., Aragão, L., Andela, N., Bellassen, V., Ciais, P., Kato, T., Lin, X., Nachin, B., Luyssaert, S., Pederson, N., Peylin, P., Piao, S., Pugh, T., Saatchi, S., Schepaschenko, D., Schelhaas, M., and Shivdenko, A.: The global forest age dataset and its uncertainties (GFADv1.1), https://doi.org/doi.pangaea.de/10.1594/PANGAEA.897392, 2019.
Pucher, C., Neumann, M., and Hasenauer, H.: An Improved Forest Structure Data Set for Europe, Remote Sens (Basel), 14, 395, https://doi.org/10.3390/rs14020395, 2022.
Pugh, T. A. M., Arneth, A., Kautz, M., Poulter, B., and Smith, B.: Important role of forest disturbances in the global biomass turnover and carbon sinks, Nat Geosci, 12, 730–735, https://doi.org/10.1038/s41561-019-0427-2, 2019a.
Pugh, T. A. M., Lindeskog, M., Smith, B., Poulter, B., Arneth, A., Haverd, V., and Calle, L.: Role of forest regrowth in global carbon sink dynamics, Proc Natl Acad Sci U S A, 116, 4382–4387, https://doi.org/10.1073/pnas.1810512116., 2019b.
Pugh, T. A. M., Rademacher, T., Shafer, S. L., Steinkamp, J., Barichivich, J., Beckage, B., Haverd, V., Harper, A., Heinke, J., Nishina, K., Rammig, A., Sato, H., Arneth, A., Hantson, S., Hickler, T., Kautz, M., Quesada, B., Smith, B., and Thonicke, K.: Understanding the uncertainty in global forest carbon turnover, Biogeosciences, 17, 3961–3989, https://doi.org/10.5194/bg-17-3961-2020, 2020.
Le Quéré, C., Andres, R. J., Boden, T., Conway, T., Houghton, R. A., House, J. I., Marland, G., Peters, G. P., Van Der Werf, G. R., Ahlström, A., Andrew, R. M., Bopp, L., Canadell, J. G., Ciais, P., Doney, S. C., Enright, C., Friedlingstein, P., Huntingford, C., Jain, A. K., Jourdain, C., Kato, E., Keeling, R. F., Klein Goldewijk, K., Levis, S., Levy, P., Lomas, M., Poulter, B., Raupach, M. R., Schwinger, J., Sitch, S., Stocker, B. D., Viovy, N., Zaehle, S., and Zeng, N.: The global carbon budget 1959-2011, Earth Syst Sci Data, 5, 165–185, https://doi.org/10.5194/essd-5-165-2013, 2013.
Le Quéré, C., Barbero, L., Hauck, J., Andrew, R. M., Canadell, J. G., Sitch, S., and Korsbakken, J. I.: Global Carbon Budget 2016 Global Carbon Budget 2016, Earth Syst Sci Data, 0, 2141–2194, 2018.
Rabin, S. S., Melton, J. R., Lasslop, G., Bachelet, D., Forrest, M., Hantson, S., Kaplan, J. O., Li, F., Mangeon, S., Ward, D. S., Yue, C., Arora, V. K., Hickler, T., Kloster, S., Knorr, W., Nieradzik, L., Spessa, A., Folberth, G. A., Sheehan, T., Voulgarakis, A., Kelley, D. I., Colin Prentice, I., Sitch, S., Harrison, S., and Arneth, A.: The Fire Modeling Intercomparison Project (FireMIP), phase 1: Experimental and analytical protocols with detailed model

descriptions, Geosci Model Dev, 10, 1175–1197, https://doi.org/10.5194/gmd-10-1175-2017, 2017.
Rabin, S. S., Alexander, P., Henry, R., Anthoni, P., Pugh, T. A. M., Rounsevell, M., and Arneth, A.: Impacts of future agricultural change on ecosystem service indicators, Earth System Dynamics, 11, 357–376, https://doi.org/10.5194/esd-11-357-2020, 2020.
Rabin, S. S., Gérard, F. N., and Arneth, A.: The influence of thinning and prescribed burning on future forest fires in fire-prone regions of Europe, Environmental Research Letters, 17, 055010, https://doi.org/10.1088/1748-9326/ac6312, 2022.
Rammer, W. and Seidl, R.: A scalable model of vegetation transitions using deep neural networks, Methods Ecol Evol, 10, 879–890, https://doi.org/10.1111/2041-210X.13171, 2019.
Repo, A., Rajala, T., Henttonen, H. M., Lehtonen, A., Peltoniemi, M., and Heikkinen, J.: Age-dependence of stand biomass in managed boreal forests based on the Finnish National Forest Inventory data, For Ecol Manage, 498, https://doi.org/10.1016/j.foreco.2021.119507, 2021.
Santoro, M., Cartus, O., Carvalhais, N., Rozendaal, D. M. A., Avitabile, V., Araza, A., De Bruin, S., Herold, M., Quegan, S., Rodríguez-Veiga, P., Balzter, H., Carreiras, J., Schepaschenko, D., Korets, M., Shimada, M., Itoh, T., Moreno Martínez, Á., Cavlovic, J., Gatti, R. C., Da Conceição Bispo, P., Dewnath, N., Labrière, N., Liang, J., Lindsell, J., Mitchard, E. T. A., Morel, A., Pacheco Pascagaza, A. M., Ryan, C. M., Slik, F., Vaglio Laurin, G., Verbeeck, H., Wijaya, A., and Willcock, S.: The global forest above-ground biomass pool for 2010 estimated from high-resolution satellite observations, Earth Syst Sci Data, 13, 3927–3950, https://doi.org/10.5194/essd-13-3927-2021, 2021.
Scheel, M., Lindeskog, M., Smith, B., Suvanto, S., and Pugh, T. A. M.: Increased Central European forest mortality explained by higher harvest rates driven by enhanced productivity, Environmental Research Letters, 17, https://doi.org/10.1088/1748-9326/ac9635, 2022.
Schelhaas, M. J., Fridman, J., Hengeveld, G. M., Henttonen, H. M., Lehtonen, A., Kies, U., Krajnc, N., Lerink, B., Dhubháin, Á. N., Polley, H., Pugh, T. A. M., Redmond, J. J., Rohner, B., Temperli, C., Vayreda, J., and Nabuurs, G. J.: Actual European forest management by region, tree species and owner based on 714,000 re-measured trees in national forest inventories, PLoS One, 13, e0207151, https://doi.org/10.1371/journal.pone.0207151, 2018.
Schelhaas, M.-J., Hengeveld, G., Filipek, S., König, L., Lerink, B., Staritsky, I., de Jong, A., and Nabuurs, G.-J.: EFISCEN-Space 1.0 model documentation and manual, 2022.
Seidl, R., Schelhaas, M. J., Rammer, W., and Verkerk, P. J.: Increasing forest disturbances in Europe and their impact on carbon storage, Nat Clim Chang, 4, 806–810, https://doi.org/10.1038/nclimate2318, 2014.
Seiler, C., Melton, J. R., Arora, V. K., Sitch, S., Friedlingstein, P., Anthoni, P., Goll, D., Jain, A. K., Joetzjer, E., Lienert, S., Lombardozzi, D., Luyssaert, S., Nabel, J. E. M. S., Tian, H., Vuichard, N., Walker, A. P., Yuan, W., and Zaehle, S.: Are Terrestrial Biosphere Models Fit for Simulating the Global Land Carbon Sink?, J Adv Model Earth Syst, 14, https://doi.org/10.1029/2021MS002946, 2022.
Senf, C. and Seidl, R.: Mapping the forest disturbance regimes of Europe, Nat Sustain, 4, 63–70, https://doi.org/10.1038/s41893-020-00609-y, 2021.
Severino, L. G., Kropf, C. M., Afargan-Gerstman, H., Fairless, C., de Vries, A. J., Domeisen, D. I. V., and Bresch, D. N.: Projections and uncertainties of winter windstorm damage in Europe in a changing climate, Natural Hazards and Earth System Sciences, 24, 1555–1578, https://doi.org/10.5194/nhess-24-1555-2024, 2024.
Sims, K., Reith, A., Bright, E., McKee, J., and Rose, A.: LandScan Global 2021, 2022.
Sitch, S., Smith, B., Prentice, I. C., Arneth, A., Bondeau, A., Cramer, W., Kaplan, J. O., Levis, S., Lucht, W., Sykes, M. T., Thonicke, K., and Venevsky, S.: Evaluation of ecosystem dynamics, plant geography and terrestrial carbon cycling in the LPJ dynamic global vegetation model, Glob Chang Biol, 9, 161–185, https://doi.org/10.1046/j.1365-2486.2003.00569.x, 2003.
Smith, B., Prentice, I. C., and Sykes, M. T.: Representation of vegetation dynamics in the modelling of terrestrial ecosystems: Comparing two contrasting approaches within European

climate space, Global Ecology and Biogeography, 10, 621–637, https://doi.org/10.1046/j.1466-822X.2001.00256.x, 2001.
Smith, B., Wårlind, D., Arneth, a., Hickler, T., Leadley, P., Siltberg, J., and Zaehle, S.: Implications of incorporating N cycling and N limitations on primary production in an individual-based dynamic vegetation model, Biogeosciences, 11, 2027–2054, https://doi.org/10.5194/bg-11-2027-2014, 2014.
Suvanto, S., Esquivel-Muelbert, A., Schelhaas, M.-J., Astigarraga, J., Astrup, R., Cienciala, E., Fridman, J., Henttonen, H. M., Kunstler, G., Kändler, G., König, L. A., Ruiz-Benito, P., Senf, C., Stadelmann, G., Starcevic, A., Talarczyk, A., Zavala, M. A., and Pugh, T. A.: Understanding Europe's forest harvest regimes, EarthArXiv, https://eartharxiv.org/repository/view/5858/, 2023.
Tagesson, T., Tian, F., Schurgers, G., Horion, S., Scholes, R., Ahlström, A., Ardö, J., Moreno, A., Madani, N., Olin, S., and Fensholt, R.: A physiology-based Earth observation model indicates stagnation in the global gross primary production during recent decades, Glob Chang Biol, 27, 836–854, https://doi.org/10.1111/gcb.15424, 2021.
Talvitie, I., Kinnunen, A., Amiri, A., and Junnila, S.: Can future cities grow a carbon storage equal to forests?, Environmental Research Letters, 18, https://doi.org/10.1088/1748-9326/acc677, 2023.
Teobaldelli, M., Somogyi, Z., Migliavacca, M., and Usoltsev, V. A.: Generalized functions of biomass expansion factors for conifers and broadleaved by stand age, growing stock and site index, For Ecol Manage, 257, 1004–1013, https://doi.org/10.1016/j.foreco.2008.11.002, 2009.
Thonicke, K., Spessa, A., Prentice, I. C., Harrison, S. P., Dong, L., and Carmona-Moreno, C.: The influence of vegetation, fire spread and fire behaviour on biomass burning and trace gas emissions: results from a process-based model, Biogeosciences, 7, 1991–2011, https://doi.org/10.5194/bg-7-1991-2010, 2010.
Tomppo, E., Gschwantner, T., Lawrence, M., and McRoberts, R. E.: National Forest Inventories Pathways for Common Reporting, https://doi.org/10.1007/978-90-481-3233-1, 2010.
Ulyshen, M., Urban-Mead, K. R., Dorey, J. B., and Rivers, J. W.: Forests are critically important to global pollinator diversity and enhance pollination in adjacent crops, Biological Reviews, 98, 1118–1141, https://doi.org/10.1111/brv.12947, 2023.
Usoltsev, V. A.: Forest biomass of Northern Eurasia: Database and geography, 2001.
Viana-Soto, A. and Senf, C.: European Forest Disturbance Atlas (Version 2.1.1.), 2024.
Virtanen, P., Gommers, R., Oliphant, T. E., Haberland, M., Reddy, T., Cournapeau, D., Burovski, E., Peterson, P., Weckesser, W., Bright, J., van der Walt, S. J., Brett, M., Wilson, J., Millman, K. J., Mayorov, N., Nelson, A. R. J., Jones, E., Kern, R., Larson, E., Carey, C. J., Polat, İ., Feng, Y., Moore, E. W., VanderPlas, J., Laxalde, D., Perktold, J., Cimrman, R., Henriksen, I., Quintero, E. A., Harris, C. R., Archibald, A. M., Ribeiro, A. H., Pedregosa, F., van Mulbregt, P., Vijaykumar, A., Bardelli, A. Pietro, Rothberg, A., Hilboll, A., Kloeckner, A., Scopatz, A., Lee, A., Rokem, A., Woods, C. N., Fulton, C., Masson, C., Häggström, C., Fitzgerald, C., Nicholson, D. A., Hagen, D. R., Pasechnik, D. V., Olivetti, E., Martin, E., Wieser, E., Silva, F., Lenders, F., Wilhelm, F., Young, G., Price, G. A., Ingold, G.-L., Allen, G. E., Lee, G. R., Audren, H., Probst, I., Dietrich, J. P., Silterra, J., Webber, J. T., Slavič, J., Nothman, J., Buchner, J., Kulick, J., Schönberger, J. L., de Miranda Cardoso, J. V., Reimer, J., Harrington, J., Rodríguez, J. L. C., Nunez-Iglesias, J., Kuczynski, J., Tritz, K., Thoma, M., Newville, M., Kümmerer, M., Bolingbroke, M., Tartre, M., Pak, M., Smith, N. J., Nowaczyk, N., Shebanov, N., Pavlyk, O., Brodtkorb, P. A., Lee, P., McGibbon, R. T., Feldbauer, R., Lewis, S., Tygier, S., Sievert, S., Vigna, S., Peterson, S., More, S., Pudlik, T., et al.: SciPy 1.0: fundamental algorithms for scientific computing in Python, Nat Methods, 17, 261–272, https://doi.org/10.1038/s41592-019-0686-2, 2020.
Winkel, G., Lovrić, M., Muys, B., Katila, P., Lundhede, T., Pecurul, M., Pettenella, D., Pipart, N., Plieninger, T., Prokofieva, I., Parra, C., Pülzl, H., Roitsch, D., Roux, J. L., Thorsen, B. J., Tyrväinen, L., Torralba, M., Vacik, H., Weiss, G., and Wunder, S.: Governing Europe's forests for multiple ecosystem services: Opportunities, challenges, and policy options, https://doi.org/10.1016/j.forpol.2022.102849, 1 December 2022.

Winkler, K., Fuchs, R., Rounsevell, M., and Herold, M.: Global land use changes are four times greater than previously estimated, Nat Commun, 12, 2501, https://doi.org/10.1038/s41467-021-22702-2, 2021.
Yu, Z., Ciais, P., Piao, S., Houghton, R. A., Lu, C., Tian, H., Agathokleous, E., Kattel, G. R., Sitch, S., Goll, D., Yue, X., Walker, A., Friedlingstein, P., Jain, A. K., Liu, S., and Zhou, G.: Forest expansion dominates China's land carbon sink since 1980, Nat Commun, 13, https://doi.org/10.1038/s41467-022-32961-2, 2022.
Zhang, Y., Yu, G., Yang, J., Wimberly, M. C., Zhang, X., Tao, J., Jiang, Y., and Zhu, J.: Climate-driven global changes in carbon use efficiency, Global Ecology and Biogeography, 23, 144–155, https://doi.org/10.1111/geb.12086, 2014.

Appendix B: Combining empirical and mechanistic understanding of spruce bark beetle dynamics in vegetation modelling

Combining empirical and mechanistic understanding of spruce bark beetle outbreak dynamics in vegetation modelling

Fredrik Lagergren[1], Anna Maria Jönsson[1], Mats Lindeskog[1], and Thomas A. M. Pugh[1,2,3]

[1] Department of Physical Geography and Ecosystem Science, Lund University, Lund, Sweden.
[2] School of Geography, Earth and Environmental Sciences, University of Birmingham, Birmingham, UK.
[3] Birmingham Institute of Forest Research, University of Birmingham, Birmingham, UK.

Abstract

For evaluating the forests' performance in a future with changing climate for different management alternatives, dynamic vegetation models are important tools. One of the functions in such models that has a big influence on the results is tree mortality. Bark beetles are important for the pattern of mortality in forest, especially for needle leaved forest in the temperate and boreal zones. The European spruce bark beetle (SBB*, Ips typographus*) has in the most recent years replaced wind as the most important disturbance agent in European forest. Historically, SBB damage is typically triggered by wind storms as they create breeding material with no defences to overcome for the beetles. Drought can contribute to increased damage and prolonged outbreaks by lowering the defences of the trees, but has been the main driver of some of the European damage in the last decade. In this study we have implemented a SBB damage module in a dynamic vegetation model (LPJ-GUESS) that includes representation of wind damage and forest management. The module was calibrated against observations of storm and SBB damage in Sweden, Switzerland, Austria and France. An index of the SBB population size that changed over time driven by phenology, drought, storm-felled spruce trees and density of the beetle population, was used to scale modelled damage. The model was able to catch the start and duration of outbreaks triggered by storm damage reasonably well, but there was a large variability that partly can be related to salvage logging of storm felled forest and sanitary cutting of infested trees. The model showed increased damage in most recent years with warm and dry conditions, although below the level reported, which may suggest that the drought stress response of spruce in LPJ-GUESS is underestimated. The new model forms a basis to explore vulnerability of European forests to spruce bark beetle infestations.

1. Introduction

Intensified forest management, reforestation and fertilization effects from increased CO_2 concentration and nitrogen deposition have tended to increase the growing stock of European forests over recent decades (Ciais et al., 2008; Scheel et al., 2022). However, over the most recent years this trend no longer exists, due to increased harvest and disturbances (Palahi et al., 2021; Patacca et al., 2022; Wernick et al., 2021). The disturbances and associated tree mortality can be related to weather and climate, directly or in combination with a biological agent, but the forest's structure and species composition is equally important, as most epidemic species are selective in host preference (Balla et al., 2021). The prevailing paradigm of European forestry has tended to increase the vulnerability of forests to these disturbances by reducing the diversity of tree species (Forzieri et al., 2021). Forest policy in Europe is primarily determined at the national and European Union levels. This means that

tools that can provide accurate projections of how these disturbances are likely to change under different climate conditions or management actions at these national-to-continental scales are crucial to be able to develop appropriate forest policy.

Bark beetles are a group of insect species that in most cases colonize dead or stressed trees. A few species are, however, also able to kill healthy trees, potentially leading to outbreaks that can cause severe mortality, especially in temperate and boreal needle-leaved forests (Kautz et al., 2017; Lindgren and Raffa, 2013). In Europe, the most damaging bark beetle is the spruce bark beetle (*Ips typographus*, hereafter referred to as SBB), causing tree death corresponding to tens of million m^3 wood per year (Patacca et al., 2022). The most recent years have seen accelerating losses of trees from SBB outbreaks, mainly related to droughts reducing the capacity of trees to defend themselves and climate warming accelerating the lifecycle of the beetles (Hlásny et al., 2021). Historically, however, outbreaks have mainly been triggered by storm damage, which creates breeding material in which the beetles are not required to overcome the defence mechanisms of the trees (Schroeder, 2001). Norway spruce (*Picea abies*), the host tree, is favoured by forestry and is often managed with thinning and clear-cuts that creates dense even-aged stands, that over time becomes increasingly vulnerable to both storm damage and spruce bark beetle attacks. The interaction of these multiple drivers makes spruce bark beetle damage challenging to model at any scale. Whilst landscape- and national-level models for SBB exist (de Bruijn et al., 2014; Jönsson et al., 2012; Seidl et al., 2014), the capability to explicitly model forest damage from SBB is not currently available in a European-scale forest model.

The life cycle and temperature dependent phenology of SBB are well studied (Wermelinger and Seifert, 1998) and have been incorporated in mechanistic models (Jönsson et al., 2007; Jönsson et al., 2012). However, to be able to evaluate model simulations on spruce bark beetle population dynamics and the shift between endemic and epidemic conditions, not only mechanistic understanding is needed, but also detailed knowledge about forest conditions. This includes stand composition and structure, timing and magnitude of storm damage, and subsequent management actions such as sanitary and salvage cutting (Jönsson et al., 2012). So far, empirical approaches have been applied in SBB modelling at continental (Marini et al., 2017) and regional scale (Soukhovolsky et al., 2022). Most empirical models include response functions of storm felling, temperature and precipitation deficit, but require prior knowledge of the SBB population, as the output from such models is a relative change in SBB population or damage, limiting the simulation of full outbreak cycles. In detailed mechanistic models, the timing of salvage and sanitary cutting is an important component (Jönsson et al., 2012), which makes data availability a limitation to large-scale model calibration. A model without mechanistic responses of climate and forest structure may, however, not be able to project future conditions and the effect of adaption in proactive and reactive forest management strategies. Conversely, the SBB lifecycle has several temperature dependent stages for reproduction and survival, which makes representation by a continuous response function, as typically employed by empirical models, difficult. Yet, when working over large regions with gridded climate datasets, the weather variability within a grid cell related to altitude, aspect and forest edge effects smooth out some of the non-linearity. This means that an empirical approach can be efficient in applications over large regions, also when considering the highest resolution of gridded climate data available today (typically 3 km, e.g. Lind et al., 2020). An approach that blends the insight of mechanistic modelling with the ability of large-scale empirical assessments to capture the net effects of unrepresented smaller-scale processes is needed.

Here, we seek to develop and evaluate a model for forest damage from SBB outbreaks within the LPJ-GUESS dynamic vegetation model (Smith et al., 2001; Smith et al., 2014). Because the model will be

applied at relatively large scales with a focus on carbon cycling, forest productivity and resilience, the aim is to accurately characterise the behaviour of the system, rather than predict specific events. For instance, it is not necessary to capture the particular year that specific outbreaks occur, but rather the typical magnitude and frequency of large outbreak events, as well as the typical background rates. It is, however, important to be able to simulate the impacts of management interventions such as salvage and sanitary cutting, and systematic changes in forest structure. Furthermore, because SBB is only one of many bark beetles that have large impacts on forest dynamics across northern forests (Kautz et al., 2017), there is also a need to develop a model structure that is flexible to simulate a category of pest with multiple bark beetle species with different characteristics across a wide variety of forest across the temperate and boreal forest biomes. The aim of this study was therefore to develop a model with the following characteristics:

1. To be able to catch outbreak dynamics, triggered by storm damage, drought stress and temperature-driven changes in beetle phenology.
2. To utilise simple empirical relationships where available, but also make use of suitable mechanistic knowledge that is relevant at the scale of interest.
3. To capture the general outbreak dynamics without detailed accounting of SBB population.
4. To generate fractions of killed individuals in vegetation in tree size/age cohorts for feedback to modelled vegetation dynamics
5. To provide a generalised concept to use for different types of bark beetles by changing the underlying functions related to weather and insect – host tree interactions.

2. Material and Methods

2.1. General description of LPJ-GUESS

LPJ-GUESS is a dynamic vegetation model adapted to both global and European simulation domains, which simulates the development of vegetation cohorts belonging to different plant functional types (PFT) in replicate patches (1000 m^2) (Smith et al., 2001; Smith et al., 2014). The cohorts compete for water, nutrients and light within the patches, driven by climate, nitrogen deposition and atmospheric CO_2 concentration. The PFTs differ in parameters related to physiological response functions, allometry and bioclimatic restrictions. Replicate patches are subject to the same climatic and edaphic conditions, but differ due to stochastic elements in the processes of cohort establishment and individual tree mortality and disturbance. A range of different forest management classes can be simulated in each model grid cell, for instance clear-cut or continuous harvesting following a particular regime or unmanaged vegetation (Lindeskog et al., 2021). Within these classes, there may be patches of different ages since the last patch-destroying (i.e. stand-replacing) natural disturbance or clear-cut harvest event. Processes in the model includes e.g. light absorption, photosynthesis, auto- and heterotrophic respiration, allocation and different types of mortality. Patch destroying disturbances apart from fire have typically been simulated as random events with a fixed average return time.

In the present study LPJ-GUESS version 4.1, subversion revision 13130 was used. In addition to the standard trunk version of the model, this revision also included the storm damage module from Lagergren et al. (2012). In this module, the simulated storm-damaged fraction of a cohorts is the product of a cohort's sensitivity index (SI), the triggering wind load (WL) and a calibration factor (CF).

$$DF_{cohort} = SI_{cohort} \times WL \times CF \qquad \text{Eq. 1}$$

The SI is based on tree shape (height to diameter ratio), neighbouring cohorts' and stands' height and time since thinning.

2.2. Setup of simulations representing the current state of spruce forest

The global set of PFTs were used in the simulations, as the aim was to produce a biotic model that could be applied routinely in the standard version of LPJ-GUESS. This set has seven boreal and temperate tree PFTs, of which spruce is represented by the shade tolerant boreal needle leaved evergreen tree type (BNE). The spruce forest for each region/country was represented in the simulations by nine age classes of clear-cut forestry with a 90-year rotation period established at 10-year intervals after year 1859, continuous-cover forestry (CCF) with short cutting interval (12 years, 15% of biomass removed at each occasion) and long (25 years, 30%) and unmanaged forest. For the clear-cut rotations thinning was done at age 9, 27 and 45 years with strength of 10%, 30% and 25% of biomass removed. Planting or establishment in the managed forest types were set to BNE only. The results were weighted by weights based on the age-class distribution from Poulter et al. (2019) for year 2010. The data had a regional resolution for France and a national for Austria and Switzerland. For Sweden national inventory data for 2008-2012 were used instead (Skogsdata 2013, https://www.slu.se/en/Collaborative-Centres-and-Projects/the-swedish-national-forest-inventory/foreststatistics/skogsdata/). The age classes 91-110 and 111-140 years were represented by short and long CCF respectively, and potential natural vegetation (PNV) represented forest older than 140 years. The weights, related to the age in 2010, were used as input to the landcover functionality in LPJ-GUESS (Lindeskog et al., 2021) and were held constant over the simulations. Each age class, CCF type and natural forest was run for five replicate patches in each grid cell. Random patch-destroying disturbances were initially set to a return time of 500 years, but after the introduction of management in a patch, these were turned off to avoid resetting the age structure. In Europe, BNE also represents silver fir (*Abies alba*), which is not attacked by SBB, this could potentially lead to overestimation of SBB damage in stands simulated as unmanaged, as BNE in those stands would represent both species. In Switzerland that has the highest fraction of PNV (25%), silver fir only makes up 6.6% of the total spruce and fir standing volume. In the French regions there are 0-12% PNV, but here silver fir makes up 49% of total fir and spruce. Austria has only 7% PNV and in Sweden there are no silver fir. Since PNV multiplied by fir fraction was low (<6%) in all regions/countries, we ignored this problem. Furthermore, as Picea abies is the primary species constituting the BNE PFT within Europe, the parameterisation here can also be considered applicable in the European version of the model (Pugh et al., Appendix A).

2.3. Implementation of a bark beetle damage module in LPJ-GUESS

European storm and bark beetle damage statistics were compiled by Marini et al. (2017), and they used the dataset to derive empirical models describing the increase rate (R) of forest volume loss due to bark beetles (D_{SBB}) to one year (t) from the previous year (t-1):

$$R = \log_e(D_{SBB\,t} / D_{SBB\,t\text{-}1}) \qquad \text{Eq. 2}$$

The top-rated model was:

$$R = -0.099 + 0.223T_t + 0.265D_{storm\,t\text{-}1} - 0.351\,D_{SBB\,t\text{-}1} - 0.151W_{t\text{-}1} - 0.052W_t - 0.233T_t\,D_{storm\,t\text{-}1} + 0.153T_t\,W_{t\text{-}1} + 0.233D_{storm\,t\text{-}1}\,W_t \qquad \text{Eq. 3}$$

depending on the thermal sum between 1 May and 30 July (T) with a threshold of + 5° C, storm felled volume (D_{storm}), D_{SBB}, and cumulative rainfall between 1 March and 31 July (W). All variables were standardized to mean 0 and standard deviation 1, D_{storm} was log-transformed before standardization.

Using this concept, we implemented an additive model for bark beetle damage in LPJ-GUESS, taking advantage of the existing LPJ-GUESS formulations for water stress and mortality of trees (L, stem litter

from spruces larger than a limit (d_{lim}) killed by other agents than bark beetles last year), and the bark-beetle phenology of Jönsson et al. (2007).

$$R = f(P_{gridcell\ t-1}) + f(P_{patch\ t-1} / L) + f(\text{water stress}) + f(\text{phenology}) \quad \text{Eq. 4}$$

$$P_{patch} = e^{R} P_{patch\ t-1} \quad \text{Eq. 5}$$

$$M = P_{patch}\, k_0 = e^{R} P_{patch\ t-1}\, k_0 \quad \text{Eq. 6}$$

In which an index of the population size at the start of the year (P_{t-1}), calculated both at patch and grid-cell level, determines the mass of bark-beetle killed trees (M) together with R and a calibration factor (k_0). Of the components of R (Figure 2), $f(P_{patch} / L)$ represents the negative feedback from a denser population relative to the amount of substrate with no defence (L) for a group of trees (patch), $f(P_{gridcell})$ represent the negative feedback when a high population in the landscape leads to lower patch level R because of swarming induced competition, f(water stress) has a positive impact on R as the defence in healthy trees is reduced with water limitation, and f(phenology) has a positive impact resulting from faster phenological development of the SBB.

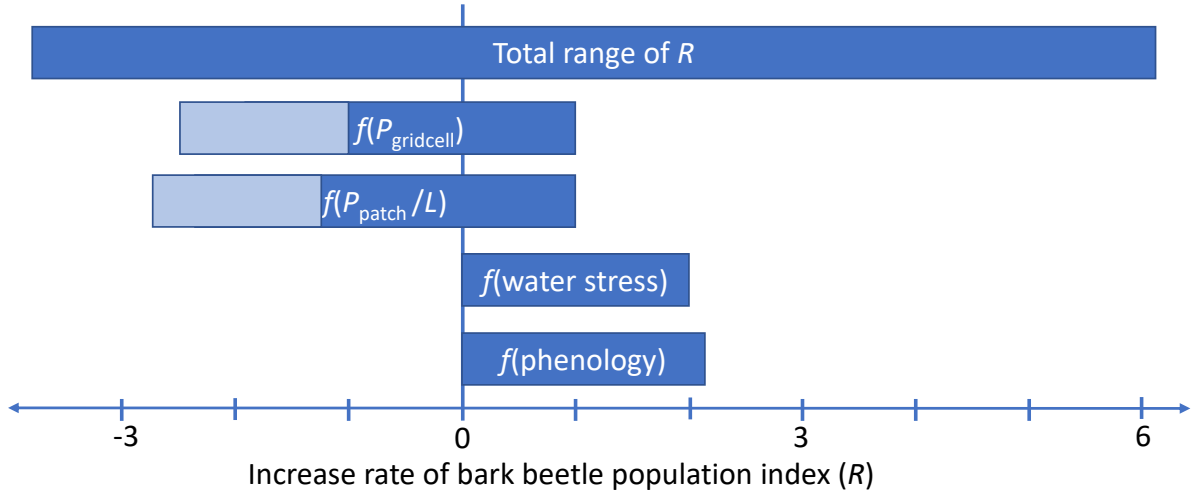

Figure 1. The different components of the increase rate of the bark beetle population index (R). For $f(P_{gridcell})$ and $f(P_{patch} / L)$, the light shaded areas show the range with different parameters for the minimum of $f(P_{gridcell})$ and $f(P_{patch} / L)$. To have the possible total negative feedback from the population index constant, the minimums of the ranges were dependent on each other, such that the sum always equalled -3.8.

The fraction of the different age and management classes, from the landcover functionality in LPJ-GUESS, were used to calculate $P_{gridcell}$ weighted over the classes. The possible range of the different parts of the model were given weights of the same magnitude as in the (Marini et al., 2017) model. The range of the components were adjusted to give a total maximum range of R (Figure 1) comparable to R calculated (Eq. 2) from the damage statistics data (see section 2.4 below). The maximum R can also be translated to the population increase rate with two successful generations in a year with 21 female offspring per mother ($e^{6.1} = 21.1^2$). To enable that an outbreak can also be sustained at the highest population levels, the lowest possible total negative feedback from population size is just below the highest possible positive feedback from water stress and phenology.

The response function for the $P_{gridcell}$ component of R (Figure 2a) was:

$$R_{gridcell} = \text{MIN}(k_{gc\_max}, \text{MAX}(k_{gc\_min}, -\log_e(P_{gridcell} \times k_1) \times k_2)) \quad \text{Eq. 7}$$

where k_{gc_max} and k_{gc_min} determine the range, k_1 the intercept and k_2 the slope of the expression. The same type of function was used for the combined response of P_{patch} and L (Figure 2b):

$$R_{patch} = \text{MIN}(k_{p\_max}, \text{MAX}(k_{p\_min}, -\log_e(P_{patch} / L \times k_3) \times k_4)) \quad \text{Eq. 8}$$

where the min and max are set by k_{p_max} and k_{p_min} respectively, and k_3 and k_4 set the intercept and slope. To avoid division by zero, a fixed background level (k_{base_bm}, set to 0.0001 kg C m^{-2}) was added to the available brood material (L):

$$L = k_{base\_bm} + L_{mort} \quad \text{Eq. 9}$$

where L_{mort} is C mass of stem mortality of spruce trees above a diameter threshold (d_{lim}) for previous year caused by other reasons than bark beetles (including storm), d_{lim} was set to 15 cm (Jönsson et al., 2012). The ratio between water supply to the canopy and canopy water demand (wscal), as calculated by LPJ-GUESS, that goes from zero at complete shutdown of photosynthesis and transpiration to one at no stress, was used to assess the dependency of drought (1 - wscal, Figure 2c):

$$R_{water} = \text{MIN}(k_{drought\_max}, (1 - \text{wscal}_{mean}) \times k_5) \quad \text{Eq. 10}$$

where k_5 is the slope, determining the point of full effect on R. The mean wscal was calculated over the month May-July for both previous year and current year, using data for BNE. Based on the (Marini et al., 2017) model, the data from the previous year were given a three times higher weight in the default setting, but in the calibration and sensitivity analysis (see below) the previous year weight (k_{pyw}) was varied between ¼ to 4. For a more mechanistic approach of taking phenology into account, the dependency of T in the (Marini et al., 2017) model was replaced with a dependency of the length of the autumn swarming period (ASP) from the Jönsson et al. (2007) model (Figure 2d):

$$R_{phen} = \text{ASP} \times k_6 / (\text{ASP30} + k_7) \quad \text{Eq. 11}$$

where the slope depends on the grid-cell-level 30-year running mean of ASP (ASP30) and two parameters k_6 and k_7. Calculated ASP was capped at 90 days (ASP_{max}). Normalizing with ASP30 instead of a direct relationship ($R_{phen} = \text{ASP} \times 2 / \text{ASP}_{max}$) gives a more responsive function at lower ASP30. We avoided to use a discrete function (based on 0, 1, 2 or 3 generations) as it will not take climate variability within a grid cell into account, which can be caused by altitude, slope aspect and brood tree exposure. Similar to Marini et al. (2017), the calculation of ASP also involves a thermal sum with a 5 °C threshold, but in addition includes heat-sum targets and triggering thresholds for development stages (Jönsson et al., 2007).

In the managed forest of Europe, countermeasures against outbreaks are often performed. We included functionality of salvage cutting of storm-felled trees and sanitary cutting of infected trees (SSC). The salvage cutting part was done by reducing L_{mort} by 90% for larger storm events (>5 m^3 wood at patch level). The total grid-cell maximum salvage cutting capacity (salvmax) was set to 50% of the 10-year average harvest rate, as it has to be done before the new generation of bark beetles emerge (which occurs approximately 6 months into the year) in order to have an effect. If the 90% of the storm damage (damage_available) was > salvmax, L_{mort} was reduced by salvmax/damage_available instead of 90%. Sanitary cutting was applied by reducing P_{patch} by 25% if the fraction of available spruce volume that would be killed was >1%. This reduction was done before Eq. 6 was applied.

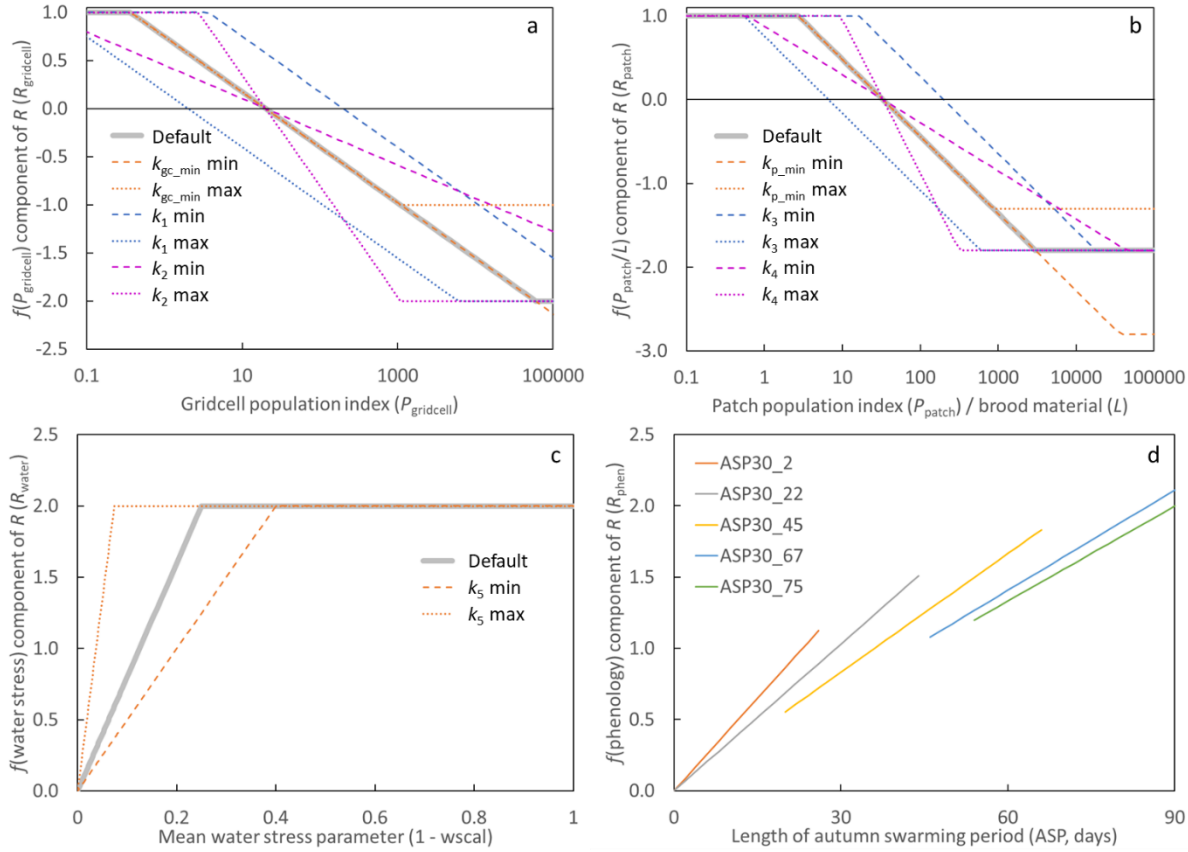

Figure 2. Shape of the functions for the components of the increase rate of the bark beetle population index (*R*). The default parameter setting is shown by thick grey lines (a-c). The functions are also shown in colour for the min and max value of parameters included in the calibration and sensitivity analysis, using the default setting for the other parameters. For *f*(phenology), no parameters were tested but the response depends on the grid-cell's 30-year running mean of the length of the autumn swarming period (ASP, ASP30) and function are shown for ASP30 from 2 to 75 days (d).

2.4. Data of storm and bark beetle damage to forest in Europe

Data of damaged volume of spruce forest were combined with statistics of standing spruce volume to assess the fractions in a country/region damaged by storm (DF_{storm}) or killed by SBB (DF_{SBB}), which were calculated and used for further analysis.

European storm and bark beetle damage statistics were compiled by Marini et al. (2017), for some countries separated into administrative or topographical units. From that data set we used damage statistics (m^3 yr^{-1}) from South Sweden (data separated into 10 counties), North-East France (five former administrative units, from here on called "old counties"), Switzerland (lowland and mountains) and Austria (whole country). As storms in Europe mainly occur in autumn and winter, and as the vegetation and bark beetle effect will be the same for a storm event in October or in February the next year, the storm damage statistics for a specific year were compiled for a storm season of July specified year until June the following year.

Data of spruce standing volume were available by year (1961-2010) for Sweden (https://www.slu.se/en/Collaborative-Centres-and-Projects/the-swedish-national-forest-inventory/long-time-series/time-series-from-1953/), for year 2008 for France (https://inventaire-forestier.ign.fr/spip.php?rubrique250), for year 1985, 1995 and 2006 for Switzerland

(https://www.lfi.ch/publikationen/publikation-en.php) and for 2008 in Austria (https://www.bfw.gv.at/en/departments-en/forest-inventory/). For the other countries than Sweden with data only for one or three years, the data were interpolated between the inventory years and kept constant before the first and after the last year.

In recent years Europe has faced several SBB outbreaks that have been driven by warm and dry conditions rather than triggered by storm events (Nardi et al., 2023; Trubin et al., 2022). To test the impact of this shift in driving factor for the parameterization, national level storm and bark beetle damage statistics from the Standardized Disturbance Index (SDI) dataset (Patacca et al., 2022) 2011-2019 for Switzerland and Austria were used. For Switzerland the damage was split between Lowland and Mountain assuming that the proportion of the country totals for Lowland and Mountain parts were the same as in the 1990-2010 data described above.

Table 1. Summary of available storm and SBB damage data from Marini et al. (2017), data used in the primary calibration and additional data from SDI (Patacca et al., 2022) used in the validation as well as the number of simulated climate grid-cells in the different parts.

Country or part of country	Regions	Gridcells per region	Available years (Marini et al., 2017)	Primary calibration years (Marini et al., 2017)	Additional calibration years (Patacca et al., 2022)
South Sweden	10	3-9	1961-2010	1990-2010	
Switzerland	2	8-9	1901-2010	1990-2010	2011-2019
Austria	1	39	1966-2010	1990-2010	2011-2019
East France	5	4-17	2000-2010	2000-2010	

Wind load (WL) calculated (Eq. 6 in Lagergren et al., 2012) from CRU wind data (see below), which is normally used to force the wind damage module, was poorly related to the observed timeseries of wind damage (DF_{storm}, fraction of spruce forest damaged). Therefore, in order to focus on bark beetle outbreak dynamics without introducing additional uncertainties associated with wind damage modelling, we adjusted WL such that it followed DF_{storm} (denoted WL_{stat}). This approach means that we take advantage of the wind damage module to distribute the damage at cohort level (Eq. 1) but, as general functions were used to go from DF_{storm} to WL_{stat}, the exact DF_{storm} time series will not be reproduced by the model. In a first step, a factor of 2 was found to approximately generate the same average level of WL_{stat} calculated from DF_{storm} as WL calculated from wind data for years 1990-2010.

$$WL_{stat} = DF_{storm} \times 2 \quad \text{Eq. 12}$$

After evaluating the quotient between preliminary LPJ-GUESS simulation results and inventoried DF_{storm} at regional level for all available years (Table 1), we concluded to use a separate function for northern Europe (Sweden) depending also on latitude (LAT):

$$WL_{stat} = DF_{storm} \times 2 / f(\text{LAT}) \quad \text{Eq. 13}$$

$$f(L) = -0.00412 \times L^2 + 0.425 \times \text{LAT} - 9.94 \quad \text{Eq. 14}$$

where Eq. 14 was fitted to DF_{storm} quotients in S Sweden 1965-2010. The scaling with LAT, as a proxy for productivity (LAT explains 82% of the variation in county average site quality class in Southern Sweden and 92% for all counties in Sweden (Tab. 3.11a, Skogsdata 2023, https://www.slu.se/en/Collaborative-Centres-and-Projects/the-swedish-national-forest-

inventory/foreststatistics/skogsdata/), is reasonable as a higher WL is needed to trigger a certain level of damage when the cohorts have a lower SI (as they have with lower productivity).

2.5. Climate data and area delimitation

The simulations were driven by daily weather data 1901-2019 at 0.5° resolution from the CRU-JRA V2.1 dataset (https://catalogue.ceda.ac.uk/uuid/10d2c73e5a7d46f4ada08b0a26302ef7). For nitrogen deposition, monthly data from Lamarque et al. (2010) were used. The model was run with forest vegetation for all grid cells within each region/country (Figure 3). For the years with no wind damage statistics, WL was calculated from CRU windspeed from the cubed exceedance of the 99.5 percentile of daily wind speed accumulated over storm season as in Lagergren et al. (2012). Wind damage was applied from 1951 and forward in the simulations.

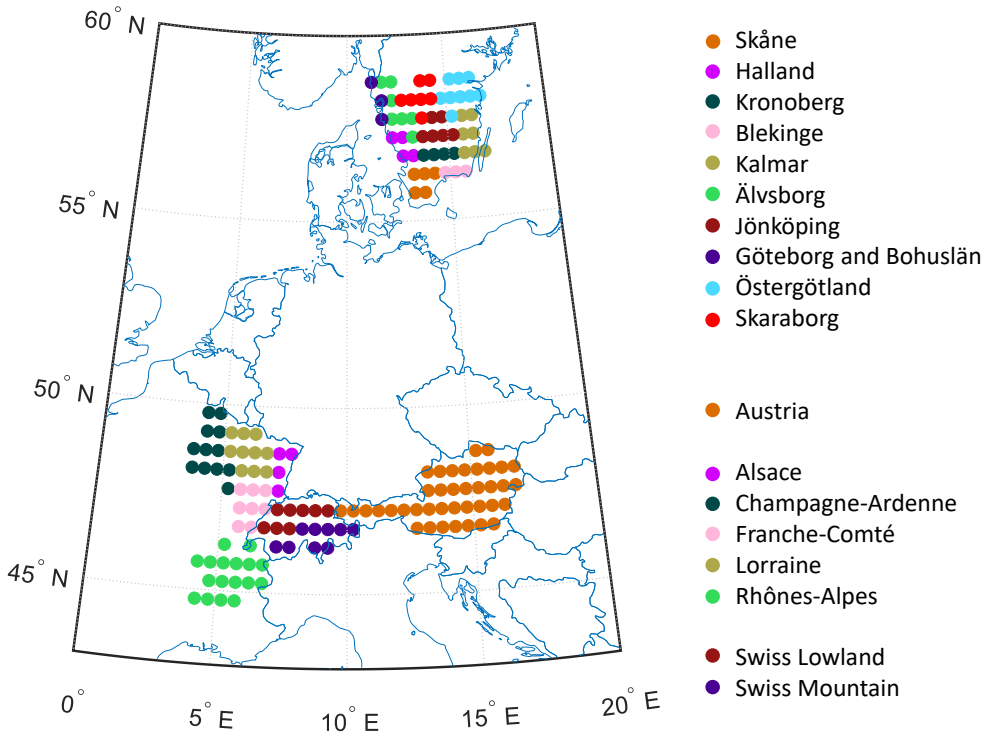

Figure 3. The climate grid cells simulated for the ten counties in South Sweden, the five old counties in North-East France, the two larger regions in Switzerland and in Austria.

2.6. Calibration and sensitivity test

For calibrating and testing the parameter sensitivity of the model, data for 1990-2010 from the 10 southern counties in South Sweden (excluding the Gotland island, which has a low fraction of spruce forest and non-typical soils), 5 old counties in North-East France (only data for 1999-2010), Austria (whole country) and the lowland and mountain regions of Switzerland were used. For South Sweden, North-East France and Switzerland the modelling results and calibration data of DF_{SBB} were averaged over the counties/regions for use in the calibration and sensitivity test. The parameters were first adjusted based on expert judgement, giving a default set of parameters (Table 2).

Table 2. Parameters in the bark beetle model. Min and max value shown for parameters used in the calibration and sensitivity analysis.

Parameter	Part of model	Default	Min	Max
k_{gc_min}	f(Pgridcell)	-2.0	-2.5	-1.0
k_{gc_max}	f(Pgridcell)	1.0		
k_1	f(Pgridcell)	0.05	0.005	0.5
k_2	f(Pgridcell)	0.25	0.15	0.5
k_{base_bm}	f(Ppatch / L)	0.0001		
k_{p_min}	f(Ppatch / L)	-1.8	-2.8	-1.3
k_{p_max}	f(Ppatch / L)	1.0		
k_3	f(Ppatch / L)	0.03	0.005	0.15
k_4	f(Ppatch / L)	0.4	0.25	0.8
k_{pyw}	f(water stress)	3	0.25	4
$k_{drought\_max}$	f(water stress)	2.0		
k_5	f(water stress)	8	5	27
k_6	f(phenology)	3.33		
k_7	f(phenology)	75		

Eight of the 14 parameters were then selected for a calibration procedure and a sensitivity test. These selected parameters were mainly related to the shape of the functions; other parameters were not included as we wanted to keep the range of the response functions at approximately the same magnitude as the weight of the original Marini et al. (2017) model (Eq. 3). To further reduce the number of calculations and to keep the total weight of the population size dependency constant, the sum of the minimum of the ranges $f(P_{gridcell})$ and $f(P_{patch} / L)$ was kept constant ($k_{gc\_min} + k_{p\_min} = -3.8$). This meant that the number of tested parameters could be reduced to 7 as k_{p_min} could be replaced with $-3.8 - k_{gc\_min}$. For each tested parameter 7 discrete numbers were used, evenly spread between the ranges in Table 2. LPJ-GUESS was first run with the default parameter setting. Output at cohort level of all variables used in the bark beetle module was produced for this simulation. These data were then applied in a stand-alone version of the bark beetle module implemented in Matlab (R2018b) for all 7^7 parameter combinations. This approach misses the feedback from bark-beetle mortality to the vegetation state that is simulated within LPJ-GUESS, but greatly reduces the calculation time. Each parameter combination was first run with the default k_0, k_0 was then iteratively adjusted until the mean quotient between simulated and observed maximum DF_{SBB} for the calibration period over the four regions/countries equalled 1. The results were sorted by R^2, root mean square error (RMSE) and absolute bias both at country level (arithmetic mean over the 1-10 regions, Table 1) and by arithmetic mean over the four countries' mean values, and the "best" parameter combination was selected based on highest R^2, lowest RMSE and lowest absolute Bias. A combined statistic measure (CSM) was also calculated for all 7^7 models (X) by summing normalized $1 - R^2$, absolute RMSE and Bias as:

$$CSM_X = ((1 - R^2_X) - (1 - R^2_{mean})) / ((1 - R^2_{max}) - (1 - R^2_{min})) + (RMSE_X - RMSE_{mean}) / (RMSE_{max} - RMSE_{min}) + (|Bias_X| - |Bias|_{mean}) / (|Bias|_{max} - |Bias|_{min}) \quad \text{Eq. 15}$$

where the normalization is based on deviation from mean relative to the range (max-min). The CSM_X values were sorted in ascendant order and we present parameters and statistics for the highest rated model as well as the range of parameters for the 50 highest rated models.

LPJ-GUESS was run both with and without SSC, then the parameter testing and calibration procedure was repeated both with and without inclusion of the 2011-2019 calibration data for Switzerland and Austria. As a final test of the impact of SSC for the results, the stand-alone implementation was also run with inclusion of SSC for the parameter set obtained without SSC and vice versa. The setting including SSC using only the 1990-2010 data was considered as the main base run, results from the other runs are in most cases presented in the Supplement.

2.7. Exploring the climate change signal

To test the robustness of the approach to test the model for different parameter combinations with structure and L_{mort} prescribed from an LPJ-GUESS simulation with default parameters, LPJ-GUESS was finally run with the optimized parameter set, with feedback of the damage associated with that setting to the simulated vegetation. A simple test of climate sensitivity was also done for this setting by applying +2 °C to the climate data throughout the simulation.

3. Results

3.1. Model optimization

The optimal set of model parameters differed depending on the country or region assessed (Table 3), the calibration period included and whether SSC was included or not. Most of the parameters of the common model with the main base-run optimization for all four regions (with SSC and not including calibration data for Switzerland and Austria 2011-2019) had a large span within the "top 50" models (Table 3) but only one parameter value or a narrow span was dominant. It should be noted that the calibration always was based on data from all countries, also when the optimum model for the regions countries was selected.

Table 3. Parameters in the main base run setting (with SSC and not including calibration data for Switzerland and Austria 2011-2019), for the model with the best combined statistics of bias, RMSE and R^2 for all four regions/countries together and for each region/country separately. For all four regions/countries together, also the parameter range for the top 50 combinations is shown (min_50, max_50). The k_0 values are the results of the calibration, LPJ-GUESS was run with a k_0 of 0.003. The numbers in parenthesis is the order number (from smallest to largest) of the seven values tested within the full parameter range (Table 2).

	k_1	k_2	k_{gc_min}	k_{pyw}	k_3	k_4	k_5	$k_0 \times 1000$
Default	0.05 (4)	0.25 (3)	-2 (3)	3 (6)	0.03 (4)	0.4 (4)	8 (3)	2.89
All four	0.005 (1)	0.5 (7)	-1.75 (4)	0.25 (1)	0.15 (7)	0.8 (7)	5 (1)	5.12
min_50	0.005 (1)	0.15 (1)	-1.75 (4)	0.25 (1)	0.005 (1)	0.5 (5)	5 (1)	
max_50	0.5 (7)	0.5 (7)	-1 (7)	4 (7)	0.15 (7)	0.8 (7)	20 (6)	
S Sweden	0.5 (7)	0.15 (1)	-2 (3)	0.5 (3)	0.009 (2)	0.8 (7)	27 (7)	0.0989
Switzerland	0.005 (1)	0.15 (1)	-2.25 (2)	1 (4)	0.005 (1)	0.25 (1)	6 (2)	0.192
Austria	0.12 (5)	0.15 (1)	-2.5 (1)	1 (4)	0.15 (7)	0.5 (5)	27 (7)	0.00272
NE France	0.005 (1)	0.35 (4)	-2.5 (1)	4 (7)	0.15 (7)	0.4 (4)	20 (6)	0.0428

3.2. Model performance

The optimization procedure resulted in reduced bias and RMSE and increased R^2 compared to the default setting (Table 4, Figure 4). The model captured the outbreak dynamics well for S Sweden. In Switzerland R^2 was rather low, mainly because the peak in damage after the 1999 storm in 2001 was

not captured. In North-East France there was a large spread in the observed outbreak after the 1999 storm, with Alsace and Lorraine having a large peak in 2001, while the other counties had a more slowly evolving progress. In Austria the outbreak starting in 2003 after the 2002 storm, with significant storm damage also in 2008 and 2008, lasted almost a decade though the response from the functions of phenology and drought did not indicate that these factors supported the outbreak, resulting in low R^2. Including years 2011-2019 data from Austria and Switzerland in the calibration resulted in similar outbreak pattern (Figure 4).

Table 4. Statistics for different parameter settings; default (Table 2), the one with highest average R^2 of the lowest 0.001 quantile of absolute average bias for all four regions/countries together and the one with highest average R^2 within the same bias criteria for each region/country, in the main base run.

	Default			Combined all four			Region/country		
	R^2	RMSE	Bias	R^2	RMSE	Bias	R^2	RMSE	Bias
All four	0.30	0.29%	0.10%	0.40	0.22%	0.04%			
S Sweden	0.54	0.28%	0.21%	0.76	0.12%	0.07%	0.72	0.08%	0.01%
Switzerland	0.34	0.31%	-0.02%	0.43	0.38%	0.07%	0.45	0.34%	0.01%
Austria	0.03	0.20%	0.10%	0.19	0.18%	0.08%	0.26	0.15%	0.07%
NE France	0.29	0.59%	-0.30%	0.21	0.64%	-0.28%	0.44	0.60%	-0.08%

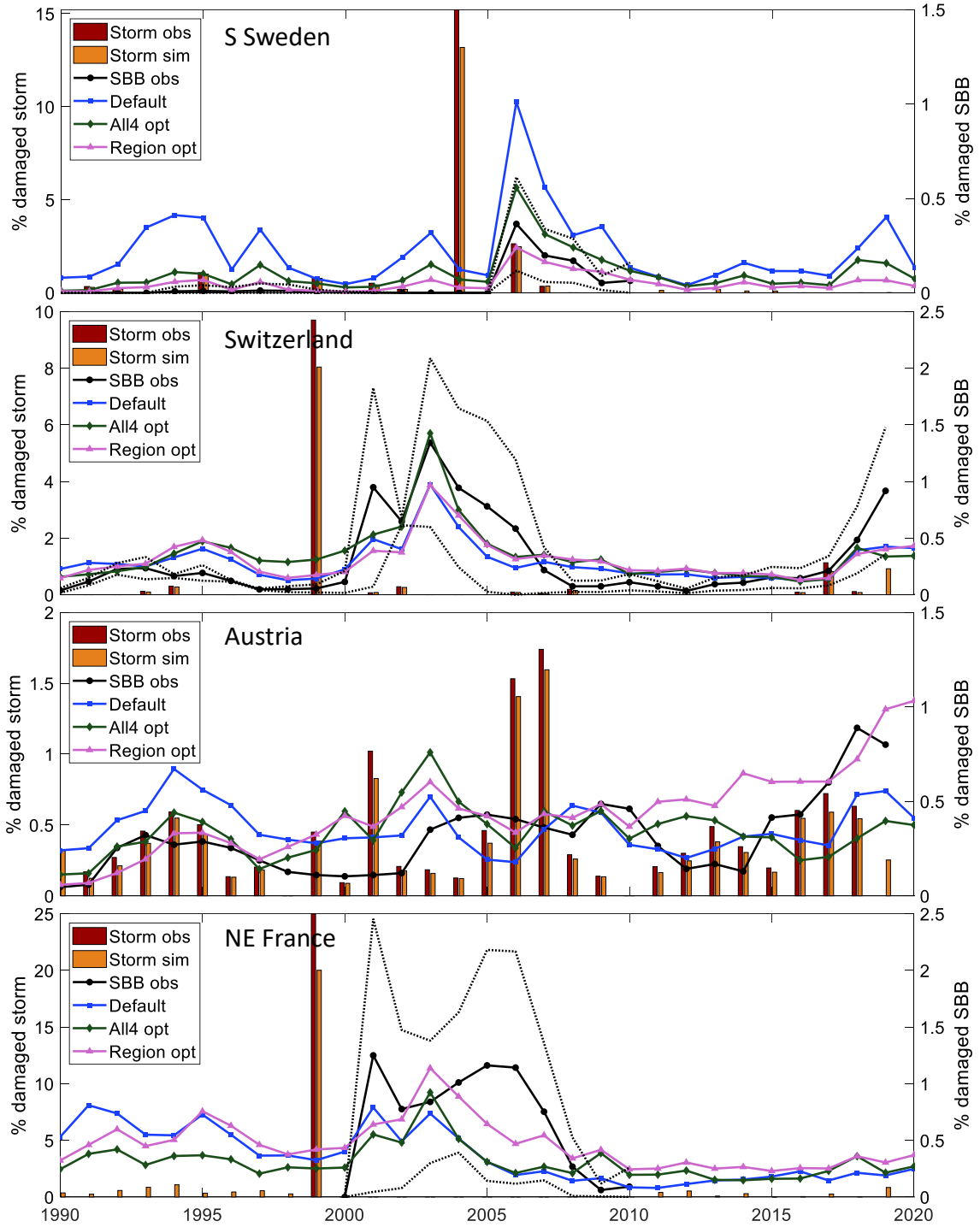

Figure 4. Observed and modelled fraction of spruce forest damaged by storm (left y-axis) and SBB (right y-axis) in four regions/countries, with modelled SBB damage from different parameter settings (Table 3) in the main base run. For Sweden (n = 10), Switzerland (n =2) and France (n = 5) +/- standard deviation between regions in observed SBB damage is shown with dotted lines.

Accumulating the SBB damage over time show that level of damage during outbreak situations was generally well captured for all four region/countries (Figure 5). The difference depending on setting for the calibration was quite large, and in the main base run the total damage for SE France was underestimated. During non-outbreak situation in Sweden the accumulated damage is higher than

observed while it agrees better in Austria and Switzerland but this may to a large extent depend on the way damage is reported, as discussed in Section 4.

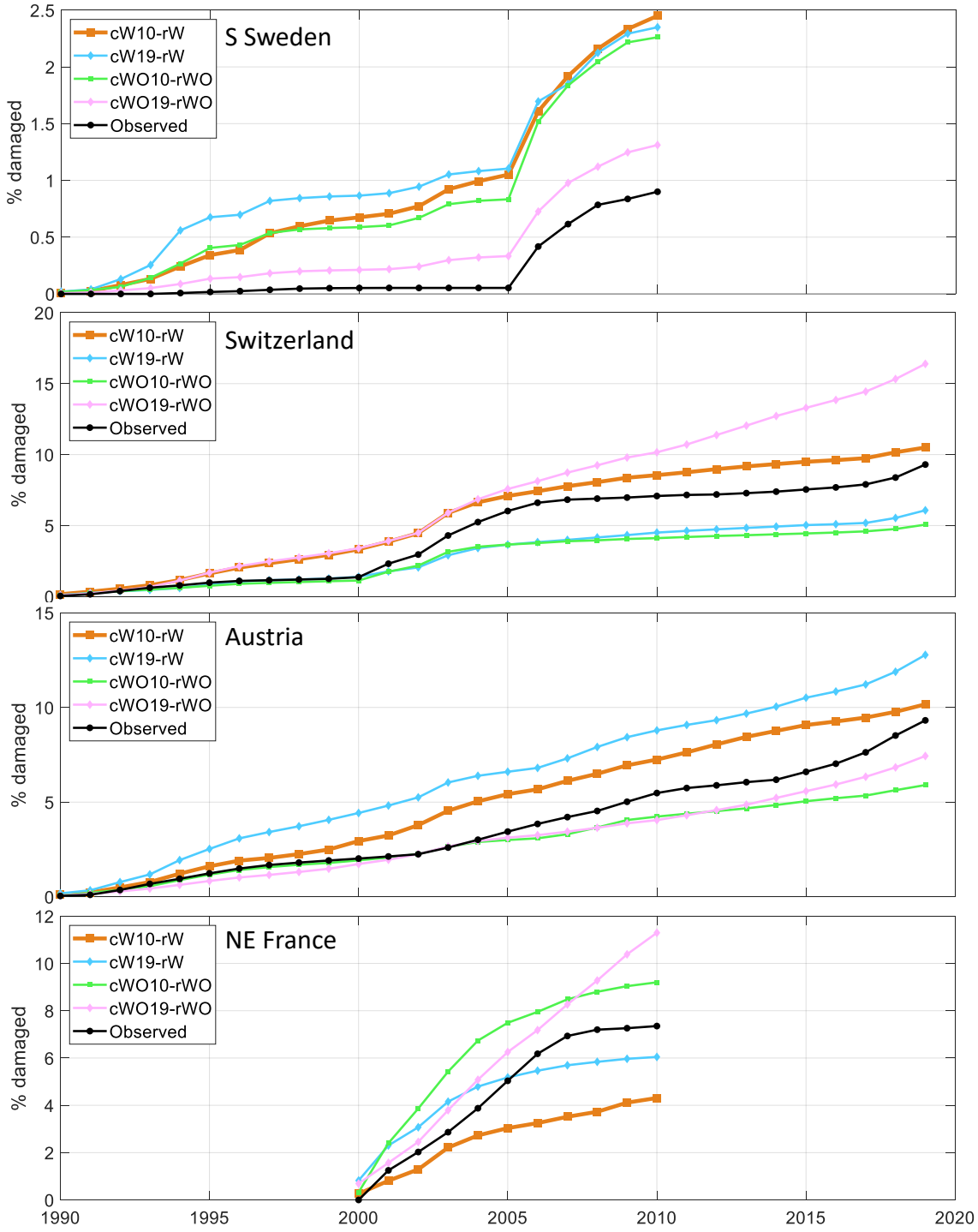

Figure 5. Accumulated fraction of simulated and observed spruce forest damaged by SBB over the period with observations. Calibrations are shown using only data up until 2010 (10) and also including data for Switzerland and Austria 2011-2019 (19) as well as with (W) or without (WO) salvage and sanitary cutting. The main base run setting, cW10-rW, is showed by bold line.

3.3. Model sensitivity

Including the 2011-2019 data for Austria and Switzerland in the calibration resulted in higher accumulated SBB damage in Austria and NE France but lower level in Switzerland with SSC (Figure 5). Without SSC it resulted in substantially higher accumulated damage in Switzerland and NE France as the outbreaks continued at a high level for more years.

Applying the parameter set obtained with SSC without SSC resulted in 1.7 (Austria) to seven (Sweden) times higher simulated damage levels and the calibration without SSC run with SSC showed reductions of similar magnitude (Figure 6). It should though be noted that the negative feedback on forest vulnerability when trees are killed is not included in these stand-alone implementations, giving a higher background damage level in the run without SSC.

Up to this point all results are for the stand-alone Matlab implementation based on the vegetation from the default LPJ-GUESS run. Applying the calibrated parameter set of the main base run in LPJ-GUESS showed a very good match for S Sweden, a minor underestimation in NE France and underestimations by 35% and 70% in Switzerland and Austria, respectively (Figure 7). An in-depth analysis for Austria showed that the difference was due to one grid cell where the missing negative feedback from spruce killing resulted in accumulated modelled damage that widely exceeded the availability of spruce trees in the stand-alone version. Removing this grid cell gave similarly low levels, showing that the applied optimization methodology had a shortcoming in this case.

The simple climate sensitivity test of increasing the temperature by 2 °C resulted in an expected increase in SBB damage in S Sweden and Austria (Figure 7). In Switzerland and NE France, the warming resulted in significantly reduced biomass of the boreal BNE PFT and consequently a reduction in SBB damage.

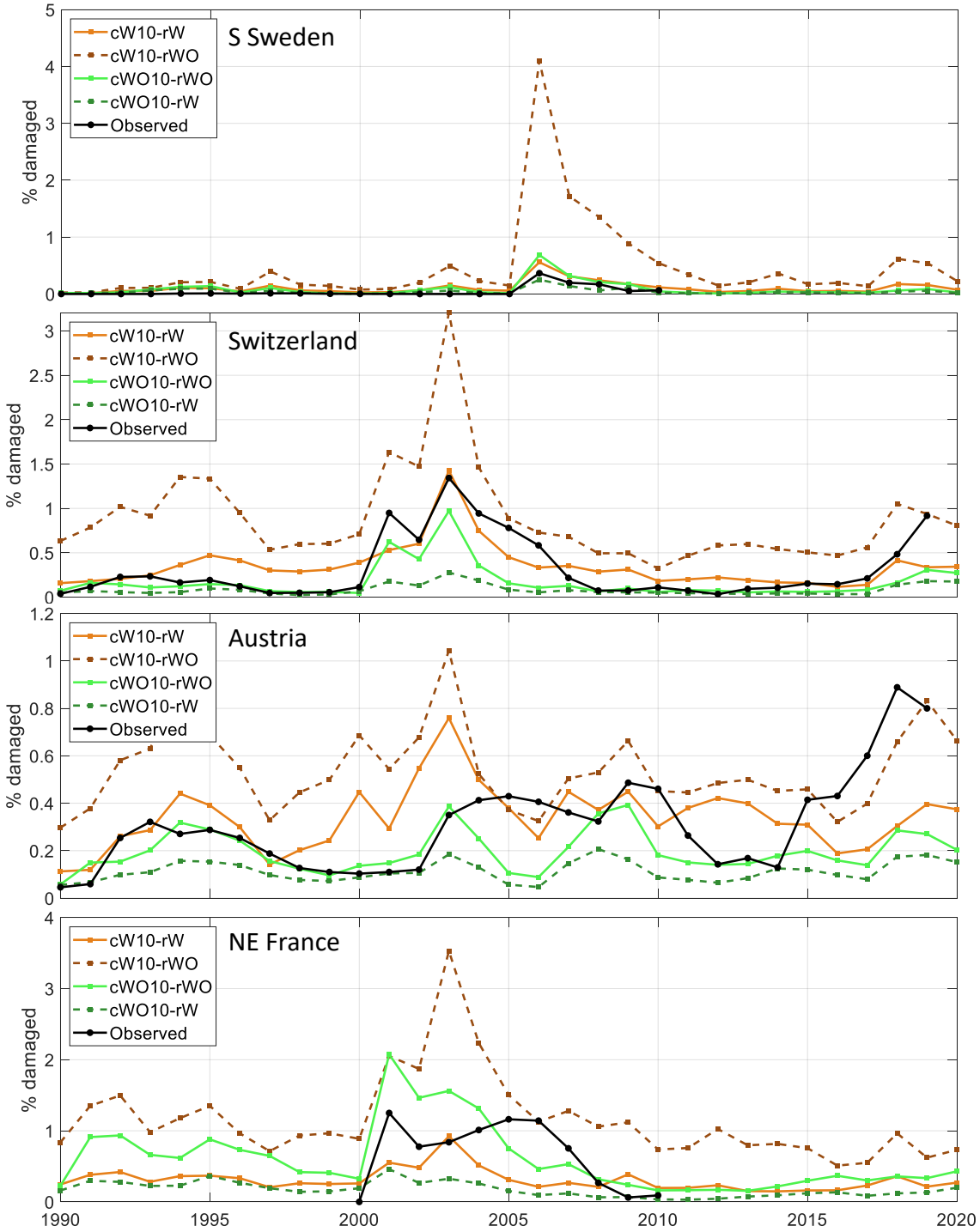

Figure 6. Test of the sensitivity of including salvage cutting of storm felled trees and sanitary cutting of infected trees (SSC) for the fraction of SBB killed trees. The calibrations with (cW) and without (cWO) SSC using calibration data for 1990-2010 (10) were run both with (rW) and without (rWO) SSC.

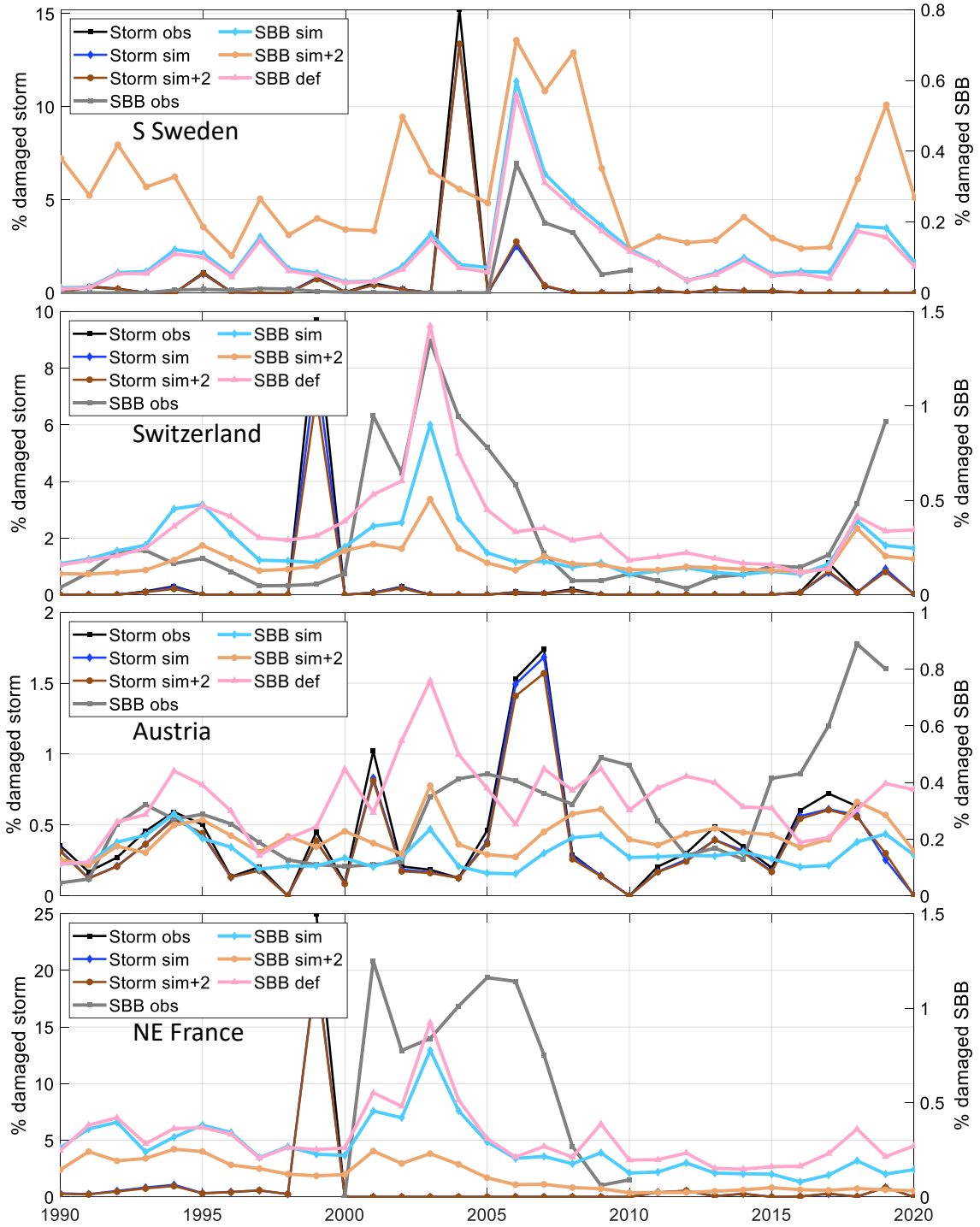

Figure 7. Sensitivity test of modelled storm and spruce bark beetle damage for temperature and model environment. Model output from the calibrated stand-alone version with tree structure and storm damage input from the default LPJ-GUESS run (def, "All4 opt" in Figure 4) and the calibrated model run with LPJ-GUESS with normal climate (SBB sim) and with +2 ° temperature (sim+2) compared to observations (obs).

4. Discussion

The course of a of an insect outbreak can be boiled down to predisposing, triggering and contributing factors (Saxe, 1993), a summary of these factors are shown in Figure 8. In this study, damage was assessed for the spruce fraction of the forest simulated for stands planted with the BNE PFT. The predisposition is, therefore, mainly determined by the amount of spruce stem volume with a diameter larger than 15 cm (d_{lim}), which depends on tree allometry, age-class distribution, growth rate and tree density. The diameter limit has no direct physiological relationship to SBB preference but is related to bark thickness, which is directly related to the possibility to breed (Schlyter and Anderbrant, 1993), with more bark beetle offspring per unit bark area in larger trees (Weslien and Regnander, 1990). In thinner trees there may be parts of the stem that has thick enough bark for successful breeding, but the beetles need a dense cover of galleries over a major part of the stem to overcome the defence. In larger trees the bark can be too thick at the base and the beetles attack higher up on the tree where a lower water potential in the stem (Tyree and Ewers, 1991) also contributes to the success of the attack. The tree density determines how quickly a tree reaches d_{lim} and, in turn, depends on plant number, thinning and mortality. Age- and competition-related mortality also contributes to the background endemic SBB population, which is important for the level of damage when an outbreak is triggered. In this study, the size of age classes was determined for one point in time at country or county scale, which is a simplification. Likewise, the availability of spruce trees with $d > d_{lim}$ in a grid cell is based on age-class data for the year 2010. Currently available large-scale datasets do not intersect stand age and species composition, which induces a big uncertainty when attempting to model outbreaks that are strongly dependent on the availability of trees of a particular species and size. A step forward in this respect could be to base the current stage on national forest inventories using plot level information on individual trees and use harvest and damage statistics for damage, thinning and clear-cut levels, which then in turn determine the tree composition and size distribution (Pugh et al., Appendix A).

Bark beetles commonly develop epidemic levels during the growing season following a storm event ramping up the populations in the defenceless damaged wood. This then leads to killing of trees the second season after the storm. The timing of such outbreaks is quite well captured by the presented model. In managed forest, however, the occurrence and timing of counter measures such as salvage logging of storm-felled trees, sanitary cutting of infected trees and insect traps have a very big impact on the outcome (Jönsson et al., 2012), factors that vary greatly in time and by region over Europe, as well as at finer scale (Wichmann and Ravn, 2001). By timely salvage logging, a large fraction of the beetles can be removed from the forest, substantially dampening the damage done. European-wide models calibrated over a longer time span (e.g. Marini et al., 2017) should not therefore be expected to have a high explanation of particular events in comparison to more local model applications (e.g. Soukhovolsky et al., 2022). However, they should be able to capture the general characteristics of these events well. One possible route forward to improved evaluation of large-scale models is assembling local-scale datasets that combine high-resolution information on species composition and forest structure, with detailed information on bark beetle detection and sanitary/salvage logging. With on-going developments in remote sensing of forest structure and composition combined with datasets on forest harvesting, this may be increasingly feasible in the near future (e.g. Jamali et al., 2024).

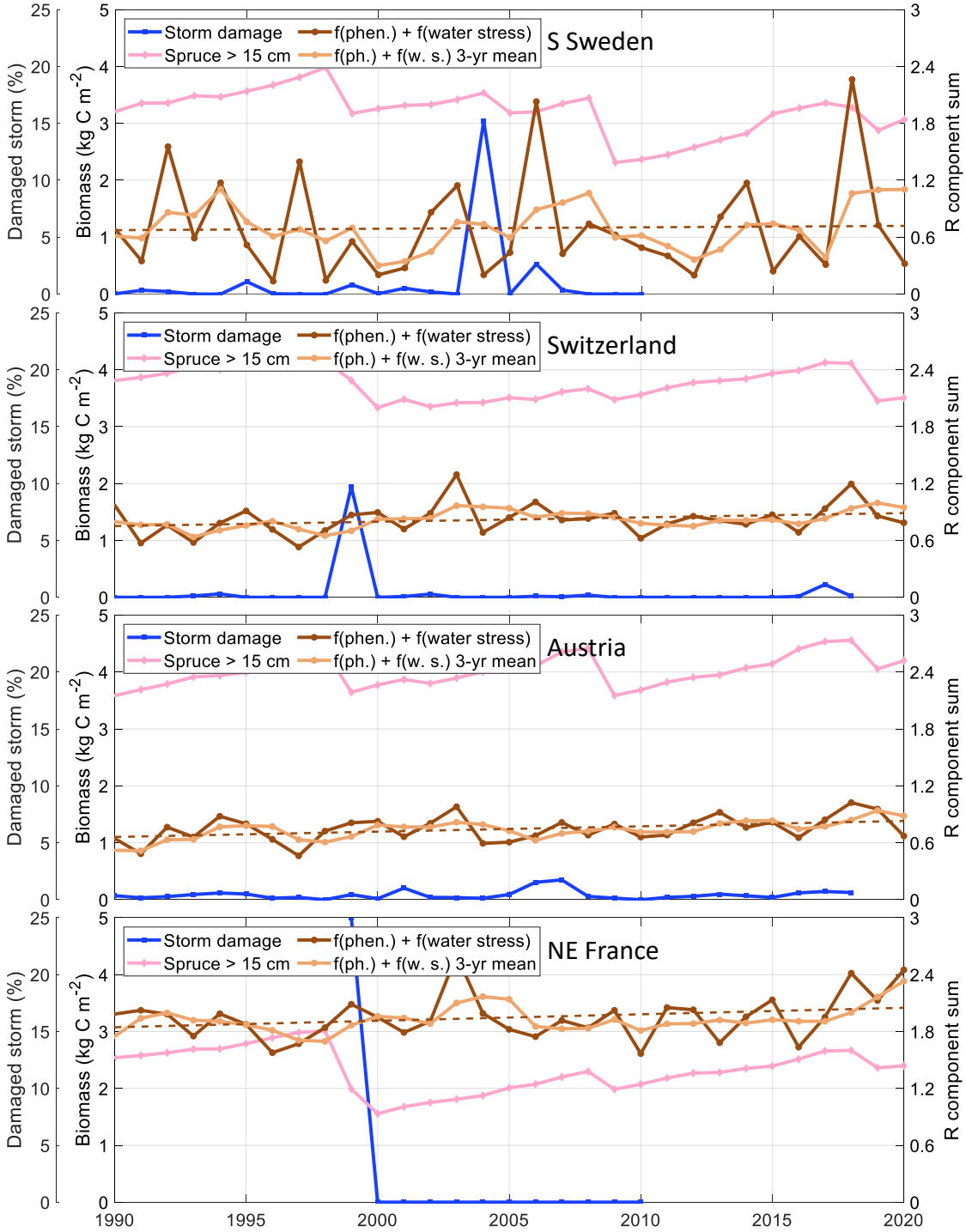

Figure 8. Sensitivity for SBB outbreak divided in predisposing (biomass of spruce trees with a diameter larger than 15 cm), triggering (fraction of spruce volume damaged by storm) and contributing (the sum of the phenology and water stress related components for the increase rate of the bark beetle population index, *R* Eq. 4) factors. For the *R* component sum the running 3-year mean and the trend over time (dashed line) are also shown.

After a major storm, the remaining trees may have disturbed root systems making them more vulnerable to drought, which may enhance SBB outbreaks, but also making them unstable – predisposing them to further storm damage. As SBB prefers defenceless trees even in an outbreak situation, such wind damage can serve as traps for the beetles, if the wood is salvaged in time. This

situation occurred in Southern Sweden when the 2006-2007 storm dampened the outbreak following the major 2004-2005 storm. This relatively subtle mechanism is not captured in our model, which overestimated SBB damage in this outbreak. The outcome after a trigger depends on the initial level of the SBB population. Many SBB models require an initial population or damage level, which means that they work in relative terms (Marini et al., 2017; Soukhovolsky et al., 2022), but this is not feasible in a dynamic forest model operating over large spatial scales.

The way damage is inventoried and reported may also be different between countries and over time. For example, the neighbouring countries Austria and Switzerland have very different reported patterns, in which Austria has a relatively high damage level for almost all years for both wind and SBB damage but relatively low peaks, while Switzerland has large storm damage followed by large SBB damage after the 1999 storm, but low or absent storm damage except from that. We consider it unlikely that the periods of zero bark beetle damage recorded in Sweden and France truly mean that there was no bark beetle damage during this period, but rather that the outbreaks were not large enough to be surveyed. E.g., the country level compilation and gap filling of the DFDE database (Patacca et al., 2022) show seven times higher expert gap filled SBB damage than reported 1990-2005 for Sweden, and in France the machine learning gap filling resulted in 2.4 times higher damage 1991-2000.

Warm weather accompanied with drought are often seen as a contributing factor (e.g. Bakke, 1983), but has both triggered and contributed to sustained outbreaks of SBB in Europe in recent years (Nardi et al., 2023; Trubin et al., 2022). There was no county-level data of SBB damage available for Sweden and France later than 2010, but country totals (Patacca et al., 2022) show levels that greatly exceed our small peak in modelled damage during 2018-2019. Drought has generally been seen as the main driver of these events (George et al., 2022; Kärvemo et al., 2023). With the data used in our calibration and the additive form of the response function, we might have underestimated this response; for Austria and Switzerland the model also underestimated the drought-induced peak even when data for those years were included. Part of the reason for underestimating the damage could be that LPJ-GUESS may be failing to simulate sufficiently increased water stress in the vegetation during this time period. For instance, in Austria and Switzerland, we see no abnormally low values of the water stress scaler wscal (indicating water stress) post 2015. This may be a failing of the model parameterization for water stress or of the input climate forcing dataset (Steinkamp and Hickler, 2015). We note, however, that the 2018 drought generates a fairly strong water stress response in the simulations for southern Sweden and this is reflected in some increase in beetle damage in the years 2018 and 2019 (Figure 4). An additional contributing factor that not has been explicitly accounted for in the present study is root rot, which can significantly increase the severity of an outbreak (Honkaniemi et al., 2018).

The simple test with a 2° C higher temperature gave an expected increase in modelled damage in S Sweden and Austria. In Switzerland and NE France, however, a reduction was simulated, mainly related to a change of the predisposing species composition, as it was only controlled by spruce planting in the even-aged stands allowing the processes of mortality and establishment to change the composition. The SBB phenology response also reaches a plateau when the climate is warm enough to allow a complete second generation to emerge every year. A third generation can be completed with very hot conditions, which potentially could increase potential rate of population increase, but there is little evidence that this is a driver for SBB outbreaks in Europe (Jönsson et al., 2011).

Whilst predicting absolute damage levels is challenging, our model is generally effective at indicating when there are elevated periods of damage risk due to SBB (Figure 8). The most obvious case is year 2003 with a strong drought (Granier et al., 2007) that contributed to prolonged outbreaks in Switzerland, Austria and NE France, but also in the recent years (2017-2019) the indicators also show

increased risks coinciding with observed damage for all assessed countries (Patacca et al., 2022). Combined with the process detail related to forest structure and management, this means that the model can be a powerful tool to explore how different forest structures and climate and management scenarios might interact to shift forests towards increased or decreased vulnerability.

The model that we have developed here is parameterised for SBB only. However, many different species of bark beetles that have the potential to cause large outbreaks and tree mortality, meaning that effectively accounting for the impact of these species on large-scale forest dynamics requires that we can develop methods to generalise responses across species to some degree. These other species of bark beetles can be specific in temperature sums for evolving and dormancy periods and for density dependent defence overcome and competition (Bentz et al., 2019). A common pattern for many species is increased risk for outbreaks related to drought (Reed and Hood, 2021), which is positive for a general concept of bark beetle damage modelling. The implementation of the SBB outbreak dynamics in LPJ-GUESS has introduced a concept of insect functional types (IFTs), which can be modelled in parallel with different response functions and specific PFT hosts. With this concept the model could also be applied in other parts of the world, if sufficient data on bark beetle phenology and damage exist to parameterise and calibrate the model.

5. Acknowledgements

The model developments described in this paper have been funded under the European Union's Horizon Europe research and innovation programme (grant agreement numbers 101059888, CLIMB-Forest; 101056755, ForestPaths; 101084481) and the Horizon 2020 programme (grant agreement no. 758873, TreeMort) as well as from the ForestValue programme, the European Commission, Vinnova, the Swedish Energy Agency and Formas for the project FORECO. This study is a contribution to the Swedish government's strategic research areas BECC and MERGE and the Nature-based Future Solutions profile area at Lund University. We thank Arjan Meddens, Rupert Seidl, Nikica Ogris and Cornelius Senf for discussions on the early stages of this work and Markus Kautz for providing phenology data.

6. References

Bakke, A., 1983. Host tree and bark beetle interactions during a mass outbreak of *Ips typographus* in Norway. Journal of Applied Entomology, 96: 118-125.

Balla, A. et al., 2021. The Threat of Pests and Pathogens and the Potential for Biological Control in Forest Ecosystems. Forests, 12.

Bentz, B.J. et al., 2019. *Ips typographus* and *Dendroctonus ponderosae* Models Project Thermal Suitability for Intra- and Inter-Continental Establishment in a Changing Climate. Frontiers in Forests and Global Change, 2.

Ciais, P. et al., 2008. Carbon accumulation in European forests. Nature Geoscience, 1: 425-429.

de Bruijn, A. et al., 2014. Toward more robust projections of forest landscape dynamics under novel environmental conditions: Embedding PnET within LANDIS-II. Ecological Modelling, 287: 44-57.

Forzieri, G. et al., 2021. Emergent vulnerability to climate-driven disturbances in European forests. Nature Communications, 12.

George, J.P. et al., 2022. Long-term forest monitoring reveals constant mortality rise in European forests. Plant Biology, 24: 1108-1119.

Granier, A. et al., 2007. Evidence for soil water control on carbon and water dynamics in European forests during the extremely dry year: 2003. Agricultural and Forest Meteorology, 143: 123–145.

Hlásny, T. et al., 2021. Bark Beetle Outbreaks in Europe: State of Knowledge and Ways Forward for Management. Current Forestry Reports, 7: 138-165.

Honkaniemi, J., Ojansuu, R., Kasanen, R. and Heliövaara, K., 2018. Interaction of disturbance agents on Norway spruce: A mechanistic model of bark beetle dynamics integrated in simulation framework WINDROT. Ecological Modelling, 388: 45-60.

Jamali, S., Olsson, P.O., Müller, M. and Ghorbanian, A., 2024. Kernel-Based Early Detection of Forest Bark Beetle Attack Using Vegetation Indices Time Series of Sentinel-2. Ieee Journal of Selected Topics in Applied Earth Observations and Remote Sensing, 17: 12868-12877.

Jönsson, A.M., Harding, S., Bärring, L. and Ravn, H.P., 2007. Impact of climate change on the population dynamics of *Ips typographus* in southern Sweden. Agricultural and Forest Meteorology, 146: 70-81.

Jönsson, A.M. et al., 2011. Modelling the potential impact of global warming on *Ips typographus* voltinism and reproductive diapause. Climatic Change, 109: 695-718.

Jönsson, A.M., Schroeder, L.M., Lagergren, F., Anderbrant, O. and Smith, B., 2012. Guess the impact of *Ips typographus* - An ecosystem modelling approach for simulating spruce bark beetle outbreaks. Agricultural and Forest Meteorology, 166-167: 188-200.

Kärvemo, S., Huo, L., Öhrn, P., Lindberg, E. and Persson, H.J., 2023. Different triggers, different stories: Bark-beetle infestation patterns after storm and drought-induced outbreaks. Forest Ecology and Management, 545.

Kautz, M., Meddens, A.J.H., Hall, R.J. and Arneth, A., 2017. Biotic disturbances in Northern Hemisphere forests - a synthesis of recent data, uncertainties and implications for forest monitoring and modelling. Global Ecology and Biogeography, 26: 533-552.

Lagergren, F., Jönsson, A.M., Blennow, K. and Smith, B., 2012. Implementing storm damage in a dynamic vegetation model for regional applications in Sweden. Ecological Modelling, 247: 71-82.

Lamarque, J.F. et al., 2010. Historical (1850-2000) gridded anthropogenic and biomass burning emissions of reactive gases and aerosols: methodology and application. Atmospheric Chemistry and Physics, 10: 7017-7039.

Lind, P. et al., 2020. Benefits and added value of convection-permitting climate modeling over Fenno-Scandinavia. Climate Dynamics, 55: 1893-1912.

Lindeskog, M. et al., 2021. Accounting for forest management in the estimation of forest carbon balance using the dynamic vegetation model LPJ-GUESS (v4.0, r9710): implementation and evaluation of simulations for Europe. Geoscientific Model Development, 14: 6071-6112.

Lindgren, B.S. and Raffa, K.F., 2013. Evolution of tree killing in bark beetles (Coleoptera: Curculionidae): trade-offs between the maddening crowds and a sticky situation. Canadian Entomologist, 145: 471-495.

Marini, L. et al., 2017. Climate drivers of bark beetle outbreak dynamics in Norway spruce forests. Ecography, 40: 1426-1435.

Nardi, D., Jactel, H., Pagot, E., Samalens, J.C. and Marini, L., 2023. Drought and stand susceptibility to attacks by the European spruce bark beetle: A remote sensing approach. Agricultural and Forest Entomology, 25: 119-129.

Palahi, M. et al., 2021. Concerns about reported harvests in European forests. Nature, 592: E15-E17.

Patacca, M. et al., 2022. Significant increase in natural disturbance impacts on European forests since 1950. Global Change Biology.

Poulter, B. et al., 2019. The global forest age dataset and its uncertainties (GFADv1.1). PANGAEA.

Reed, C.C. and Hood, S.M., 2021. Few generalizable patterns of tree-level mortality during extreme drought and concurrent bark beetle outbreaks. Science of the Total Environment, 750.

Saxe, H., 1993. Triggering and predisposing factors in the “Red” decline syndrome of Norway spruce (*Picea abies*). Trees-Structure and Function, 8: 39-48.
Scheel, M., Lindeskog, M., Smith, B., Suvanto, S. and Pugh, T.A.M., 2022. Increased Central European forest mortality explained by higher harvest rates driven by enhanced productivity. Environmental Research Letters, 17.
Schlyter, F. and Anderbrant, O., 1993. Competition and niche separation between 2 bark beetles - existance and mechanism. Oikos, 68: 437-447.
Schroeder, L.M., 2001. Tree Mortality by the Bark Beetle *Ips typographus* (L.) in storm-disturbed stands. Integrated Pest Management Reviews, 6: 169-175.
Seidl, R., Rammer, W. and Spies, T.A., 2014. Disturbance legacies increase the resilience of forest ecosystem structure, composition, and functioning. Ecological Applications, 24: 2063-2077.
Smith, B., Prentice, I.C. and Sykes, M.T., 2001. Representation of vegetation dynamics in the modelling of terrestrial ecosystems: comparing two contrasting approaches within European climate space. Global Ecology and Biogeography, 10: 621-637.
Smith, B. et al., 2014. Implications of incorporating N cycling and N limitations on primary production in an individual-based dynamic vegetation model. Biogeosciences, 11: 2027-2054.
Soukhovolsky, V. et al., 2022. Wind Damage and Temperature Effect on Tree Mortality Caused by *Ips typographus* L.: Phase Transition Model. Forests, 13.
Steinkamp, J. and Hickler, T., 2015. Is drought-induced forest dieback globally increasing? Journal of Ecology, 103: 31-43.
Trubin, A., Mezei, P., Zabihi, K., Surový, P. and Jakuš, R., 2022. Northernmost European spruce bark beetle *Ips typographus* outbreak: Modelling tree mortality using remote sensing and climate data. Forest Ecology and Management, 505.
Tyree, M.T. and Ewers, F.W., 1991. The hydraulic architecture of trees and other woody plants. New Phytologist, 119: 345-360.
Wermelinger, B. and Seifert, M., 1998. Analysis of the temperature dependent development of the spruce bark beetle *Ips typographus* (L) (Col, Scolytidae). Journal of Applied Entomology, 122: 185-191.
Wernick, I.K. et al., 2021. Quantifying forest change in the European Union. Nature, 592: E13-E14.
Weslien, J. and Regnander, J., 1990. Colonization densities and offspring production in the bark beetle *Ips typographus* (L.) in standing spruce trees. Journal of Applied Entomology, 109: 358-366.
Wichmann, L. and Ravn, H.P., 2001. The spread of *Ips typographus* (L.) (Coleoptera, Scolytidae) attacks following heavy windthrow in Denmark, analysed using GIS. Forest Ecology and Management, 148: 31-39.

Appendix C: Disturbance modules in EFISCEN-Space

General approach

Disturbance simulations in EFISCEN-Space are structured in three components: i) Hazard, ii) Exposure and iii) Vulnerability (Figure C1). The hazard component is represented by the disturbance scenarios. Those consist of a time-series for each plot that indicates which year the plot is hit by a disturbance. These scenarios are external to the model to allow flexibility of alternative climate forcings and/or methods of scenario construction. The exposure is represented by the plot state at the moment of the disturbance event in terms of forest biomass and structure. The vulnerability is given by the characteristics of the species present in the forest. This confers to the differences among tree species in response to different disturbance types. Disturbance types currently simulated in EFISCEN-Space are windstorms and wildfires, which have separate impact modules as described in the next sections.

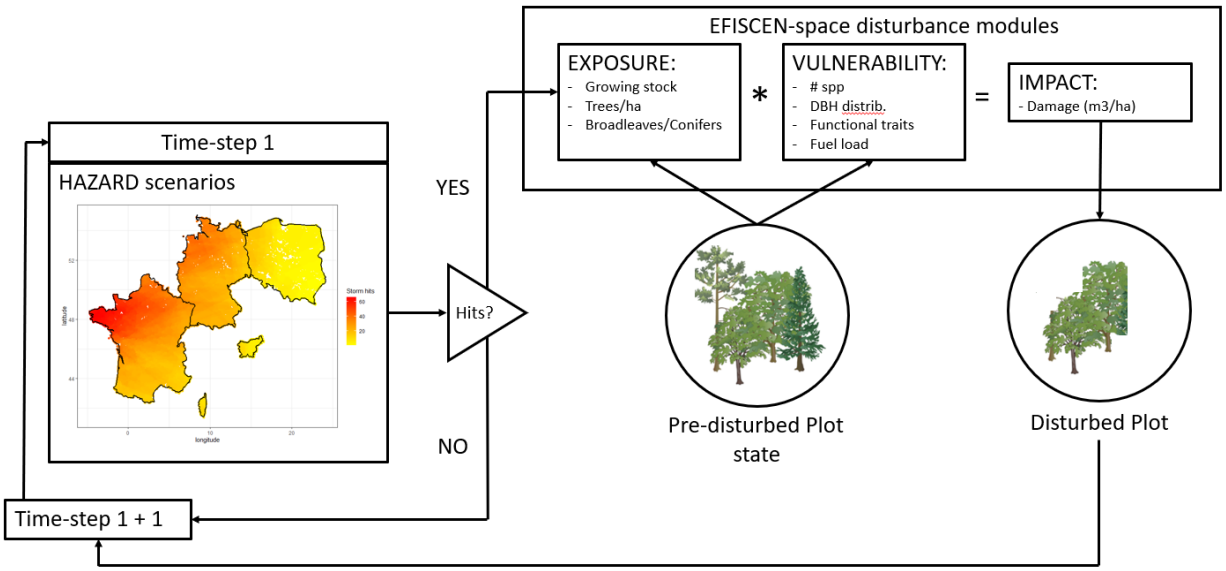

Figure C1. Conceptual diagram of disturbance modules in EFISCEN-Space

Fire impact model

The impact of a wildfire is simulated at the stand level and is assessed based on 1) the climatic conditions determining the degree of flammability of the available fuel at the forest floor, 2) the structural characteristics of the forest and 3) tree species specific characteristics. At each annual time step we calculate the fuel load based on Equation 1 (Schumacher et al., 2006).

$$\text{Fuel load} = Kfc1 + Kfc2 * FWI * Bleaves + Kfc3 * FWI * Bwoody \quad \text{(Eq.1)}$$

Where *FWI* is the Canadian Fire Weather Index of the plot during the European fire season (June, July, August), as available from the Copernicus Climate Change Service, Climate Data Store (2020). FWI is included to account for fuel load flammability induced by drought conditions.

Bleaves and *Bwoody* are respectively the leaves and the woody biomass litter available in the soil carbon model YASSO (Tuomi et al., 2009, 2011) at the forest floor as given by the litter turnover in that time-step before decomposition, which is assumed to happen in wintertime. *Kfc1*, *Kfc2* and *Kfc3* are empirical parameters set to 0.8, 0.2 and 0.4, respectively (Keane et al., 2011; Schumacher et al., 2006; Seidl et al., 2014). Then we calculate the fraction (%) of the crown of each tree of the stand killed by fire (ck) as a function of fuel load (which determines fire intensity) and DBH as proxy for tree size (Equation 2 - Seidl et al., 2014, Appendix A). Below a DBH of 400 mm, ck is calculated as:

$$ck=\min(\text{Fuel load}*(ck1+ck2*DBHt);1) \quad \text{(Eq.2)}$$

where c*k1* and *ck2* are constants (Schumacher et al., 2006), and *DBHt* is the tree diameter at breast height. Above the DBH threshold ck is set to zero, assuming no crown fires occur in trees of this size (Schumacher et al., 2006; Seidl et al., 2014). The probability of tree mortality (*Pmort*) is calculated as a function of *ck* and resistance to fire given by the bark thickness of the tree species (Equation 3).

$$Pmort=11+e-1.466+1.91*(DBH*rBT)-0.1775*(DBH*rBT2)-0.000541*ck2 \quad \text{(Eq.3)}$$

where *rBT* is the species-specific relative bark thickness. *rBT* has been computed for all the tree species in Europe following (Patacca et al., in prep.). *Pmort* is computed at the cohort level (i.e. each DBH class of a species). Because a cohort consists of a number of trees of the same size and species, *Pmort* is applied as a fraction to determine the share of the cohort that is killed.

Wind impact model

ForestGALES (FGR, Gardiner et al., 2008) is a hybrid empirical-mechanistic model (Hale et al., 2015). It is among the most used models in the literature to simulate the effect of wind on forest stands. The model includes parameters both at the stand and the tree level to calculate the Critical Wind Speed (CWS) needed to damage a certain tree in a stand (Locatelli et al., 2016). Being initially developed in the United Kingdom to assess windstorm hazard in conifer plantation (Hale et al., 2015), the amount of tree species parametrized has often been a constraint for broader geographic applications, especially for the lack of many common broadleaves species. The input as required by FGR at the species and stand level is summarised in Table C1. Parametrizing FGR for new species is a tedious and expensive job (Locatelli et al., 2016), as tree pulling and wind tunnel experiments are usually performed to calculate the main species specific parameters needed as model input (Nicoll et al., 2006). Instead of physical methods of determining required parameters, we used species-specific functional traits to compute the species level information. A set of non-parametric machine learning models that take into account both phylogenetic and environmental variation on trait expression (Maynard et al., 2022) were employed to impute average functional traits for all the species available in EFISCEN-Space. Species groups as defined in EFISCEN-space (e.g. long-lived broadleaves) were calibrated with the functional trait value of the original species as measured in the forest inventory raw data. The architectural parameters of tree species assessed empirically with tree-pulling and wind-tunnel tests were copied from FGR-parametrised species and matched with the species not parametrised but present in EFISCEN-Space. The matching was done according to tree species functional type

and whole plant architecture (Table C2). Specific values of wood mechanical properties and rooting depth were derived from functional traits.

Table C1. Species and stand parameters needed to couple FGR to EFISCEN-space

Species level	**Stand level**
Green wood density	Max stand height (m)
Module Of Rupture	Tree spacing (m)
Module Of Elasticity	Distance from the edge (m)
Rooting depth	Upwind gap (m)
Canopy volume (m3) (optional)	Soil type

Table C2. Pairing of architectural characteristic of the missing species in FGR to EFISCEN-Space species.

EFISCEN-space species	**Matched FGR species**
Long-lived broadleaves	Fagus sylvatica
Short-leaved broadleaves	Betula spp.
Castanea sativa	Quercus robur & petrea
Populus plantations	Eucalyptus spp.
Quercus ilex	Quercus robur & petrea

The trait Canopy volume (m3) was left to be dynamically calculated by FGR at each time step applying allometric equations as function of tree size (dbh, height) and spacing. Stand level attributes were re-calculated at each time-step (n) from the stand condition simulated by EFISECN-Space. Tree height is calculated from tree diameter at breast height (dbh) and species following Equation 1:

$$h = e^{\wedge}(ln(v/dc1*ec2)/c2) \qquad \text{(Eq.1)}$$

Where *h* is the tree's height, *v* the tree's volume calculated in EFISCEN-Space, *d* is the diameter at breast height (DBH) of the tree, and c1, c2 and c3 are species specific parameters. From the highest tree in the stand we derived the maximum stand height. Tree spacing (m) was calculated from the number of trees per hectare as Equation 2:

$$sp = \text{sqrt}(10000 / Ntrees) \qquad (Eq.2)$$

We calculated the distance from the edge of the forest plot and the upwind gap for all EFISCEN-Space plots and all the eight main cardinal directions (N; NE; E; SE; S; SW; W; NW). We did so by overlaying a uni-grid of 1x1 km cell-grid size over the EU Joint Research Centre (JRC) 2020 forest cover map. For each plot we calculated the distance from the plot to the forest edge in meters (distance from the edge) and the distance from the forest edge to the next forest fragment (Upwind gap: the space available for wind to accelerate in gusts), as shown in Figure C2.

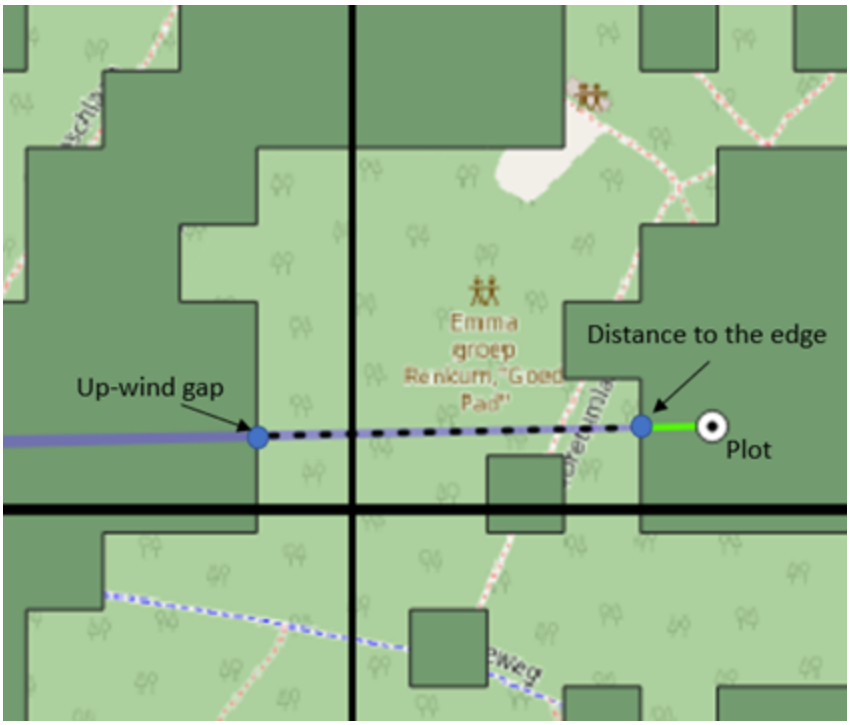

Figure C2: Distance from the edge and up-wind gap visualisation example for one inventory plot.

We derived soil type for each plot from the SoilGrids dataset and matched it with the soil categories of FGR. At each time step, if a plot is hit by a storm, the model is informed with storm max windspeed and wind direction. Then FGR is run to calculate the CWS for each single tree in the stand as function of species mechanical properties, functional traits and stand conditions (see Hale et al., 2015 for more details).

We then assessed an index of topographic ruggedness (TOPEX, Chapman et al., 2000) to adjust the storm windspeed with the terrain exposition of the forest stand to wind direction. Ultimately, we calculate a damage probability factor by comparing the adjusted storm windspeed with the CWS needed to turn down trees (as calculated by the FGR model), following Equation 3 (as in Gardiner et al., 2024):

$$Damage = 1/1+e\ (-(stormWS*(1-(TopexPlot/TopexMax))-CWS)/S) - 1/1+e(CWS/S) \quad (Eq.3)$$

Similar to fire, the wind damage probability is applied as a fraction of the cohort damaged.

References

Chapman, L., 2000. Assessing topographic exposure. Meteorol. Appl. 7, 335–340. https://doi.org/10.1017/S1350482700001729.

Copernicus Climate Change Service, Climate Data Store, (2020): Fire danger indicators for Europe from 1970 to 2098 derived from climate projection. Copernicus Climate Change Service (C3S) Climate Data Store (CDS). DOI: 10.24381/cds.ca755de7

Gardiner, B., Byrne, K., Hale, S., Kamimura, K., Mitchell, S. J., Peltola, H., & Ruel, J. C. (2008). A review of mechanistic modelling of wind damage risk to forests. *Forestry*, *81*(3), 447-463.

Gardiner, B., Lorenz, R., Hanewinkel, M., Schmitz, B., Bott, F., Szymczak, S., ... & Ulbrich, U. (2024). Predicting the risk of tree fall onto railway lines. Forest Ecology and Management, 553, 121614.

Hale, S. E., Gardiner, B., Peace, A., Nicoll, B., Taylor, P., & Pizzirani, S. (2015). Comparison and validation of three versions of a forest wind risk model. *Environmental Modelling & Software*, *68*, 27-41.

Keane et al., 2011;

Locatelli, T., Gardiner, B., Tarantola, S., Nicoll, B., Bonnefond, J. M., Garrigou, D., ... & Patenaude, G. (2016). Modelling wind risk to Eucalyptus globulus (Labill.) stands. *Forest Ecology and Management*, *365*, 159-173.

Maynard, D. S., Bialic-Murphy, L., Zohner, C. M., Averill, C., van den Hoogen, J., Ma, H., ... & Crowther, T. W. (2022). Global relationships in tree functional traits. Nature Communications, 13(1), 3185

Nicoll, B. C., Gardiner, B. A., Rayner, B., & Peace, A. J. (2006). Anchorage of coniferous trees in relation to species, soil type, and rooting depth. *Canadian Journal of Forest Research*, *36*(7), 1871-1883.

Patacca et al., in prep Tree diversity increases functional stability of European forests

Schumacher, S., Reineking, B., Sibold, J., & Bugmann, H. (2006). Modeling the impact of climate and vegetation on fire regimes in mountain landscapes. *Landscape Ecology*, *21*, 539-554.;

Seidl, R., Rammer, W., & Spies, T. A. (2014). Disturbance legacies increase the resilience of forest ecosystem structure, composition, and functioning. *Ecological Applications*, *24*(8), 2063-2077.

Tuomi, M., Thum, T., Järvinen, H., Fronzek, S., Berg, B., Harmon, M., ... & Liski, J. (2009). Leaf litter decomposition—Estimates of global variability based on Yasso07 model. Ecological Modelling, 220(23), 3362-3371.

Tuomi, M., Laiho, R., Repo, A., & Liski, J. (2011). Wood decomposition model for boreal forests. *Ecological modelling*, *222*(3), 709-718.

Appendix D: Mortality model for EFISCEN-Space

Introduction

Natural mortality is an important demographic process in forests. In the first version of EFISCEN-Space (Schelhaas et al. 2022a) it was implemented as a fixed rate per diameter class and species, parameterised per country on repeated NFI data (Schelhaas et al., 2018b). As a next step we developed species-specific dynamic mortality models, which allows a wider range of management scenarios to be simulated, because the mortality will react to changes in forest structure. This also facilitates to include the impact of climate change on mortality. To do so, we collected repeated national forest inventory (NFI) data across Europe and amended it with repeated inventory data from forest reserve networks to cover a wider range of density and management situations.

Methods and data

We compiled repeated NFI data from 13 countries and additional forest reserve data from 12 countries in Europe. Several countries had multiple cycles available. We only included plots that had no trees reported as being harvested during the observation period. Our dataset covered in total a bit over 100 thousand plots with almost 1.5 million repeated tree observations, with nearly 120 thousand tree deaths recorded. The trees were grouped into 20 the major species groups as used in EFISCEN-Space. We followed the same statistical fitting procedure as for the increment model (Schelhaas et al. 2018a), i.e. a 10-fold forward selection process with 80% of the data for fitting and 20% for validation to identify potential predictors, followed by a backward selection process on the full dataset using the pre-selected variables. We used the same set of potential explanatory variables, representing forest structure, soil, deposition, weather and climate. We added diameter, ln(diameter) and diameter squared to accommodate different shapes. We also added the growth ratio as a predictor. The growth ratio is calculated as the ratio between the predicted growth of the tree under the observed stand conditions divided by the predicted growth of the tree under standardised conditions at the same site, being a tree with a neutral social status (rDiffDq=0) in a stand with a basal area of 10 m^2/ha. The growth ratio was introduced based on the observation that observed growth is one of the best predictors of future mortality (Hülsmann et al. 2017). For the basic statistical model we followed the approach of Portier et al. (2021), employing a generalized linear model with a complementary log-log (cloglog) link function and using the interval as on offset. This specific function is well-suited for modeling natural mortality because of its asymmetrical structure (Penman & Johnson, 2009), which accommodates cases where one outcome of the dependent variable is significantly less common than the other.

$$log(-log(1-p)) = \beta 0 + bj + \beta 1x1 + \cdots + \beta kxk$$

We then built in the new mortality model into the EFISCEN-Space modelling framework and tested its performance by simulating for a few countries a business-as-usual scenario using the new rule-based approach, as well as a scenario where management was absent. Both simulations were performed for a period of 100 years. Based on the results, we decided to add an additional parameter that stops the growth of a stand if a certain species-specific stand basal area is reached. This was needed as the model was clearly not capable of simulating realistic increment and mortality responses when reaching densities close to the self-thinning line, resulting in extremely high and unrealistic simulated basal areas. We set this parameter to the 99th percentile observed in the calibration data.

Results

All species include one or more variables that represent plot structure (Table D1), amended with a limited number of variables from one of the other classes. Ln(diameter) was the variable most often selected, being included in 13 models. The negative sign indicates a decreasing mortality with increasing diameter, reflecting the strong self-thinning process in small trees. In contrast, only 7 models included diameter or diameter squared, which is needed to create a pattern of increasing mortality with increasing diameter. Competition is an important variable, with 16 models including either a direct effect via plot basal area or social status (rDiffDq), or indirectly via the growth ratio. The maximum basal area per species after which the growth is stopped is generally in the range of 45-80 m^2 ha^{-1} (Table D2). This is somewhat higher than generally observed in old-growth forests (Trippleton et al. 2021) but takes into account the high values that can be observed in relatively small inventory plots. For most countries, simulated mortality in the first 5-year period aligns closely with those reported by Avitabile et al. (2024) (Figure D1). For the Netherlands, one of the outliers, the (harmonised) value as reported by Avitabile et al. seems very low compared to published values in the national NFI report. The simulated value of 1.14 m^3 ha^{-1} yr^{-1} actually lies well in the reported range of 0.91 m^3 ha^{-1} yr^{-1} for the period 2003-2013 and 1.70 m^3 ha^{-1} yr^{-1} for the period 2013-2021 (Schelhaas et al. 2022b). The other outliers will be studied in more detail.

Table D1. Species-specific parameters of the final mortality model

	speciesName	Abies spp.	Larix spp.	Picea abies	Picea sitchensis	Pseudotsuga menziesii	Pinus sylvestris	Pinus nigra+ mugo
	index	1	2	3	4	5	6	7
	intercept	-4.99778	4.498553	-9.71958	-13.6947	4.05406	2.174342	-6.7291
Forest structure	PlotBasalArea	0.021322						
	rDiffDq			-1.04037			-0.42428	
	lnPlotBasalArea		0.802931	0.391007			0.298673	
	lnDiameter_mm		-2.11706	-0.59019		-1.35475	-1.63076	-0.85164
	Diameter_mm			0.003955			0.003346	
	GrowthRatio				-3.11603	-3.07684	-0.8675	
	sqDiameter_mm		4.41E-06				2.04E-06	
Deposition	avgDepOxNnc						0.000404	0.004723
	avgDepRedNnc							
	avgDepOxSnc							
Soil	PHIHOX			0.095022	0.079268			0.187186
	SLTPPT							
	ORCDRC			0.010586				
	CRFVOL						-0.01677	-0.02556
	CEC			-0.05844				
Weather	MaT			0.112673			0.030269	
	aTR							
	TaP						0.000297	
	TaR						-0.00015	-0.00062
	MaDR							
	MINmP	-0.03952						
	ISO							
	ThHUi		0.012105					
	ThARi							
	SDmR				0.032823			
	SDmPET							
	MwaqP		-0.01296					
	MweqT							
	McoqP							
	MweqPET							
Climate	var20							
	var33							
	var3						0.020986	-0.11653
	bio9			-0.00386				
	var32		-0.0019					
	var23						-0.02175	
	bio8		-0.00494					-0.01277

	speciesName	Other ind. Pinus	Other conifers	Betula spp.	Castanea sativa	Eucalyptus spp.	Fagus sylvatica	Robinia pseudoacacia
	index	8	9	10	11	12	13	14
	intercept	-0.42437	-5.83371	-5.83247	2.190693	-4.87509	-1.43553	-7.76732
Forest structure	PlotBasalArea	0.01464	0.024265					
	rDiffDq		-1.23992	-1.05732			-0.33919	-1.0191
	lnPlotBasalArea							
	lnDiameter_mm	-0.58252			-1.07378		-0.56524	
	Diameter_mm							
	GrowthRatio				-0.94832			
	sqDiameter_mm						2.31E-06	
Deposition	avgDepOxNnc	0.000898						
	avgDepRedNnc							
	avgDepOxSnc					-0.00066		
Soil	PHIHOX			0.032047				
	SLTPPT	0.043344						
	ORCDRC_sd3							
	CRFVOL							
	CEC		-0.05559					
Weather	MaT							0.289092
	aTR							
	TaP							
	TaR		-0.00022					
	MaDR	-0.03592					0.23259	
	MINmP							
	ISO	-3.0168						
	ThHUi	0.002791	0.002529					
	ThARi						-0.02077	
	SDmR							
	SDmPET						-0.04685	
	MwaqP							
	MweqT		0.174637	0.009929				
	McoqP							
	MweqPET							
Climate	var20							
	var33							
	var3	-0.06304						
	bio9							
	var32							
	var23	0.02454		-0.01731				
	bio8							

	speciesName	Populus plantations	Quercus robur&petraea	Quercus ilex	Quercus suber	long-lived broadleaves	short-lived broadleaves
	index	15	16	17	18	19	20
	intercept	4.581486	-0.56921	-1.6847	-7.02664	0.513274	-2.97486
Forest structure	PlotBasalArea		-0.01859			0.00615	0.002711
	rDiffDq		-0.50657			-0.29725	-0.50072
	lnPlotBasalArea	-0.36662	1.057826			0.172575	0.075497
	lnDiameter_mm	-1.65723	-1.26972	-0.54121		-1.44096	-0.43158
	Diameter_mm	0.004484				0.004093	
	GrowthRatio	-2.1001					
	sqDiameter_mm		1.89E-06				
Deposition	avgDepOxNnc					0.000492	-0.00044
	avgDepRedNnc	0.000497	0.000172			0.00025	0.000396
	avgDepOxSnc				0.001009		
Soil	PHIHOX						
	SLTPPT						
	ORCDRC_sd3						
	CRFVOL		-0.04612	0.035994			
	CEC						
Weather	MaT	0.06947				0.069724	
	aTR						0.020395
	TaP						
	TaR						
	MaDR						
	MINmP		0.029399				
	ISO					-2.25665	
	ThHUi				-0.00669	0.001845	
	ThARi		-0.01283				-0.00847
	SDmR						0.004051
	SDmPET						
	MwaqP						
	MweqT						
	McoqP			0.030093			
	MweqPET				0.023116		
Climate	var20				-0.00222		
	var33	0.001296					
	var3			-0.09934			
	bio9				0.008		
	var32						
	var23						
	bio8						-0.00095

Table D2. Species-specific maximum basal area at which the growth is stopped

Species index	Species name	Maximum plot basal area
1	Abies spp.	79.99
2	Larix spp.	76
3	Picea abies	72.75
4	Picea sitchensis	77.55
5	Pseudotsuga menziesii	88.33
6	Pinus sylvestris	57.56
7	Pinus nigra+mugo	61.97
8	Other indigenous Pinus	58.27
9	Other conifers	63.4
10	Betula spp.	51.73
11	Castanea sativa	77.26
12	Eucalyptus spp.	52.91
13	Fagus sylvatica	70.83
14	Robinia pseudoacacia	70.87
15	Populus plantations	68.11
16	Quercus robur&petraea	61.84
17	Quercus ilex	43.82
18	Quercus suber	43.73
19	long-lived broadleaves	61.48
20	short-lived broadleaves	65.32

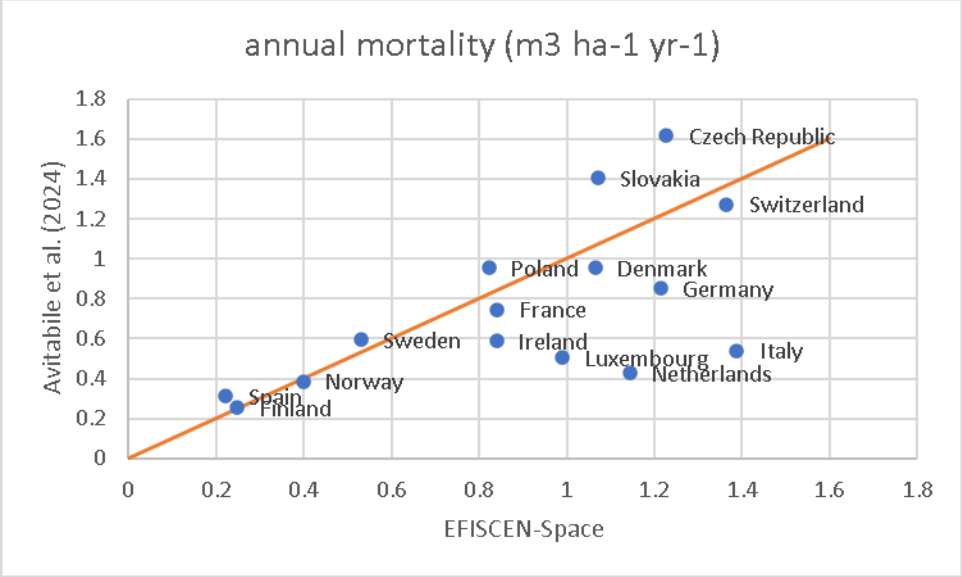

Figure D1. Comparison of simulated mortality by EFISCEN-Space in the business-as-usual scenario (using the rule-based approach) and annual natural losses as reported by Avitabile et al. (2024). In orange the 1:1 line is shown.

References

Avitabile, V., Pilli, R., Migliavacca, M., Duveiller, G., Camia, A., Blujdea, V., ... & Mubareka, S. (2024). Harmonised statistics and maps of forest biomass and increment in Europe. *Scientific data*, *11*(1), 274.

Hülsmann, L., Bugmann, H., & Brang, P. (2017). How to predict tree death from inventory data—lessons from a systematic assessment of European tree mortality models. *Canadian Journal of Forest Research*, *47*(7), 890-900.

Penman, A. D., & Johnson, W. D. (2009). Complementary log–log regression for the estimation of covariate-adjusted prevalence ratios in the analysis of data from cross-sectional studies. *Biometrical Journal: Journal of Mathematical Methods in Biosciences*, *51*(3), 433-442.

Portier, J., Wunder, J., Stadelmann, G., Zell, J., Abegg, M., Thürig, E., & Rohner, B. (2021). 'Latent reserves': A hidden treasure in National Forest Inventories. *Journal of Ecology*, *109*(1), 369-383.

Schelhaas, M. J., Hengeveld, G. M., Heidema, N., Thürig, E., Rohner, B., Vacchiano, G., ... & Nabuurs, G. J. (2018a). Species-specific, pan-European diameter increment models based on data of 2.3 million trees. *Forest Ecosystems*, *5*, 1-19.

Schelhaas, M. J., Fridman, J., Hengeveld, G. M., Henttonen, H. M., Lehtonen, A., Kies, U., ... & Nabuurs, G. J. (2018b). Actual European forest management by region, tree species and owner based on 714,000 re-measured trees in national forest inventories. *PLoS One*, *13*(11), e0207151.

Schelhaas MJ, Hengeveld GM, Filipek S, König L, Lerink B, Staritsky I, de Jong A, Nabuurs GJMM (2022a) *EFISCEN-Space 1.0 model documentation and manual.* Wageningen, Wageningen Environmental Research, Report 3220 https://edepot.wur.nl/583568

Schelhaas, M. J., Teeuwen, S., Oldenburger, J., Beerkens, G., Velema, G., Kremers, J., ... & Clerkx, A. P. P. M. (2022b). *Zevende Nederlandse Bosinventarisatie: methoden en resultaten* (No. 142). Wettelijke Onderzoekstaken Natuur & Milieu.

Thrippleton, T., Hülsmann, L., Cailleret, M., & Bugmann, H. (2021). An evaluation of multi-species empirical tree mortality algorithms for dynamic vegetation modelling. *Scientific Reports*, *11*(1), 19845.

Appendix E: Propagation of uncertainty from input data into EFISCEN-Space projections: A case study of Romanian forests

Propagation of uncertainty from input data into EFISCEN-Space projections: A case study of Romanian forests

Ioan Dutca, Mart Jan Schelhaas, Sara Filipek, Gert Jan Nabuurs, Sergey Zudin, Igor Staritsky

Abstract

Forest resource projection models, such as EFISCEN-Space, are often used to investigate the future development of forests over large forest areas. They typically use the National Forest Inventory (NFI) data to initialize the model, and future projections are produced over a period of several decades. However, the uncertainty of these projections is expected to originate, among other sources related to the model, in the uncertainty of the input data to initialize the model. Here we performed an uncertainty analysis for EFISCEN-Space model using Romanian NFI as a case study. Three types of uncertainty were considered: (i) plot sampling uncertainty, (ii) tree measurement uncertainty and (iii) allometric volume model prediction uncertainty. These uncertainty types were integrated within the following EFISCEN-Space input files: (i) plotNrPerHa.csv, (ii) plotAttributes.csv, (iii) volumeParameters.csv and (iv) mortalities.csv. We used a Monte Carlo error propagation procedure in 42 steps, constructed in R, to integrate the three types of uncertainty into the four input files. To propagate the errors from these input files into the EFISCEN-Space projections we performed 1000 replications. For each replication, new input files were produced based on resampled plot data while including measurement uncertainty and volume model prediction residual uncertainty, launched the EFISCEN-Space model for a period of 40 years and retained the aggregated results at the country level (output6.csv). The uncertainty of projections was assessed by calculating the standard error (SE) and coefficient of variation (CV) of projected values for each simulation year. Overall, the uncertainty in the resulting projections was relatively low, due to the large number of plots used to initialize the model. However, the greatest initial uncertainty was observed for the annual harvest, with CV reaching 2.35%. During the simulation period, the greatest relative increase in uncertainty, measured by CV change, occurred for basal area per hectare and tree number per hectare, which saw increases of +90% and +89.6%, respectively. In terms of SE increase, the largest change was observed for mean volume per hectare, which increased by +137.2%. Interestingly, the mean annual harvest was the only variable that experienced a reduction in uncertainty during the simulation period, with uncertainties decreasing by -31.8%. Analysing these changes over time highlights the cumulative impact of uncertainty on forest projection reliability, guiding future improvements in data collection and model accuracy. We acknowledge this analysis provides only a partial picture about the uncertainty of forest resources projections. Therefore, further development of this analysis is advised, to investigate the effects of other sources of uncertainty such as uncertainty from the D increment models, dynamic mortality models and dynamic ingrowth models.

1. Introduction

Forest resource modelling plays a critical role in understanding forest growth, mortality, and biomass/carbon changes over time. Models like EFISCEN-Space are essential for projecting forest dynamics, especially as forests face pressures from climate change, human intervention, and natural growth cycles. EFISCEN-Space, a spatially explicit model, uses National Forest Inventory (NFI) data to initialize and predict forest changes at various temporal and spatial scales, providing valuable insights for forest management and policymaking (Schelhaas et al., 2022).

However, the in the process of decision-making, the uncertainty of the estimates plays a vital role. Having knowledge on the level of uncertainty of forest resources projections can help decision makes taking the most appropriate decisions. Creating robust projections does not necessarily mean that uncertainty is reduced, but it is transparently presented (Wei & Xia, 2024). Therefore, estimation of uncertainty of forest estimates has increased in popularity in the last decade, also because of requirements on uncertainty reporting within the carbon mitigation efforts in the forestry sector (Vorster et al., 2020; Yanai et al., 2018, 2020).

The uncertainty in forest NFI estimates typically originates from plot sampling and tree prediction and measurement of individual trees within plots, because forest volume or biomass are based on the cumulative tree predictions within sample plots (McRoberts et al., 2015; McRoberts & Westfall, 2014). The uncertainty from tree prediction and measurement is often disregarded, due to difficulties in error propagations or simply because the necessary information, such as the variance-covariance matrix and the residual variance is often lacking.

The uncertainty from allometric model predictions significantly contributes to the total uncertainty in large-area forest biomass estimates, as highlighted in multiple studies (McRoberts et al., 2015, 2016; McRoberts & Westfall, 2014; Vorster et al., 2020; Yanai et al., 2020). This prediction uncertainty arises from four main sources: (i) the choice or potential misspecification of the allometric model, (ii) measurement errors in the independent variables, (iii) uncertainty in the model's parameter estimates, and (iv) residual variance (McRoberts et al., 2016; McRoberts & Westfall, 2014). The sample size of the calibration dataset used to fit the models has been identified as a crucial factor affecting biomass estimation uncertainty at the national level, as it influences both model parameter and residual variance uncertainties (Duncanson et al., 2015). Distribution of the calibration sample is also an important feature that affects the efficacy of observations in the model prediction uncertainty (Dutcă & McRoberts, 2024), as does the independence of observations (Dutcă, Mather, et al., 2018; Dutcă, Stăncioiu, et al., 2018).

The use of remote sensing, particularly in model-assisted estimation frameworks, can effectively reduce sampling uncertainty in National Forest Inventories (NFIs). Integrating remote sensing data, such as LiDAR or satellite imagery, with field measurements enhances estimations by using wall-to-wall coverage for variables like biomass and tree volume (Gregoire et al., 2016; Saarela

et al., 2020). Remote sensing acts as auxiliary data that, when applied in model-assisted methods, maintains unbiased estimates while increasing precision by leveraging extensive spatial data across vast forest areas (Ståhl et al., 2016). For example, combining airborne LiDAR data with field plot samples has shown to reduce variance in biomass estimates by providing detailed, consistent spatial information (Condés & McRoberts, 2017; McRoberts et al., 2016).

Monte Carlo error propagation is a statistical technique used to assess uncertainty in forest attribute estimates, such as biomass or carbon stock, by simulating possible outcomes based on input variability. Multiple random samples are generated from these distributions, and for each sample set, NFI calculations are performed to produce a range of possible outputs. This process is repeated many times, creating a distribution of results that reflects the combined effect of input uncertainties on the final estimate. The spread of this distribution indicates the level of uncertainty in the attribute of interest, providing insights into the reliability of forest inventory estimates. This approach is particularly valuable for complex, non-linear models and allows decision makers to make more informed decisions by understanding how measurement errors and natural variability affect estimates (McRoberts et al., 2015).

In this report we used a Monte Carlo error propagation procedure in R, to investigate how the uncertainty in the input data affected the uncertainty of EFISCEN-Space projections for Romanian forests, over a period of 40 years.

2. Material and methods

2.1. Romanian NFI data

For this analysis we used the Romanian National Forest Inventory (NFI) data from the first cycle (NFI1) and from the second NFI cycle (NFI2). Romanian NFI is a continuous forest inventory with a cycle of 5 years. The first cycle period is 2007-2012 and the second cycle was between 2012-2017. It consists of clusters of four sample plots located at the intersection of a 4x4 km grid for the mountain and hilly area and a 2x2 km for the plain area. To increase sampling efforts efficiency, at the intersection of grid lines, there are 4 plots, with 250 m between plots. Each plot is permanent and consists of two subplots:

- a large subplot of 500 m^2 where only trees with $D > 28.5$ cm are measured.
- a small subplot of 200 m^2, concentrical to the large subplot, where trees with $5.6 \leq D \leq 28.5$ cm are measured.

Because the two subplots are concentrical, within the small subplot all trees are measured, whereas in the circle sector of the large subplot remaining outside the small subplot (i.e., the annulus), only trees with $D > 28.5$ cm are measured.

The NFI1 data consists of 7514 plot clusters that contains 20781 plots and 437750 unique trees. The NFI2 contains 7573 plot clusters with 21286 plots and 514352 trees. Of these, 398823 trees have been identified in both NFI1 and NFI2. The NFI1 and NFI2 were further used to generate the input files for EFISCEN-Space. From the NFI database we generated three files that were used as a starting point for the Monte Carlo error propagation procedure:

1. Tree data (TD.csv) that contains tree information based on NFI2
2. Plot data (PD.csv) that contains information on plots from NFI2
3. Mortality and harvest data (MH.csv) that contains information on tree mortality and harvest.

2.2. Pre-processing of tree data (TD.csv)

The TD.csv was originated from NFI2 (i.e., the second cycle of Romanian NFI). Within the error propagation procedure, the TD.csv will be used to produce plotNrPerHa.csv and volumeParameters.csv EFISCEN-Space input files.

The NFI2 has been cleaned and prepared for processing:

- Each plot was renamed as a combination of “RO_2_sondaj_spinsondaj”, where “sondaj” was the code of the plot cluster, and “spinsondaj” was the code of the plot within the cluster.

- Each tree was given a unique code, composed of "sondaj_spinsondaj_treeinsp", where the "treeinsp" is the code of the tree within the plot.
- Retain only the trees with unique tree codes (duplicated plots were also removed during this procedure).
- Retain only the plots reported under land use category "forest" and only the trees reported as "alive".
- Because the Latin name of the tree species in the NFI2 may have been slightly different than that in the "efiscen_species.csv", where species are grouped in 20 species classes (i.e., speciesIndex), we checked the name of each tree species and made sure the species name is in a format that matches the efiscen_species.csv file.
- Assign the speciesIndex class (1 to 20) for each tree within the NFI2 dataset.
- For each tree in the NFI2 dataset, calculate the corresponding number of trees per hectare as a product between the share of forest within the small (i.e., 200 m^2) or large (i.e., 500 m^2) subplot and the expansion factor per hectare (i.e., 50 for the small subplot and respectively 20 for the large subplot). Plots reported with 0% forest were removed from the analysis.
- Assign the representative area for each plot. If the plot was within the 4x4 km grid, the representative area for each plot was 400 ha (given that there are 4 plots within each intersection of the grid); if the plot was within the 2x2 km grid, the representative area was 100 ha.
- Determine the measurement year for each plot (derived from the date of the measurement).

The TD.csv was created from NFI2, restricted to the following columns:

1. plotName – the name of the plot
2. sp – the Latin species name, necessary for calculating the tree volumes
3. speciesIndex – the species index as in efiscen_species.csv.
4. D – diameter at breast height in mm
5. H – tree height, in cm
6. NperHa – tree number per hectare

2.3. Pre-processing of plot data (PD.csv)

The PD.csv will be used to produce plotAttributes.csv input file. The PD.csv was obtained by reducing NFI2 to the necessary columns:

- plotName
- nfiYear – the year of measurement
- reprArea – the representative area (i.e., 100 or 400 ha)

- latitude – these are not the exact coordinates of the plot, but the centre of 1km Inspire cell, in m (EPSG:3035)
- longitude – in m (EPSG:3035)

The second step was to retain only the unique plot values in the PD.csv.

Attaching abiotic data

The abiotic data "abiotics.csv" containing bioclimatic and soil variables (as in Table 3.5 from EFISCEN-Space 1.0 documentation and manual (Schelhaas et al., 2022)) was extracted for each plot based on its coordinates. The "abiotics.csv" data was attached to PD.csv by "plot coordinates".

Attaching weather data (weatherVariable.csv)

The weather data such as temperature and precipitation over a 25 by 25 km grid (see Table 3.6 from EFISCEN-Space 1.0 documentation and manual) was attached to PD.csv dataset by the "grid no".

Besides the abiotic and weather data, the PD.csv contains the variables mortalityNat, mortalityMgt, volumeRegion, branchBiomassRegion, foliageBiomassRegion, rootsBiomassRegion, woodDensityRegion, stemBiomassRegion, and costRegion, see Table 3.38 from (Schelhaas et al., 2022).

2.4. Pre-processing of mortality and harvest data (MH.csv)

The MH.csv file is originated from both NFI2 and NFI1 (first NFI cycle).

- For both NFI2 and NFI1, a unique "TreeID" was determined based on combination of plot cluster, plot and tree within plot "sondaj_spinsondaj_treeinsp".
- For both NFI1 and NFI2, the plotName was assigned as "RO_sondaj_spinsondaj".
- Checking the species names in both NFI1 and NFI2 to match the species names in efiscen_species.csv.
- Determine the speciesIndex by merging NFI1 with efiscen_species.csv by "scientificName"

Retain from NFI2 only trees labelled as:

1. Trees that were identified in both NFI1 and NFI2
2. Trees that were harvested
3. Trees with the stem broken under 1.3 m from the ground.

Merge NFI1 with the NFI2 datasets by “TreeID”, in order to assign to each tree in the NFI2 its diameter from NFI1.

The MH.csv dataset has the following columns:

- plotName – name of the plot
- TreeID – the unique ID of each tree
- D – diameter at breast height in mm, recorded from NFI1
- speciesClass – this is the speciesIndex determined based on efiscen_species.csv
- VM1 – the status of the tree in NFI1 (dead or alive)
- VM2 – the status of the tree in NFI2 (dead or alive). The trees in NFI2 with the stem broken under 1.3 m were assumed being dead in NFI2.
- Statut – the status of the trees in NFI2 (e.g., “Identified in both NFI1 and NFI2”, “Harvested” or “Broken under 1.3m”).

2.5. Preparatory steps for the application of Monte Carlo error propagation procedure

a. *Prepare the volume model parameter list*

Within the “model_params” list we defined the allometric model parameters for 107 tree species present in NFI1. The Romanian NFI uses distinct volume model parameters for 40 tree species (Marin et al., 2019). Besides these 40 species, for the remaining 67 species (67=107-40), the volume model parameters were assigned from one of those 40 species, based on species similarities. The allometric volume model parameters are for a polynomial function using both D and H in logarithmic scale to estimate tree volume:

$$V_i = 10^{(a+b\cdot log_{10}(D_i)+c\cdot[log_{10}(D_i)]^2+d\cdot log_{10}(H_i)+e\cdot[log_{10}(H_i)]^2)} \qquad \text{Eq. (1)}$$

Where D is the diameter at breast height (in cm), H is the tree height (in m), and V is the predicted tree volume (in m^3). A function was created “predict_V” based on Eq. (1), which aims to predict the volume of individual trees, based on the allometric volume model parameters for each species (from “model_params” list).

b. Prepare the plot vector to be resampled

plot_vector - A vector containing unique plotNames

2.6. Propagating uncertainty from allometric volume models

The official Romanian allometric volume models were developed in the 70's, therefore, apart from the model parameter estimates, no other information was published (Giurgiu et al., 1972; Giurgiu & Draghiciu, 2004). To propagate errors from allometric model predictions it is required information on (i) the variance-covariance matrix of model parameters plus the residual variance or (ii) original observations used to fit the model. None of these two options can be achieved, since no observations were available nor the variance-covariance matrix including the residual variance. It is acknowledged that uncertainty from residual variance is greater when compared to uncertainty sourced in the variance-covariance matrix.

Because the residual standard error (RSE) was not provided, we estimated the RSE. For the main (in terms of tree numbers) 12 tree species within the NFI, we collected tree volume measurements from international databases. For each species we created a dataset containing measurements of D, H and V. For each tree in the dataset the residual r_i was calculated as the difference between volume observation (V_i) and the volume prediction ($\hat{V}_i$) based on Eq. (1), in log scale:

$$r_i = \log(V_i) - \log(\hat{V}_i) \qquad \text{Eq. (2)}$$

We assumed the differences between $\log(V_i) - \log(\hat{V}_i)$ were homoscedastic as a result of logarithmic transformation (Dutcă et al., 2022), therefore, we further calculated the standard deviation of differences (Eq. 2) as a substitute for RSE:

$$SD_{diff} = \sqrt{\frac{\sum_{i=1}^{n}(r_i - \bar{r}_i)^2}{n-1}} \qquad \text{Eq. (3)}$$

We created a list of standard deviations of differences (Eq. 3) for each of the 12 main tree species "residual_sd". As for the "model_params" list, we assimilated the remaining 95 species (95=107-12) to one of the 12 species.

2.7. The Monte Carlo error propagation procedure

The procedure was implemented in R, in 42 steps. Within this procedure, the following EFISCEN-Space input files were produced: plotNrPerHa.csv, plotAttributes.csv, volumeParameters.csv and mortalities.csv. The uncertainty implemented is from (i) plot sampling, (ii) measurement of D and H and (iii) residual variance of volume allometric model predictions.

For the i^{th} replication:

Step (1): Resample with replacement the plot_vector, producing "Resampled_plots" vector.

Step (2): Create a new dataset (Resampled_plots_dataset) that contains two columns: (i) "plotName" - the "Resampled_plots" vector and (ii) "plotName1", which is the renamed plot. The plots were renamed using "RO_2_index", where the "index" is the index of the plot in the resampled vector (i.e., from 1 to the length of the "Resampled_plots" vector). When

resampling with replacement some plots will appear more than once in the resampled vector. That becomes problematic when resembling the original dataset based on the resampled plots. If the plots are not renamed, those plots appearing more than once will still appear as one plot but having double (or multiplied) number of trees. To distinguish between individual plots, the resampled plots were renamed, so that the further plot level separation was possible.

development of plotNrPerHa.csv file

Step (3): Merge the "Resampled_plots_dataset.csv" with "TD.csv, by "plotName", into TD1.csv.

Step (4): Select a random value (muD) for each line within the merged dataset from step (3), from N(0,1).

Step (5): Add the measurement uncertainty for each D measurement in TD.csv as:

$$D_{u_i} = D_i + muD_i \cdot 0.00255 \cdot D_i \qquad \text{Eq. (4)}$$

where muD is the random value from step (4), and 0.00255 derived from FIA protocol stating that 95% of D measurements are to be within 0.5% of true D (McRoberts et al., 2016).

Step (6): Determine the new dbh.class based on Du:

$$dbh.class_i = \frac{D_{u_i}}{25} + 1 \qquad \text{Eq. (5)}$$

For $dbh.class_i > 40$, replace the $dbh.class_i$ with 40.

Step (7): Create a new dataset TD2.csv derived from TD.csv that contains the columns: plotName, speciesIndex, dbh.class and NPerHa.

Step (8): Group the TD2.csv by plotName, speciesIndex and dbh.class, while calculating the sum of NPerHa for each group.

Step (9): Create a matrix (TD2grouped) where on Y axis are the groups plotName, speciesIndex while on X axis the dbh.classes. For each combination of plotName, speciesIndex and dbhclass get the sum of NPerHa from step (8). Replace NA values with 0.

Step (10): Export the TD2grouped as a csv file called plotNrPerHa.csv, to the following location: "efiscenspace/efiscenspace/scenariodefinition/plots".

development of plotAttributes.csv file

Step (11): Merge the "Resampled_plots_dataset.csv" with "PD.csv, by "plotName", creating PD1.csv. Delete "plotName" column and rename "plotName1" to "plotName" within the PD1.csv.

Step (12): Export the PD1.csv renamed as plotAttributes.csv, to the following location: "efiscenspace/efiscenspace/scenariodefinition/plots".

development of volumeParameters.csv file

Step (13): Create a new VMP.csv dataset from TD1.csv that already contains the resampled plots.

Step (14): Select a random value (muH from N(0,1)) for each line within VMP.csv.

Step (15): Add the measurement uncertainty for each H measurement in VMP.csv as:

$$H_{u_i} = H_i + muH_i \cdot 0.06079 \cdot H_i \qquad \text{Eq. (6)}$$

where muH is the random value from step (14), and 0.06079 is a factor derived from the statement that 90% of H measurements are to be within 10% of true H (McRoberts et al., 2016).

Step (16): Predict the volume of each tree in VMP.csv using "predict_V" function that uses "model_params" list. The function uses Eq. 1 and species-specific volume model parameters to predict volume of individual trees. The independent variables Du and Hu used to predict the volume are those to which measurement uncertainty were added.

Step (17): Select a random value R_v from N(0,1) for each line within VMP.csv.

Step (18): Add uncertainty to volume predictions from step (16) as:

$$\widehat{V_{u_i}} = e^{(\log(\widehat{V_i}) + R_{v_i} \cdot SD_{diff_i})} \qquad \text{Eq. (7)}$$

where SD_{diff} is the standard deviation of differences between observed and predicted V (Eq. 3), which is an estimate of RSE (residual standard error of an allometric model in log scale).

Step (19): Create as many datasets from VMP.csv as classIndex levels.

Step (20): To each dataset created at step (19), fir a quadratic model to data that uses Du to predict Vu:

$$V_u = q_0 + q_1 D_u + q_1 {D_u}^2 + \varepsilon \qquad \text{Eq. (8)}$$

Step (21): Create a data frame (volumeParameters) containing the region (i.e., Romania), speciesIndex (i.e., 1 to 20), function (i.e., quadratic), q_0, q_1, q_2 and minVol (i.e., the minimum volume Vu).

Step (22) Export the volumeParameters as volumeParameters.csv, to the following location: "efiscenspace/efiscenspace/scenariodefinition/ expansionfactors".

development of mortalities.csv file

Step (23): Merge the "Resampled_plots_dataset.csv" with "MH.csv, by "plotName", into MH1.csv.

Step (24): Select a random value (rD) for each line within the merged dataset from step (3), from N(0,1).

Step (25): Add the measurement uncertainty for each D measurement in MH1.csv as:

$$D_{u_i} = D_i + rD_i \cdot 0.00255 \cdot D_i \qquad \text{Eq. (9)}$$

Step (26): Determine the new dbh.class based on Du in the MH1.csv:

$$dbh.class_i = \frac{D_{ui}}{25} + 1 \qquad \text{Eq. (10)}$$

For $dbh.class_i > 40$, replace the $dbh.class_i$ with 40

Step (27): Create a dataset "HVdata" based on MH1.csv, that contain only harvested trees (statut = harvested).

Step (28): Create a dataset named "MOdata" based on MH1.csv that contain trees that were alive in NFI1 (VM1 = alive) and dead in NFI2 (VM2 = dead).

Step (29): Group MH1.csv dataset by speciesClass and dbh.class, while accounting the total number of trees in each group (i.e., MHg). Create an index of that contains speciesClass number and dbh.class number (i.e., speciesClass_dbh.class). Rename the column containing the number of trees in each group as "REF".

Step (30): Group the HVdata.csv by speciesClass and dbh.class, while accounting the total number of trees in each group (i.e., HVg). Create an index as in step (29). Rename the column containing the number of trees in each group as "HV".

Step (31): Group the MOdata.csv by speciesClass and dbh.class, while accounting the total number of trees in each group (i.e., MOg). Create an index as in step (29). Rename the column containing the number of trees in each group as "MO".

Step (32): Merge the data frames MHg, HVg and Mog by "index" into MHg.

Step (33): Calculate the probability of trees being harvested (PrH) or die (PrM) for each combination of speciesIndex and dbh.class as (Schelhaas, Fridman, et al., 2018):

$$PrH = 1 - \left(1 - \frac{HV}{REF}\right)^{\frac{1}{mY}} \qquad \text{Eq. (11)}$$

$$PrM = 1 - \left(1 - \frac{MO}{REF}\right)^{\frac{1}{mY}} \qquad \text{Eq. (12)}$$

where REF is the total number of trees for each combination of speciesIndex and dbh.class, HV is the number of trees being harvested for each combination of speciesIndex and dbh.class and MO is the number of trees that died for each combination of speciesIndex and dbh.class; mY is the average duration between measurements in NFI1 and NFI2. To calculate the mY, the number of years between NFI1 and NFI2 was determined for each plot, and further calculate the mean number of years between NFI1 and NFI2 over all plots.

Step (34): A new datasets named "Harvest" was derived from MHg, containing the following columns: speciesIndex, dbh.class and PrH.

Step (35): Similarly for mortality. The dataset "Mortality" was derived from MHg, containing the following columns: speciesIndex, dbh.class and PrM.

Step (36): The "Harvest" data frame was arranged by dbh.class (on X axis) and speciesIndex (on Y axis); the PrH was shown in the matrix for each combination of dbh.class and speciesIndex. Check if any dbh.class is missing and include a column for the missing class with PrH = NA.

Step (37): The "Mortality" data frame was arranged by dbh.class (on X axis) and speciesIndex (on Y axis); the PrM was shown in the matrix for each combination of dbh.class and speciesIndex. Check if any dbh.class is missing and include a column for the missing class with PrM = NA.

Step (38): Merge Harvest and Mortality data frames into "mortalities" data frame. Replace all NA values in the mortalities data frame with zero.

Step (39): Export the mortalities data frame as mortalities.csv, to the following location: "efiscenspace/efiscenspace/scenariodefinition/growthandmortality".

Step (40): Launch EFISCEN-Space from R. Within the settings.csv file the startYear was set to 2015, Duration to 40 years, numpy_randomseed to 123. The following variables were set to 1: BiomassOutput, NumberOutput, useStaticMortality and makeCSVOutput. All the remaining variables were set to 0.

Step (41) Import EFISCEN-Space aggregated output6.csv into R.

Step (42) Retain the following variables from output6.csv for each replication:

- average basal area (m^2/ha)
- average harvest (m^3/ha/yr)
- average mortality (m^3/ha/yr)
- average number of trees per hectare (N/ha)
- average volume per hectare (m^3/ha)

Simulation period

The simulation period was from 2015, which is the mid of the second NFI cycle, until 2055, therefore, over a period of 40 years.

2.8. Presentation of uncertainty

For each parameter of interest, and for each of the 40 years of the simulation period, we calculated the standard deviation of all 1000 repeated values of variable X, which is the standard error:

$$SE = \sqrt{\frac{1}{1000}\sum_{i=1}^{1000}(X_i - \bar{X})^2} \qquad \text{Eq. (13)}$$

To better understand the magnitude of the SE in relation to the estimated mean, we calculated the coefficient of variation (CV%) as:

$$CV = \frac{SE}{\bar{X}} \cdot 100 \qquad \text{Eq. (14)}$$

3. Results

3.1. Number of trees per hectare

The number of trees per hectare increased by 2027, from about 886 to 910 trees ha^{-1} followed by a decline to about 814 trees ha^{-1} in 2055. Both the standard error and the coefficient of variation increased during the simulation period from about 5.5 trees ha^{-1} (CV = 0.6%) in 2015 to about 9.5 trees ha^{-1} (CV = 1.17%) in 2055 (Figure 1).

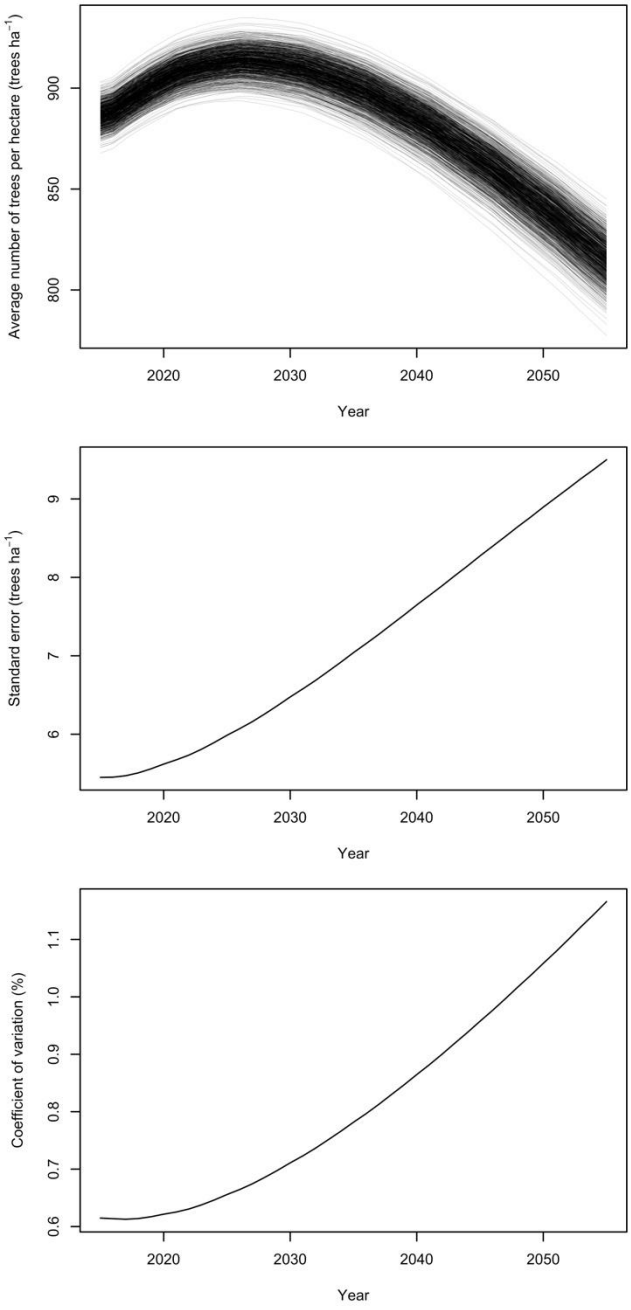

Figure 1. Number of trees per hectare with the standard error and coefficient of variation

3.2. The basal area per hectare

The average basal area per hectare increased by approximately 22%, from 28.7 m^2 ha^{-1} in 2015 to 35 m m^2 ha^{-1} in 2055. The uncertainty of basal area, although generally small, increased by a factor of two during the simulation period, from 0.14 to 0.33 m^2 ha^{-1} (the coefficient of variation, from 0.49% to 0.94%) (Figure 2).

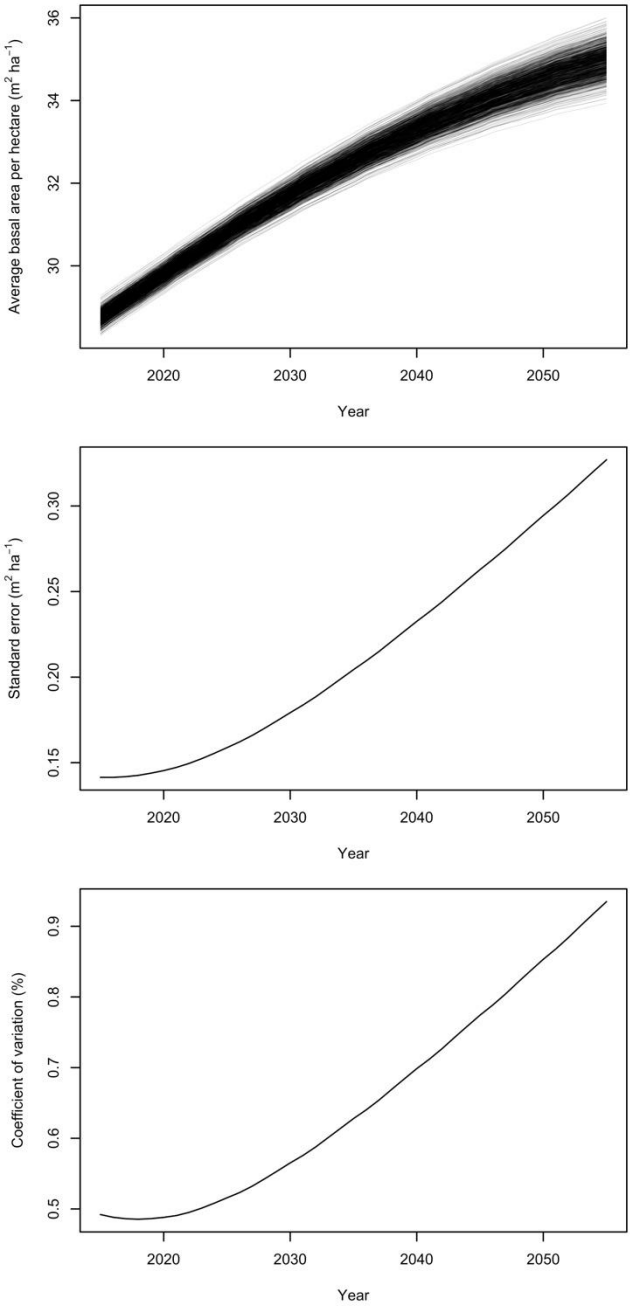

Figure 2. The average basal area per hectare with the standard error and coefficient of variation

3.3. Volume per hectare

The average volume per hectare increases from approximately 337 m^3 ha^{-1} in 2015 to approximately 437 m^3 ha^{-1} in 2055 (Figure 3), which represent an increase of about 30%. The standard error of average volume per hectare increases substantially during the simulation period from approximately 2 m^3 ha^{-1} in 2015 to about 4.9 m^3 ha^{-1} in 2055 (an increase of 137%) and the CV increased from 0.6 to 1.1%, which is an increase of 83% (Figure 3).

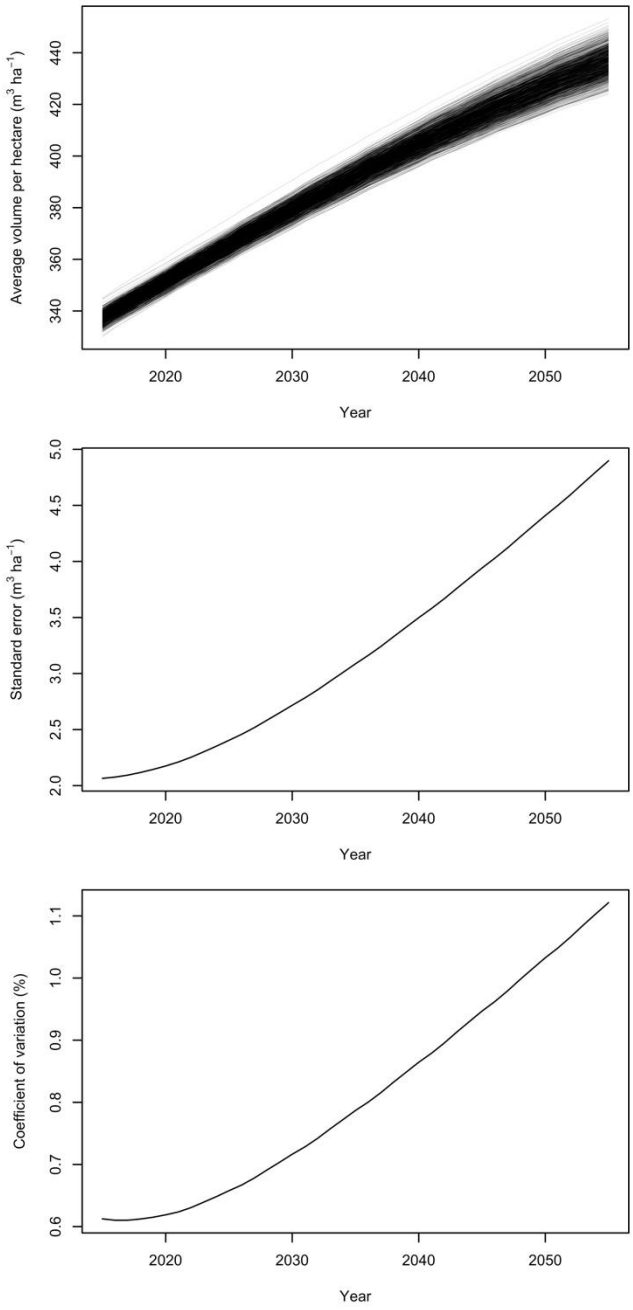

Figure 3. The average volume per hectare with the standard error and coefficient of variation

3.4. Annual tree mortality per hectare

Average tree mortality increased during the simulation period from approximately 1.78 m^3 ha^{-1} yr^{-1} in 2015 to approximately 2.0 m^3 ha^{-1} yr^{-1} in 2055. The coefficient of variation of tree mortality per hectare increased from 2% in 2015 to about 2.6% in 2055 (Figure 4).

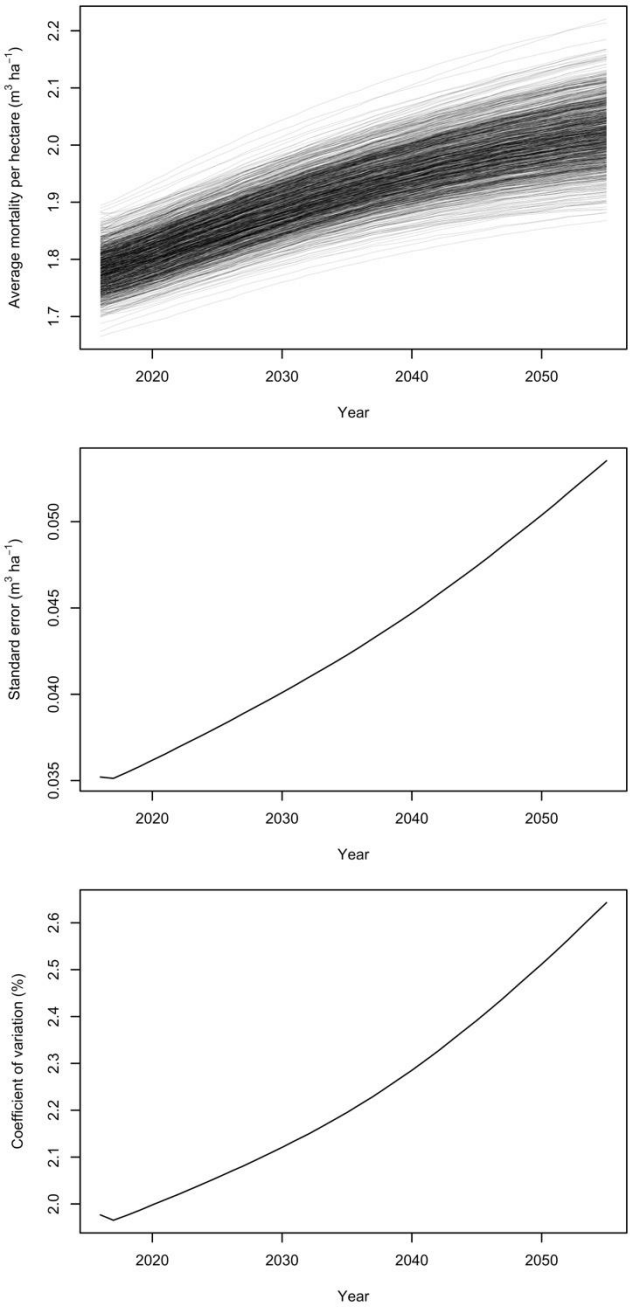

Figure 4. The annual average mortality per hectare with the standard error and coefficient of variation

3.5. Annual tree harvest per hectare

The tree harvest per hectare started from approximately 4.9 m^3 ha^{-1} yr^{-1} to approximately 6.7 m^3 ha^{-1} yr^{-1} in 2055. The uncertainty in tree harvest, unlike for the other variables investigated, decreased during the simulation period, from about 2.4% (or 0.11 m^3 ha^{-1} yr^{-1}) in 2015 to about 1.6% (or 0.1 m^3 ha^{-1} yr^{-1}) in 2055 (Figure 5).

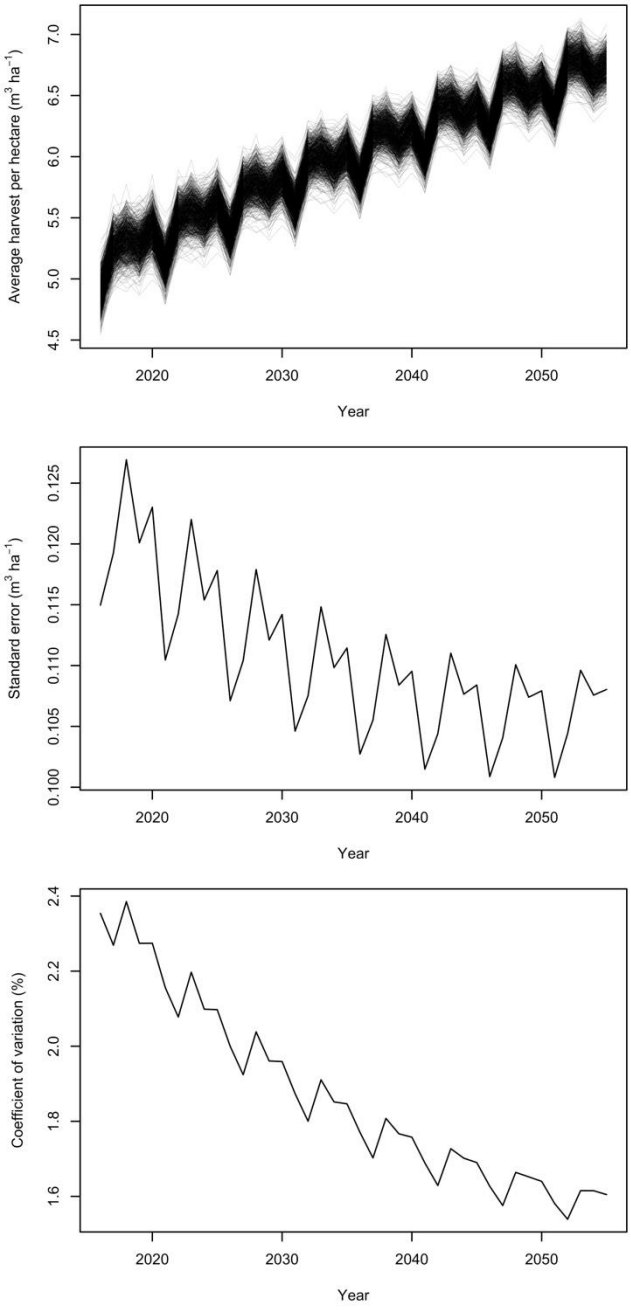

Figure 5. The average annual harvest per hectare with the standard error and coefficient of variation

3.6. Gross annual increment

The gross annual increment is expected to increase during the simulation period up to a peak increment that is expected to happen in 2050. The increase is from about 9.8 m^3 ha^{-1} yr^{-1} in 2015 to about 10.6 m^3 ha^{-1} yr^{-1} in 2055, which represent an increase of ~9%. The uncertainty will decrease slightly until 2027 and increase after. The standard error was about 0.04 m^3 ha^{-1} yr^{-1} in 2015 and about 0.07 m^3 ha^{-1} yr^{-1} in 2055. The coefficient of variation increased from about 0.45% in 2015 to about 0.67 % in 2055.

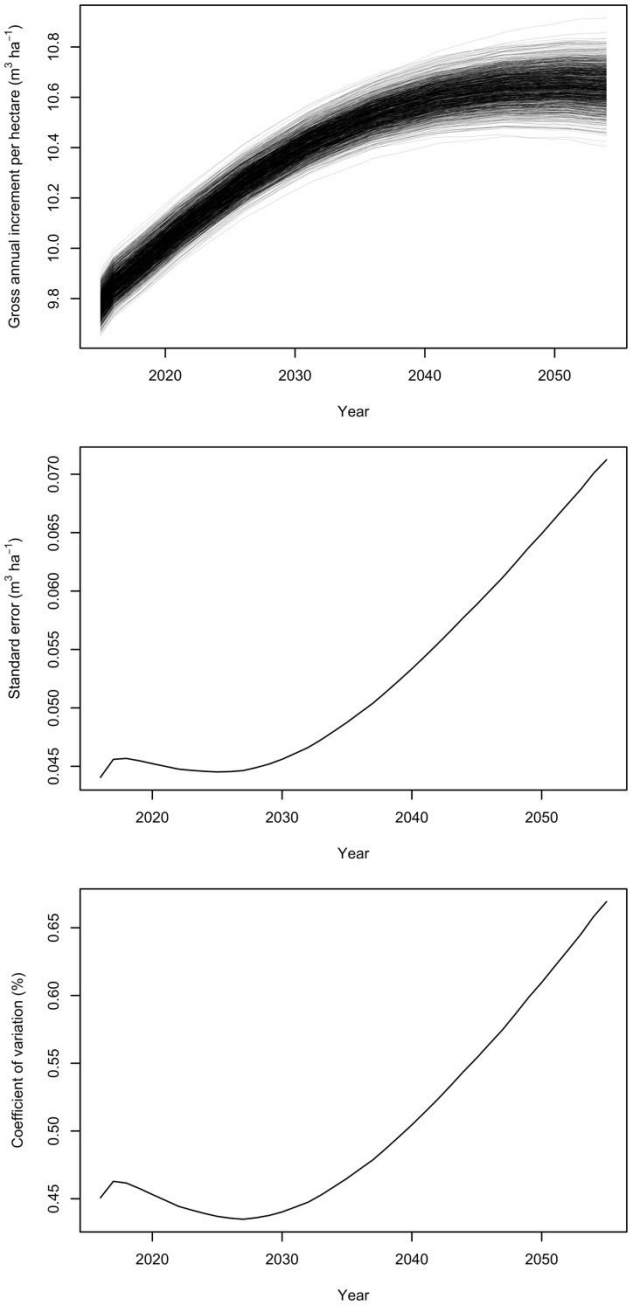

Figure 6. The gross annual increment with the standard error and coefficient of variation

3.7. Synthesis

The synthesis of results is presented in table 1:

- The greatest increase in estimate during simulation period was attributed to mean annual harvest and total harvest (i.e., +37.8%) whereas the number of trees per hectare decreased by 8.1%.
- The variable that had the greatest initial uncertainty in terms of CV, were also the mean annual harvest (2.354%) and the variable with the lowest initial CV was the gross increment per hectare (0.451%).
- The variable with the greatest uncertainty (CV) in 2055 was the annual mortality and total mortality with 2.643 and respectively 2.661%. The lowest CV in 2055 is attributed again to gross increment per hectare.
- The greatest increase in SE corresponds to mean volume per hectare (+137.2%) and the lowest increase corresponds to mean annual harvest which was the only variable to experience a decrease of uncertainty during simulation period.
- The greatest increase in coefficient of variation occurred for the basal area per hectare and tree number per hectare (+90 and respectively +89.6%) whereas the lowest increase in CV is attributed to mean annual harvest (-31.8%).

Table 1. Synthesis of results

Variable[1]	Units	The estimate, in		Standard error (SE), in		Coefficient of variation (CV, %), in		Change in estimate (%)	Change in SE (%)	Change in CV (%)
		2015	2055	2015	2055	2015	2055			
1	m^3ha^{-1}	337.1	436.8	2.0648	4.8981	0.612	1.121	+29.6	+137.2	+83.1
2	m^2ha^{-1}	28.746	34.979	0.1414	0.3270	0.492	0.935	+21.7	+131.2	+90.0
3	N ha^{-1}	886.5	814.8	5.4501	9.4996	0.615	1.166	-8.1	+74.3	+89.6
4	m^3ha^{-1}	1.7810	2.0253	0.0352	0.0535	1.977	2.643	+13.7	+52.0	+33.7
5	m^3ha^{-1}	4.884	6.732	0.1150	0.1080	2.354	1.605	+37.8	-6.0	-31.8
6	m^3ha^{-1}	9.774	10.644	0.0441	0.0712	0.451	0.669	+8.9	+61.7	+48.5

[1]Variables:

1. Volume per hectare
2. The basal area per hectare
3. Number of trees per hectare
4. Annual tree mortality per hectare
5. Annual tree harvest per hectare
6. Gross annual increment

4. Discussions

In this report we investigated how the uncertainty in the EFISCEN-Space input data would affect the uncertainty of Romanian forest resources projections over a period of 40 years. We performed 1000 replications of the Monte Carlo error propagation to account for the uncertainty in the projections of national forest estimates.

The projections of the forest estimates show an increase in forest resources over the simulated period of 40 years. The average volume per hectare and the total volume stock increased by almost 30%, despite of both the mortality and harvest increase (the increase in mortality was 14%, but the increase in harvest was 38%). In the same time, the average tree number per hectare decreased by 8%. The basal area increase (22%) was less than that of the volume stock, suggesting that volume stock increase is caused partially by the basal area increase, but there seems to be an increase in average tree height that caused the greater increase in volume stock compared to basal area. Out of the 30% increase in volume, ~22% was caused by the basal area increase (produced by diameter increase), and the difference of ~8% was driven by the tree H increase. In a typical allometric model employing logarithmic transformation where both D and H are used to predict tree volume, the parameter of D usually takes values closed to 2.0, whereas the parameter of H is much less, about 0.6-0.7 (Zianis et al., 2005). Since allometric model parameters can be interpreted as measures of relative growth (Huxley, 1932), a parallel can be drawn between the differences in increase of volume stock caused by basal area vs. height growth (22% vs. 8%) and the difference between allometric model parameters of D and H (2% vs. 0.7%). Their ratios are relatively similar (8/22 = 0.36 vs. 0.7/2=0.35) which attempts to explain the difference between the increase of basal area and the increase of volume stock. Furthermore, there seems to be a large share of Romanian forests that are going to be in an active growing stage during the simulation period, which was reflected into the gross increment. The increment increase (8.9%) peaked around 2050, potentially caused by a shift in the growing stage of Romanian forests. This peak may have been also affected by the continuous harvest volume during the simulation period.

The decrease in tree numbers per hectare also suggests that the volume stocks in increasingly concentrated in a lower number of trees that accumulate more biomass.

Regarding the harvest, it should be noted that the simulated harvest is based only on the probabilities derived from NFI1 vs. NFI2. Therefore, harvest is simulated as a function of growing stock. Since the growing stock increased during the simulation period, it was expected that the harvest will increase. The assumption on which the harvest simulation relies is that harvest is always related to the growing stock and a certain percent is always harvested (from each species class and D-class). In reality, this assumption may not be true, because countries have policies in place to regulate

harvest, being at the same time a strong measure that can be used to control the carbon sink at a country level.

A similar assumption is valid for mortality. The mortality was simulated as a fixed probability given the species class and D-class, as for the harvest. Nevertheless, because the mortality is a natural process, the simulation is expected to represent the reality more accurately than for the harvest.

The levels of uncertainty presented here are relatively low. This is the consequence of the high number of plots used for model parameterization. A total of 20845 plots were used, resulting therefore in a relatively small standard errors of the estimate and small coefficients of variation. However, an important outcome of this analysis is the increase in uncertainty during simulation period which for some forest variables was quite substantial.

The uncertainty of tree number per hectare is sourced only from plot sampling uncertainty. The CV increased from 0.6% in 2015 to 1.17% in 2055. However, the basal area per hectare includes uncertainty from plot sampling, but also from D measurement. Despite adding a new source of uncertainty, the CV levels were lower (0.49% in 2015 to 0.94% in 2055) compared to tree number per hectare, mainly because basal area is an aggregated plot variable, therefore, less sensitive to build up uncertainty when, for example, the resampled plots contain more plots with small trees that usually show a greater number of trees per hectare. The mean volume per hectare includes uncertainty from plot sampling, tree measurement but also from volume model prediction. The CVs (i.e., 0.6% in 2015 to 1.1% in 2055) were larger compared to those of basal area.

The tree mortality and harvest include uncertainty from plot sampling, D and H measurement and also from volume model prediction. Because mortality and harvest do not occur in all plots, it was expected that uncertainty of these two variables will be larger compared to mean volume per hectare. The CV of mortality varied between 2.0% in 2015 to 2.6% in 2055, whereas the CV of harvest varied from 2.6% in 2015 to 1.6% in 2055. We suspect that the reduction of CV in harvest was caused by setting the same seed for all replications, which randomly selected the sequence of year to be harvested within each harvesting cycle (equal to the mean period between NFI1 and NFI2).

The gross annual increment was calculated as a difference between mean volume per hectare of current year minus mean volume per hectare of previous year, plus the harvest and mortality of current year. Therefore, the uncertainty of annual increment relates to the uncertainty of its components. Nevertheless, the CV of annual increment was very low, varying from 0.45% in 2015 to 0.67% in 2055, which suggests that some components of annual increment (i.e., mean volume per hectare, mortality and harvest) may have been negatively autocorrelated, resulting in a compensation of uncertainty.

Limitations of error propagation procedure

In this error propagation procedure, we propagated uncertainty from plot sampling, tree measurement and allometric prediction as affecting the following input files: plotAttributes.csv, plotNrPerHa.csv, volumeParameters.csv and mortalities.csv.

We acknowledge that this analysis, although not a complete uncertainty analysis, brings valuable insights that help producing better projections. A complete uncertainty analysis was not possible to implement due to the way the model was constructed. To perform a complete uncertainty analysis, the model should allow adding regression model prediction uncertainty every time a prediction is performed within the forest model. However, forest resource projection models such as EFISCEN-Space are already highly complex models that typically work with point estimates for the diverse regression models used within the forest model. Therefore, adding another level of complexity would make forest projection models extremely difficult, if not impossible, to operate effectively for the purpose they were designed to. Alternatively, we looked at how the uncertainty in the input data affects the uncertainty of the projections.

When propagating the uncertainty from allometric model prediction, there are two components of the model prediction that are typically included: (i) uncertainty of model parameters, which originates in the variance-covariance of allometric model parameters, and (ii) uncertainty from residual variance (McRoberts & Westfall, 2014). In this analysis, because the Romanian allometric models lacked their variance-covariance matrix and their residual variances, we derived the residual variances for the main tree species based on validation of Romanian volume models with external data from the literature (see section 2.6), since the uncertainty from residual variance has a stronger effect on the total uncertainty compared to that originated from allometric model parameter variance-covariance matrix (McRoberts et al., 2015, 2016; McRoberts & Westfall, 2014). The procedure/routine of using allometric volume models in EFISCEN-Space is to fit the NFI level data (predicted volumes from local allometric models as used in the NFI) as a function of D, using a polynomial function-based model that uses only D as predictor of tree volume. Because of this routine, for each Monte Carlo replication we actually derived new model parameters of the polynomial functions that use D to predict volume, based on original NFI data that included the residual uncertainty component of allometric model prediction. Therefore, for the uncertainty originated in the allometric model prediction, although we included the uncertainty from residual variance, that was actually translated into a kind of uncertainty of model parameters for the polynomial input model parameters. As a result, the uncertainty from allometric volume models prediction used in this analysis can be assimilated to the component of uncertainty that is related to variance-covariance of model parameters (or the uncertainty from allometric model parameters) and lacking therefore the uncertainty originated from residual variance.

One of the main drivers of uncertainty in any forest resource model is the increment model prediction, because these models will mainly dictate the rate of change in the estimate across the simulation period. In this analysis, the uncertainty in the increment model prediction was not included

because increment models in EFISCEN-Space were designed to work at European level (Schelhaas, Hengeveld, et al., 2018). These increment models are sensitive to climate conditions across Europe, therefore, although Romanian NFI data was not included in the original analysis it is expected that the dependence of the increment models to local climate would create accurate predictions of D growth.

The uncertainty from tree measurement was formulated as from (McRoberts et al., 2016). We did not have access to repeated tree measurements of D and H (in the same time, not as in NFI1 and NFI2) to estimate the uncertainty based on local measurement conditions. However, because trees are measured relatively similarly everywhere, we assumed that measurement uncertainty in the US and Romania is similar.

The soil module Yasso15 was not included into the analysis. Therefore, the analysis has focused on tree volume, and no estimations of soil carbon have been performed.

Future directions

In this report we performed a first attempt to account for the uncertainty in the forest resource projections as originated from the uncertainty of input data. Therefore, further development is required to better understand the magnitude of different sources of uncertainty in different environments and find the key sources of uncertainty that may help improve the accuracy of forest resources projections overall. Given the limited available Romanian data to account for a more complete and accurate estimation of uncertainty, extending the procedure to other countries would help validate/invalidate the findings of this report. Another important direction is to include the uncertainty from D increment, dynamic mortality and ingrowth model parameters input data, as it is believed to represent significant sources of uncertainty.

5. Conclusions

This report focuses on the propagation of uncertainties in EFISCEN-Space projections for Romanian forests, with specific attention to how uncertainties in input data impact forest resource projections. The analysis uses Monte Carlo error propagation to model the uncertainty across three key input factors: plot sampling, tree measurements, and allometric model predictions. Given the increasing need for precise forest estimates, understanding the impact of data uncertainty is vital. This study provides a comprehensive look at how different sources of input uncertainty contribute to overall projections, enhancing the reliability of the model outputs and supporting more informed forest management decisions.

The study uses Romanian NFI data from two cycles, covering extensive datasets on forest structure, tree species, and geographic variability. Input files were prepared from the NFI data and then used to simulate forest dynamics over 40 years, from 2015 to 2055, under EFISCEN-Space. The Monte Carlo approach allowed repeated simulations (1000 replications) to capture and analyse the variability induced by uncertainties in the data. The key findings are:

- The overall uncertainty of resulting projections was relatively low, due to the large number of plots used to initialize the model;
- The greatest initial uncertainty occurred for the annual harvest (CV=2.354%);
- The greatest relative uncertainty increase during the simulation period, in terms of CV increase, was recorded for basal area per hectare and tree number per hectare (changes in CV of +90 and respectively +89.6%), whereas in terms of SE increase, it was recorded for mean volume per hectare (+137.2%).
- The mean annual harvest was the only investigated variable that experienced a reduction in uncertainty during simulation period (of -31.8%).

Therefore, the results reveal the sensitivity of various forest metrics to uncertainties in the input data. Analysing these changes over time highlights the cumulative impact of uncertainty on forest projection reliability, guiding future improvements in data collection and model accuracy.

References

Condés, S., & McRoberts, R. E. (2017). Updating national forest inventory estimates of growing stock volume using hybrid inference. *Forest Ecology and Management*, *400*, 48–57. https://doi.org/10.1016/J.FORECO.2017.04.046

Duncanson, L., Rourke, O., Dubayah, R., Schilz, M. H., & Palm, C. A. (2015). Small Sample Sizes Yield Biased Allometric Equations in Temperate Forests. *Scientific Reports*, *5*, 17153. https://doi.org/10.1038/srep17153

Dutcă, I., Mather, R., Blujdea, V. N. B., Ioraș, F., Olari, M., & Abrudan, I. V. (2018). Site-effects on biomass allometric models for early growth plantations of Norway spruce (Picea abies (L.) Karst.). *Biomass and Bioenergy*, *116*, 8–17. https://doi.org/10.1016/j.biombioe.2018.05.013

Dutcă, I., & McRoberts, R. E. (2024). *Optimal sample trees diameter distribution in developing allometric biomass models*. https://doi.org/doi.org/10.21203/rs.3.rs-4222725/v1

Dutcă, I., McRoberts, R. E., Næsset, E., & Blujdea, V. N. B. (2022). Accommodating heteroscedasticity in allometric biomass models. *Forest Ecology and Management*, *505*(November), 119865. https://doi.org/10.1016/j.foreco.2021.119865

Dutcă, I., Stăncioiu, P. T., Abrudan, I. V., & Ioraș, F. (2018). Using clustered data to develop biomass allometric models: The consequences of ignoring the clustered data structure. *PLOS ONE*, *13*(8), e0200123. https://doi.org/10.1371/journal.pone.0200123

Giurgiu, V., Decei, I., & Armasescu, S. (1972). *Biometria arborilor şi arboretelor din România: Tabele dendrometrice [The biometry of trees and stands in Romania: Dendrometrical tables]*. Ceres.

Giurgiu, V., & Draghiciu, D. (2004). *Modele matematico-auxologice si tabele de productie pentru arborete [The mathematic and auxologic models, and yield tables for forest stands]*. Ceres.

Gregoire, T. G., Næsset, E., McRoberts, R. E., Ståhl, G., Andersen, H.-E., Gobakken, T., Ene, L., & Nelson, R. (2016). Statistical rigor in LiDAR-assisted estimation of aboveground forest biomass. *Remote Sensing of Environment*, *173*, 98–108. https://doi.org/10.1016/J.RSE.2015.11.012

Huxley, J. (1932). Problems of relative growth, by Sir Julian S. Huxley...With 105 illustrations. In *Problems of relative growth, by Sir Julian S. Huxley...With 105 illustrations.* L. MacVeagh, The Dial Press,. https://doi.org/10.5962/bhl.title.6427

Marin, G., Bouriaud, O., Nițu, D. M., Calotă, C. I., & Dumitru, M. (2019). *Inventarul Forestier National din Romania. Ciclul I (2008-2012) [National Forest Inventory of Romania]*. Editura Silvica. http://roifn.ro/pdfs/Inventarul_forestier_national_din_Romania_Ciclul_I_2008-2012.pdf

Mart-Jan Schelhaas, Geerten Hengeveld, Sara Filipek, Louis Konig, Bas Lerink, Igor Staritsky, Anjo de Jong, & Gert-Jan Nabuurs. (2022). *EFISCEN-Space 1.0 model documentation and manual*.

McRoberts, R. E., Chen, Q., Domke, G. M., Ståhl, G., Saarela, S., & Westfall, J. A. (2016). Hybrid estimators for mean aboveground carbon per unit area. *Forest Ecology and Management*, *378*, 44–56. https://doi.org/10.1016/J.FORECO.2016.07.007

McRoberts, R. E., Moser, P., Zimermann Oliveira, L., & Vibrans, A. C. (2015). A general method for assessing the effects of uncertainty in individual-tree volume model predictions on large-area volume estimates with a subtropical forest illustration. *Canadian Journal of Forest Research*, *45*(1), 44–51. https://doi.org/10.1139/cjfr-2014-0266

McRoberts, R. E., & Westfall, J. A. (2014). Effects of Uncertainty in Model Predictions of Individual Tree Volume on Large Area Volume Estimates. *Forest Science*, *60*(1), 34–42. https://doi.org/10.5849/forsci.12-141

Saarela, S., Wästlund, A., Holmström, E., Mensah, A. A., Holm, S., Nilsson, M., Fridman, J., & Ståhl, G. (2020). Mapping aboveground biomass and its prediction uncertainty using LiDAR and field data, accounting for tree-level allometric and LiDAR model errors. *Forest Ecosystems*, *7*(1). https://doi.org/10.1186/s40663-020-00245-0

Schelhaas, M. J., Fridman, J., Hengeveld, G. M., Henttonen, H. M., Lehtonen, A., Kies, U., Krajnc, N., Lerink, B., Dhubháin, Á. N., Polley, H., Pugh, T. A. M., Redmond, J. J., Rohner, B., Temperli, C., Vayreda, J., & Nabuurs, G. J. (2018). Actual European forest management by region, tree species and owner based on 714,000 re-measured trees in national forest inventories. *PLoS ONE*, *13*(11). https://doi.org/10.1371/journal.pone.0207151

Schelhaas, M. J., Hengeveld, G. M., Heidema, N., Thürig, E., Rohner, B., Vacchiano, G., Vayreda, J., Redmond, J., Socha, J., Fridman, J., Tomter, S., Polley, H., Barreiro, S., & Nabuurs, G. J. (2018). Species-specific, pan-European diameter increment models based on data of 2.3 million trees. *Forest Ecosystems*, *5*(1). https://doi.org/10.1186/s40663-018-0133-3

Ståhl, G., Saarela, S., Schnell, S., Holm, S., Breidenbach, J., Healey, S. P., Patterson, P. L., Magnussen, S., Næsset, E., McRoberts, R. E., & Gregoire, T. G. (2016). Use of models in large-area forest surveys: comparing model-assisted, model-based and hybrid estimation. *Forest Ecosystems*, *3*(1), 5. https://doi.org/10.1186/s40663-016-0064-9

Vorster, A. G., Evangelista, P. H., Stovall, A. E. L., & Ex, S. (2020). Variability and uncertainty in forest biomass estimates from the tree to landscape scale: The role of allometric equations. *Carbon Balance and Management*, *15*(1), 8. https://doi.org/10.1186/s13021-020-00143-6

Wei, N., & Xia, J. (2024). Robust projections of increasing land carbon storage in boreal and temperate forests under future climate change scenarios. *One Earth*, *7*(1), 88–99. https://doi.org/10.1016/j.oneear.2023.11.013

Yanai, R. D., See, C. R., & Campbell, J. L. (2018). Current Practices in Reporting Uncertainty in Ecosystem Ecology. *Ecosystems*, *21*(21), 971–981. https://doi.org/10.1007/s10021-017-0197-x

Yanai, R. D., Wayson, C., Lee, D., Espejo, A. B., Campbell, J. L., Green, M. B., Zukswert, J. M., Yoffe, S. B., Aukema, J. E., Lister, A. J., Kirchner, J. W., & Gamarra, J. G. P. (2020). Improving uncertainty in forest carbon accounting for REDD+ mitigation efforts. *Environmental Research Letters*, *15*(12). https://doi.org/10.1088/1748-9326/abb96f

Zianis, D., Muukkonen, P., Mäkipää, R., & Mencuccini, M. (2005). *Biomass and stem volume equations for tree species in Europe*. Finnish Society of Forest Science, Finnish Forest Research Institute. http://www.citeulike.org/group/15400/article/11858948